UQAC
Université du Québec
à Chicoutimi

Development of a probabilistic method in seismic microzonation mapping accounting for uncertainties of the 3D geological model and geotechnical soil parameters

Par

Mohammad Salsabili

Sous la supervision du Prof. Ali Saeidi et la co-supervision du Prof. Alain Rouleau

Thèse présentée à l'Université du Québec à Chicoutimi dans le cadre du programme offert conjointement avec l'Université du Québec à Montréal en vue de l'obtention du grade de Philosophiæ Doctor (Ph. D.) en science de la terre et de l'atmosphère

Soutenue le 20 avril 2022

Jury :

Réal Daigneault, Professeur, Département des sciences appliquées, Université du Québec à Chicoutimi, Président du Jury

Sheri Molnar, Professeur, Department of Earth Sciences, Western University, Membre externe

Julien Walter, Professeur, Département des sciences appliquées, Université du Québec à Chicoutimi, Membre interne

Québec, Canada

RÉSUMÉ

Un problème important en génie géotechnique appliquée à la séismicité est l'évaluation de l'intensité attendue des ondes et de la période de résonance dominante des terrains à un endroit donné. La connaissance des caractéristiques des sédiments de surface est importante à cet égard. En effet, les facteurs géologiques (par exemple la stratigraphie des dépôts, leur épaisseur, la topographie du bassin) et géotechniques (par exemple les types de sol, leur module de cisaillement, taux d'amortissement) des dépôts de surfaceront tendance à modifier l'amplitude et le contenu fréquentiel des ondes sismiques qui les traversent, un phénomène connu sous le nom d'effet de site. Des indicateurs d'effet de site tels que la vitesse moyenne des ondes de cisaillement des 30 premiers mètres (V_{s30}) et la période fondamentale de résonance du site (T_0) sont les principaux paramètres utilisés pour évaluer l'amplification potentielle de la secousse sismique et effectuer une cartographie de microzonation sismique.

Cette étude de microzonation sismique est menée pour affiner le modèle d'aléa sismique pour un territoire ayant une géologie de surface complexe. La géologie quaternaire sous-jacente aux basses-terres du sud du Québec, incluant le territoire de la Ville de Saguenay présente une stratigraphie glaciaire et postglaciaire complexe avec un certain nombre de vallées enfouies remplies de sédiments fluvioglaciaire et glaciomarine. Le contraste élevé d'impédance entre les formations rocheuses et les sédiments superficiels peut causer une amplification sismique. Compte tenu du cadre stratigraphique et de la variabilité des dépôts, une méthodologie stochastique à plusieurs étapes est développée pour la modélisation géologique 3D et la quantification des incertitudes associées. Le krigeage bayésien empirique (EBK) est appliqué pour générer la carte de la topographie du substratum rocheux et déterminer l'épaisseur des sédiments de till et leurs incertitudes. La moyenne et la variance localement variables estimées par la méthode EBK permettent de tenir compte de la complexité des données et de la non-stationnarité modérée. Une simulation séquentielle d'indicateurs est ensuite effectuée pour déterminer la probabilité d'occurrence des sédiments postglaciaires discontinus (argile, sable et gravier) au-dessus de la couche basale de till.

La corrélation de la vitesse des ondes de cisaillement (V_s) avec les paramètres mesurés par des essais de pénétration de piézocône (CPTu) est étudiée dans les sédiments postglaciaires des basses-terres du Saint-Laurent et du Saguenay. Les valeurs supplémentaires de V_s, obtenues grâce à ces corrélations empiriques permettent de palier la faible quantité de mesures directes de V_s et d'augmenter les bases de données géotechniques appliquées à la séismicité. La base de données ainsi compilée comprend 991 mesures CPTu-V_s sur 40 sites. Les objectifs sont d'examiner l'applicabilité de différentes corrélations CPTu-V_s, d'identifier les principaux paramètres CPTu et de développer des corrélations CPTu-V_s spécifiques en tenant compte des effets du type de sol (par exemple sableux ou argileux) et du contexte géologique (sédiments marins de la mer de Champlain ou du golfe de Laflamme). Les résultats révèlent que l'application des corrélations déjà utilisées est biaisée à des degrés divers, dénotant un besoin de corrélations spécifiques aux sites localisés dans la zone d'étude. L'analyse statistique multivariée permet de développer des corrélations empiriques entre les valeurs de V_s, les paramètres géotechniques, la profondeur et les types de sol, ainsi que l'évaluation de leurs incertitudes. La prise en compte du type de sol et du cadre géologique contribuent à une réduction des incertitudes dans les corrélations CPTu-V_s développée pour les sols à grain fin.

Un traitement combiné de diverses sources d'incertitudes est appliqué, considérant les facteurs géologiques et géotechniques, pour développer un modèle 3D de vitesse d'onde de cisaillement et évaluer l'incertitude associée Le modèle 3D de V_s est créé en utilisant des corrélations V_s et la probabilité d'occurrence des sols postglaciaires. L'incertitude propagée est également quantifiée par la prise en compte de la variance combinée et elle dépend à la fois de la variabilité géologique et géotechnique. La dernière étape consiste à transformer le modèle 3D de V_s en cartes 2D représentant la distribution spatiale de $V_{s,30}$ et T_0 avec les incertitudes associées. Les résultats

indiquent que les cartes sismiques et leur incertitude sont influencées par l'épaisseur du sol, les probabilités de type de sol et les propriétés géotechniques du sol. L'épaisseur du sol ressort comme un des facteurs les plus critiques. Dans les sédiments peu profonds, les cartes de $V_{s,30}$ et de T_0 représentent des conditions de roche ou de sol très rigide avec une réponse sismique dans de courtes périodes de vibration ≤ 0,2 s. En revanche, les régions avec des sédiments plus épais présentent des sites avec une réponse potentielle qui ressemble à des conditions de sol moyennes à molles, avec des périodes de vibration dominantes plus longues. Les cartes de variance respectives, soit $\sigma_{V_{s,30}}$ et σ_{T_0}, représentent l'incertitude aléatoire et épistémique inhérente aux modèles, qui sont associées à la fois à la variabilité spatiale des unités géologiques et à la dispersion statistique des données de V_s. En conséquence, l'incertitude combinée des modèles géologiques et géotechniques est faible à proximité des forages géologiques en raison de la plus grande certitude du modèle géologique, entraînant une plus faible incertitude de $V_{s,30}$ et de T_0.

ABSTRACT

A key aspect of geotechnical earthquake engineering is related to the evaluation of the expected intensity and the dominant period of the seismic shaking at a given location. Knowledge of the geological (e.g., stratigraphy, basin topography, and thickness) and geotechnical (e.g., soil type, shear modulus, and damping ratio) properties of the surficial sediments is important in this respect since they tend to modify the amplitude and frequency content of the incoming seismic waves, a phenomenon known as seismic site effect. Site effect proxies, such as the time-averaged shear wave velocity of the top 30 m ($V_{s,30}$) and the fundamental site period (T_0), are the main parameters commonly used for evaluating the potential amplification of seismic shaking and conducting seismic microzonation mapping.

Seismic microzonation study is conducted to refine the seismic hazard model for the study area with complex surficial geology. The Quaternary geology underlying the lowlands of southern Quebec, including the Saguenay City territory, shows complex glacial and postglacial stratigraphy with a number of buried valleys filled with glaciofluvial and glaciomarine sediments. High seismic impedance contrast between rock formations and surficial sediments may cause seismic amplification. Considering the stratigraphic setting and soil type heterogeneity, a multistep stochastic methodology is developed for 3D geological modeling and quantification of the associated uncertainties. Empirical Bayesian kriging (EBK) is applied to generate a bedrock topography map and determine the thickness of the till sediments and their uncertainties. The locally varying mean and variance obtained by the EBK method enable accounting for data complexity and moderate nonstationarity. Sequential indicator simulation is then performed to determine the occurrence probability of the discontinuous postglacial sediments (e.g., clay, sand, and gravel) on top of the basal till layer.

The correlation of shear wave velocity (V_s) with piezocone penetration test (CPTu) parameters is investigated in postglacial sediments in the lowlands of the St. Lawrence and Saguenay rivers. In establishing CPTu-*Vs* correlations, the sparsity of V_s measurements is remedied by using extensive geotechnical soil databases and the developed CPTu-*Vs* correlations. The compiled database includes 991 CPTu–V_s measurements at 40 sites. The objectives are to examine the applicability of different CPTu–V_s correlations, identify the leading CPTu parameters, and develop specific CPTu–V_s correlations considering the effects of soil type (e.g., sandy or clayey) and geological setting (Champlain or Laflamme sea sediments). Results reveal that the application of the existing correlations is biased in varying degrees, denoting a need for site-specific correlations for the study area. A multivariate statistical analysis allows the development of empirical correlations among V_s, geotechnical parameters, depth, and soil types, along with the evaluation of their uncertainties. Consideration of soil type and geological setting contributes to a reduction in uncertainties for the CPTu–*Vs* correlations for fine-grained soils.

A combined treatment of various sources of uncertainties, from geological to geotechnical, is applied to develop a 3D shear wave velocity model and evaluate the associated uncertainty. A 3D V_s model is created using V_s correlations and the occurrence probability of postglacial soils. The propagated uncertainty is also quantified by considering the combined variance of the geological and geotechnical properties. The final step involves transforming the 3D V_s model into 2D maps representing the spatial distribution of $V_{s,30}$ and T_0 together with related uncertainties. Results indicate that seismic maps and their uncertainty are influenced by soil thickness, soil geotechnical properties, and soil type probabilities. Among which soil thickness is one of the most critical; in shallow sediments, $V_{s,30}$ and T_0 maps represent rock or very stiff soil conditions with the seismic response in short vibration periods ≤ 0.2 s. By contrast, regions with thicker sediments present sites with a potential response that resembles medium to soft soil conditions with longer dominant vibration periods. The respective $\sigma_{V_{s,30}}$ and σ_{T_0} maps represent the inherent random and epistemic uncertainty in the models, which are associated with the spatial variability of the geological units and the statistical dispersion of the V_s data. Consequently, the combined uncertainty of the geological and geotechnical

models is genuinely quantified as it decreases in the vicinity of the geological boreholes due to the higher certainty of the geological model, resulting in lower uncertainty of $V_{s,30}$ and T_0.

TABLE OF CONTENTS

LIST OF TABLES

LIST OF FIGURES

LIST OF ABBREVIATIONS

CPT	Cone penetration test
CPTu	Piezocone penetration test
EBK	Empirical Bayesian Kriging
ME	Mean error
MSE	Mean standardized error
MSSE	Mean square standardized error
NBCC	National Building Code of Canada
OCR	Over-consolidation ratio
RMSE	Root mean square error
SBT	Soil behavior type
SCPTu	Seismic piezocone penetration test
SIS	Sequential indicator simulation
SPT	Standard penetration test
TIN	Triangulated irregular network

LIST OF SYMBOLES

a_n	Net area ratio
B_q	Normalized pore water pressure (=(u_2 - u_0)/(q_t - σ_{v0}))
$\tilde{C}_{00}$	Variance of point values
$\tilde{C}_{ij}$	Covariance between measured samples
$\tilde{C}_{i0}$	Covariance between measured and unknown values
D_{50}	Effective mean diameter
D	Depth
$E(Z\ )$	Mean of a random geotechnical variable
e_0	Void ratio
f_o	Fundamental site frequency
F_r	Normalized sleeve friction resistance (=f_s/(q_t - σ_{v0}))100%
f_s	Sleeve friction resistance
G_{max}	Maximum shear modulus
h	Soil thickness of each cell (or block)
h_{pg}	Soil thickness of postglacial deposits
H_n	Total soil thickness of n cells (or blocks)
H	Total soil thickness
I_c	Soil behavior type index (= [(3.47 – log Q_{tn})^2 + (log F_r+1.22)^2]$^{0.5}$)
$i(u_\alpha; k)$	Binary indicator value at location u_α and for category k
n	Stress exponent
p_a	Atmospheric pressure
p_i	Event probability of x_i
q_c	Raw cone tip resistance
q_t	Corrected cone tip resistance (= q_c + u_2 (1 – a_n))
Q_{t1}	Normalized cone resistance when n=1
Q_{tn}	Normalized cone resistance with a variable n (= [(q_t – σ$_{v0}$)/p_a] (p_a/ σ'$_{v0}$)^n)
R_f	Friction ratio (= f_s/q_t)
T_0	Fundamental site period of vibration
T_n	Natural period of vibration
u	Coordinates vector
u_0	In situ equilibrium water pressure
u_2	Pore pressure measured behind cone
V_s	Soil shear-wave velocity
V_{s1}	Normalized soil shear-wave velocity
$V_{s,30}$	Average shear-wave velocity of the top 30 m
$V_{S,avg}$	Average shear-wave velocity of the entire soil deposit
$V_{s,clay}$	Clay V_s
$V_{s,pg}$	Postglacial V_s
$V_{s,rock}$	Bedrock V_s (= 2500 m/s)
$V_{s,sand}$	Sand V_s
$V_{s,till}$	Glacial V_s (= 580 m/s)
$V_{s,n}$	Shear-wave velocity of the n^{th} cell (or block)
V_s^d	Deterministic V_s model
V_s^p	Probabilistic V_s model
$\bar{V}_{s,n}$	Averaged shear-wave velocity of n cells (or blocks)
w	Water content
$w_i w_j$	Kriging weights
x_i	Random categorical variable
z_i	Random geotechnical variable
$Z(u_\alpha)$	Random variable at location u_α

β_s	Internal damping ratio
$\hat{\gamma}(h)$	Experimental variogram
$\hat{\gamma}_I(h;k)$	Indicator variogram for category k
$\sigma^2(x_i)$	Variance of a random categorical variable
$\sigma^2(Z)$	Variance of a random geotechnical variable
$\tilde{\sigma}_k^2$	Error variance of kriging
$\sigma_{v0}, \acute{\sigma}_{v0}$	Overburden stress (total, effective)
$\sigma_{Vs,clay}$	Clay V_s standard deviation
$\sigma_{Vs,sand}$	Sand V_s standard deviation
$\sigma_{Vs,till}$	Glacial V_s standard deviation (= 175 m/s)
$\sigma^2_{Vs,n}$	V_s variance of the n^{th} cell (or block)
$\sigma^2_{\overline{V}_{s,n}}$	Averaged V_s variance of a soil column with n cells (or blocks)
$\sigma_{V_s^p}$	V_s standard deviation of a probabilistic model
σ_{T_0}	T_o standard deviation
$\sigma_{V_{s,30}}$	$V_{s,30}$ standard deviation

DEDICATION

To

my parents, *Farzaneh* and *Nader*,

for their unconditional love and inspiration of the humanity, kindness, and patience…

my sister and my brothers

for always being my support over these years.

ACKNOWLEDGMENTS

I would like to thank my supervisor Prof. Ali Saeidi for his valuable supervision, technical advice, support, and permanent encouragement during my PhD.

I would like to thank my co-supervisor Prof. Alain Rouleau for his valuable comments and suggestions throughout this research.

I would like to express my gratitude to Dr. Miroslav Nastev, who considerably helped me in completing my research study. I greatly appreciate his valuable suggestions and comments, as well as the time he dedicated to my academic research.

Prof. Daigneault, chair of the jury, Prof. Molnar, external member, and Prof. Walter, internal member of the jury, I would like to thank them for their time, comments, and valuable recommendations.

I also appreciate all my professors, colleagues, and our friendly research group members (R2EAU) at the University of Quebec at Chicoutimi for their help and comments.

I would like to thank Mr. David Noel, the technician of the geotechnical laboratory of the University of Quebec at Chicoutimi, and Mr. Ian van der Hulst at Gouda Geo-Equipment Co. for their help in performing field tests.

I would like to acknowledge the financial support from the Natural Sciences and Engineering Research Council of Canada and Hydro-Quebec.

I would like to acknowledge the Quebec Ministry of Transportation and the members of the CERM-PACES project of UQAC for their cooperation and for providing access to the database.

Finally, I want to thank my lovely family, my brother *Alireza*, and my close friends for their support throughout this period of my life.

INTRODUCTION

Statement of the problem

The characterization of local soil conditions and assessment of the related uncertainties are the first and most important step in earthquake hazard evaluation. The study begins with integrating data from geological, geotechnical and geophysical site investigations to predict the spatial distribution of site conditions known as seismic microzonation mapping. This inherent multidisciplinary effort needs an appropriate decision-making approach for data assimilation based on the geological conditions, soil geotechnical properties, and budget of the project. Usually, a deterministic approach is used for preparing seismic microzonation maps. However, there is a significant amount of uncertainty due to the random nature of soil properties, complex geology, limited measurement methods, data adequacy, uncertain empirical relationship, and uncertainty in the estimation and complexity of the studied phenomena. The development of a probabilistic microzonation approach will consider several aspects of these uncertainties.

The reliability of estimated V_s values is dependent on the quality of data obtained from geophysical, geotechnical and geological studies. Among the sources of data for seismic site classification, the 3D geological model is crucial for mapping site classes since it provides information about the spatial distribution of soil properties, subsurface layering and the thickness of the unconsolidated deposits. Due to incomplete information about reality, uncertainty will affect the geological model. The primary problem is how this uncertainty in the geological model can be quantified and how it affects the site classification and the seismic microzonation map.

Shear-wave velocity is the key parameter for the development of seismic microzonation maps. In situ *Vs* profiling can be measured by different methods and can be categorized into two main categories, namely, invasive and non-invasive (Hunter and Crow, 2015). The uncertainty of V_s measurements varies among different methods. For instance, Moss (2008) indicated that the coefficient of variation of invasive and non-invasive methods

varies from 1% to 3% and from 5% to 6%, respectively. A problem is the propagation of *Vs* measurement uncertainty into model uncertainties (*Vs* model).

Having access to sufficient in situ V_S measurements is ideal for carrying out a seismic microzonation project, however, it is challenging in regional studies. Nevertheless, geotechnical data, which have been obtained in previous geotechnical investigations, represent a useful source of information for estimating the shear-wave velocity. Among the geotechnical tests, standard penetration tests (SPTs) and cone penetration tests (CPTs) appear to be the most frequently applied tests to determine the shear-wave velocity using typical empirical relationships (Mayne and Rix, 1995; Robertson, 2009; Anbazhagan et al., 2012). These regression equations are developed based on samples collected from different sites with specific characteristics and transformation uncertainties. Regarding the different compositions of the clay in Eastern Canada in comparison with other parts of the globe, another problem to be addressed in this project is the development of empirical correlations with consideration of the specific characteristics of these clays and consequently the development of specific shear-wave velocity profiles (V_S-depth correlations).

According to the National Building Code of Canada (NRC, 2015), site-associated amplification is mainly dependent on the shear-wave velocity in the top 30 meters ($V_{s,30}$) of surficial deposits. Based on this approach, the deterministic site classes (A to F) are associated with $V_{s,30}$ ranges and this parameter constitutes the basis of most seismic microzonation maps conducted in Canada (Hunter et al., 2002; Rosset et al., 2015; Nastev et al., 2016; Foulon et al., 2018). However, due to the uncertainties propagated to the $V_{s,30}$ model, the deterministic site classification approach neglects the variabilities. A probabilistic approach can be the resolution of this problem, and the effect of input uncertainties on the resulting maps will be quantified.

Objectives

The general objective of the thesis is to develop a probabilistic seismic microzonation mapping methodology that considers the uncertainties of the developed 3D geological model and geotechnical soil parameters. The objectives of the research are set in conducting a study over the territory of the Saguenay City due to the complex geological and geotechnical soil properties. The presence of sensitive clays and the proximity of the important seismic zone of Charlevoix are critical factors for the study of the region.

To achieve this general objective, several specific objectives will be met.

a) Develop a methodology to create a 3D geological model and assess the associated uncertainty in the model.

b) Develop empirical correlations of shear-wave velocity (V_s) and soil geotechnical properties over the Saguenay City area.

c) Develop a methodology for creating a stochastic 3D geotechnical model of V_s and assessing its uncertainties.

d) Generate spatial distribution maps of $V_{s,30}$ and T_0 (fundamental site period) and the spatial uncertainties.

Methodology

GIS database

As a first step, it is necessary to gather as much data as possible about the surface and subsurface geology and, in particular, on the soft deposits present in the region, in order to characterize the geotechnical soil properties. There are various sources of information for collecting geodata, such as geotechnical investigations, borehole data, geophysical surveying results, hydrological and hydrogeological data, geological maps and sections that can be stored in a unified database.

The database of the *Programme d'acquisition de connaissances sur les eaux souterraines (PACES, 2013)* produced for the Saguenay–Lac-Saint-Jean region will help in collecting this information because of the abundance of data that it includes on surface and subsurface geology (maps of deposits, drilling logs, stratigraphic sections, geophysical data, etc.). The Hydro-Quebec geotechnical data obtained at electric high voltage power posts and along the transmission lines will be added to the PACES database. Particular attention will be given to the collection of existing data on surface deposits. This project, therefore, requires obtaining the latest data to the region's geodatabase. All these data will be stored, managed and processed in a geodatabase using a geographic information system (GIS). Consequently, the GIS information layers can be included or interpreted from the following thematic data set:

- seismologic data,
- referenced seismic ground motion parameters (PGA, spectral acceleration),
- surficial geology maps (Quaternary deposits),
- the thickness of Quaternary deposits
- bedrock basement geology (underlying unconsolidated materials),
- borehole data such as collar locations, and other specifications of drill hole operations,
- geotechnical soil properties acquired by SCPT/CPTu or SPT
- shear-wave velocity (V_S) measurement locations and values,
- groundwater table elevations,

- underlying bedrock basement elevation.

The existing subsoil database will be increased by adding the data acquired by in situ penetration tests and geophysical surveys, especially for the area of the electrical transformation sites and along the high voltage transmission lines of Hydro-Québec. All data related to the nature of the deposits, the mechanisms and the age of the deposition, the thickness of the deposits and to the geotechnical characteristics must be gathered and stored during this stage.

3D Geological model development

A geological model is a spatial representation of the distribution of sediments and rocks in the subsurface. An important phase of this study is the development of a 3D model of the subsurface, which which can be used to determine shear-wave velocity and the thickness of loose deposits. The construction of a 3D model can be carried out by implementing two approaches: *explicit* and *implicit* modelling.

The traditional explicit method is carried out by manually digitizing the boundaries of a complex geological body by viewing and interpreting the drillhole data along a series of geological cross- sections. Conventionally, 2D sections are generated in the form of polylines; then a triangulated solid body is generated by connecting these polylines together, The resulting solid body is called the wireframe model in commercial software; in geo models, it represents the volumetric distribution of soil or rock stratigraphy. The procedure of explicit modelling does not need complex data processing and analysis; it is straightforward, and the geo modeller can perceive all parts of processing. However, the digitization and connection of the boundaries are time-consuming in a complex model; in addition, the constructed model is based on the interpretation of an individual geo-modeller and could be biased. Finally, the process of updating the model is difficult and time-consuming (Cowan et al., 2003).

An implicit model can be defined as a mathematical function that directly transforms the input data to produce a model through space. For instance, a sphere with a unit radius

through space can be defined as x2+y2+z2-1=0, which represents a function in the form of $f(x, y, z) = \mathrm{C}$; this function describes a surface consisting of an infinite number of (x,y,z) in the space, implicitly by an equation (Cowen et al. 2003). In this approach, an interpolation algorithm such as kriging, radial basis functions, inverse distance weighted, and others can define this function (De Kemp, 2000; Jessell et al., 2014). The advantage of using geostatistical algorithms is that it assigns values to locations where no samples or measurements have been taken, and it allows considering the uncertainty of these estimates (e.g. kriging variance).

The consistency and accuracy of input data are significantly important in implicit modelling. By importing the data to the software and after selecting the appropriate interpolation algorithm, the geo-modeller has a lower control on the final model in comparison with the explicit modelling. It is therefore important that the raw data be checked and verified precisely, as well as cross-validating outputs. Geological data have been collected for a long time, and different geologists' insights have been involved so that the data are based on different interpretations. All relevant data, e.g. maps, profiles, cross-sections, geophysical and other data, must be checked for consistency, and, if necessary and possible, they must be revised to produce a homogeneous data set. The software *Leapfrog 3D Geo* will be used to make this model (Aranze, 2014). An important issue in this part of the project is the determination of model uncertainties, particularly associated with the thickness and spatial distribution of the soft deposit layers. The algorithm of the methodology of creating the 3D geological model is presented in Figure 1-1.

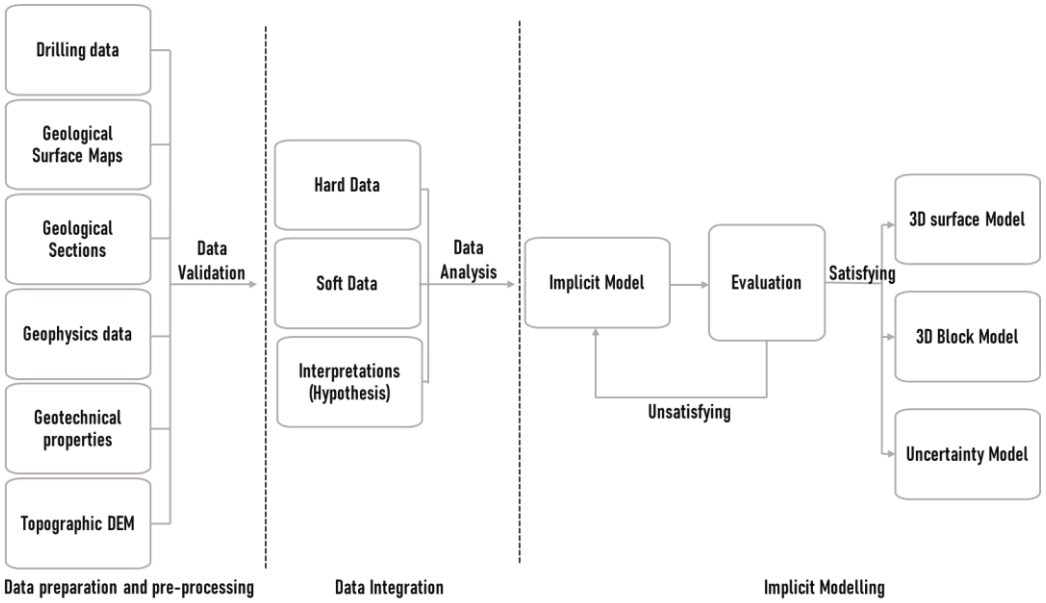

Figure 1-1. Flow diagram of developing a 3D geological model. © Mohammad Salsabili, 2022

*Hard data: Direct measurements or observations of the attributes (i.e., borehole data), Soft Data: Indirect or interpreted data (e.g. geophysical interpretations).

3D Geotechnical model development

Adequate V_S measurements from geophysical or geotechnical tests are are not available at sufficient density or resolution for all parts of the region. By developing a representative *V*s-depth profile for the study area, the shear-wave velocity variation with depth in the soil column was determined. Hence, if location *j* does not have direct V_S measurements, then the V_s-depth profile is approximately assigned indirectly from the converted CPT-V_s, and SPTn-V_S data. Such profiles will be combined with a 3D geological model to determine the variation in V_s for each site column through the region. In brief, the procedure includes two main steps: (I) developing V_s empirical correlations and (II) creating a 3D V_s model incorporating the probabilistic geologic model and V_s empirical correlations.

Several methods will be used to estimate the shear-wave velocity, according to the available data and to tests carried out during the project. First, seismic cone penetration test (SCPT) are carried out thanks to the equipment that is acquired as part of this project to directly measure V_s values, particularly at electric transformer substations in the region and under high

voltage power lines. These values can also be estimated using empirical relationships based on CPT and SPT test results. Geophysical tests are carried out with the geophysical equipment available at UQAC to determine the values of V_s and to evaluate the V_s obtained via indirect measurements. An important part of the study is the development of regional empirical correlations and the evaluation of the V_s obtained by these three methods. This offers the possibility to validate the results for several types of soil of the region, especially for sensitive clay, and to extrapolate these results over other territories. The procedure for developing the geotechnical model is as follows (Figure 1-2):

i) Analysis of the effective geotechnical and geological parameters used in the correlation with *V*s-CPT data,

ii) Development of a site-specific correlation for predicting shear-wave velocity from CPT data,

iii) Development of the *V*s-depth profiles for the Saguenay City area from integrated *V*s measurement data,

iv) Evaluation of the reliability of the V_s-depth profiles with the data obtained from direct methods such as SCPT data, seismic refraction and reflection sections.

v) Integration of the V_s correlations with the 3D geological model.

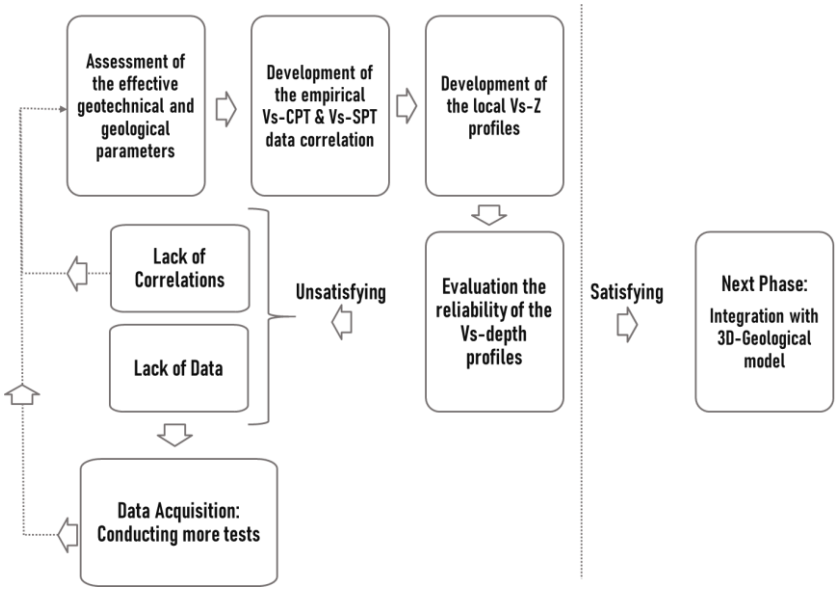

Figure 1-2. The procedure for the development of *V*s empirical correlations and geotechnical model. © Mohammad Salsabili, 2022

Seismic microzonation

The spatial distribution of seismic site parameters namely the average shear-wave velocity down to the bedrock ($V_{s,avg}$), the average velocity for the top 30 meters ($V_{s,30}$) and fundamental site period (T_0) are the most typical seismic microzonation map products. The 3D geological model determines the spatial distribution and thickness of each layer along the depth of the deposits. In addition, the developed V_s-depth profiles assist in determining the shear-wave velocity for each layer. Indeed, it would be possible to determine the values of the seismic site parameters using thickness values obtained for the different layers, as well as shear-wave velocity values for each of these strata. The spatial distribution of seismic parameters can be interpreted as a microzonation map. It should be noted that the uncertainties affecting the soil types, the thickness of the deposits and those on the V_s measurements will be considered to determine the uncertainties on the values of the site parameters.

To apply the probabilistic approach, the variability and associated uncertainties in input parameters will be expressed by determining the mean and the variance of the mean for each

variable (V_s and H). Then, the uncertainty will be propagated to the design parameters such as $V_{s,30}$ and T_0 using first order second-moment analysis. For random field variables such as thickness and geological units, the important role of modelling spatial variability relies on quantifying the related spatial uncertainty using the geostatistical approach.

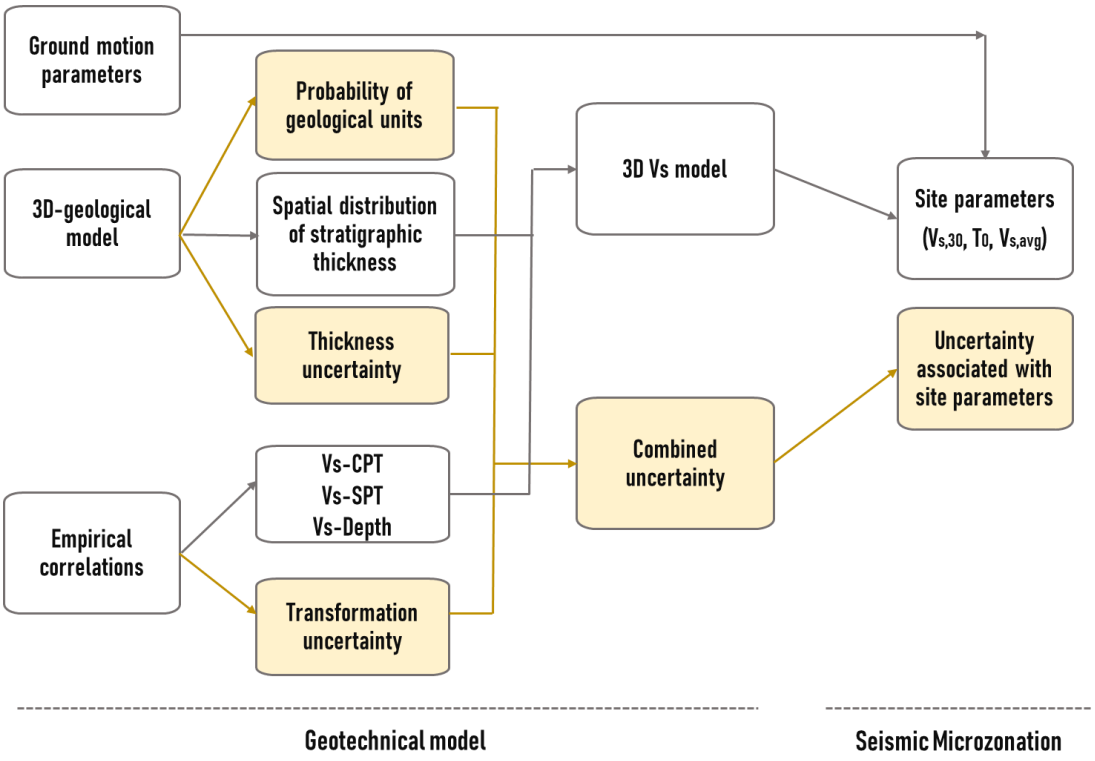

Figure 1-3. Flow diagram of code-oriented seismic microzonation. © Mohammad Salsabili, 2022

Originality and contribution

A methodology to quantify and integrate geological and geotechnical uncertainties is adopted to develop seismic microzonation maps. The methodology is based on developing a probabilistic 3D model that determines the geometrical and geotechnical soil properties and provides a basis for assessing the spatial uncertainties. The model assists in determining the seismic site parameters and associated uncertainties, including the average V_s value of the top 30 m of soil ($V_{s,30}$), the average V_s of all of the soil deposits ($V_{s,avg}$) and the fundamental site period (T_0).

A comparison between the site parameters and classification schemes is applied to evaluate the importance of the site classification parameters on the resulting microzonation maps. These results provide insight into the influencing factors of microzoning results related to geology and engineering. This approach has received only little attention in the literature, and it is described in the following published paper:

Salsabili, M., Saeidi, A., Rouleau, A. and Nastev, M., (2021) "Seismic microzonation of a region with complex surficial geology based on different site classification approaches" *Geoenvironmental Disasters*, *8*(1), pp.1-13.

Considering the stratigraphic setting and soil type heterogeneity, a multistep stochastic methodology is developed for 3D geological modelling and quantification of the associated uncertainties. In soil engineering literature, uncertainty in the geological model has been neglected and the soil units are usually modelled using a deterministic approach. The novelty of methodology is that it involves geostatistical interpolation and simulation methods to develop a probabilistic 3D geological model considering the stratigraphic rules and soil heterogeneity. Details were published as follows:

Salsabili, M., Saeidi, A., Rouleau, A. and Nastev, M. (2021) "3D Probabilistic Modelling and Uncertainty Analysis of Glacial and Postglacial Deposits of the City of Saguenay, Canada" *Geosciences*, *11*(5), p.204. https://doi.org/10.3390/geosciences11050204.

The development of empirical correlations between V_s and geotechnical properties is important given the specific characteristics of soil deposits in a region with different soil

structures, especially with sensitive clays. We attempt to study and develop CPTu-V_s correlations for a wide range of soil types in southern Quebec and for the first time. In this way, multivariate nonlinear regression analyses are conducted to develop the CPTu-V_s correlation and assess geotechnical uncertainties. In this study, we examine small- and large-strain soil properties, specifically fine-grained and sensitive clays found in Champlain and Laflamme marine sediments. Details have been presented in a submitted paper as follows:

Salsabili, M., Saeidi, A., Rouleau, A., and Nastev, M. (2022) "Development of empirical CPTu-Vs correlations for post-glacial sediments in Southern Quebec, Canada, in consideration of soil type and geological setting". Soil Dynamics and Earthquake Engineering, 154(July 2021), 107131. https://doi.org/10.1016/j.soildyn.2021.107131.

The final step deals with developing a novel probabilistic method to consider the spatial uncertainties of the geological model and propagating these uncertainties to the geotechnical response variable V_s. To the best of our knowledge, this approach introduces for the first time consideration of the influence of soil geological uncertainty on the prediction of geotechnical properties and seismic site characterization. The approach is used to develop a stochastic 3D V_s model and facilitate to assess the uncertainty associated with combining various types of uncertainties in building the geological and geotechnical models. Details are presented in a submitted paper as follows:

Salsabili, M., Saeidi, A., Rouleau, A. and Nastev, M. "3D probabilistic approach for seismic microzonation mapping and model uncertainty assessment" (Submitted to *Earthquake Spectra*, under review, 2021)

In addition, we have published abstracts and made presentations at three conferences on applications of geological, geotechnical and hazard studies:

Salsabili, M., Saeidi, A., Rouleau, A. and Nastev, M., (2021) "Le développement de corrélations entre la vitesse des ondes de cisaillement et des données de piézocône sismique: une étude dans des dépôts d'argile sensible du sud du Québec" Colloque scientifique: *Le sinistre de Saint-Jean-Vianney de 1971*, 13 et 14 mai 2021, Saguenay. Soc. Can de géotechnique, Sections Est du Québec. (conference)

Salsabili, M., Saeidi, A. and Rouleau, A., (2020) "Probabilistic 3D modeling of layered soil deposits: Application in seismic risk assessment", the Canadian Geotechnical Society, *GeoVirtual Conference*, September 14-16, 2020. (conference)

Salsabili, M., Saeidi, A. and Rouleau, A., (2019) “Comparison of code-oriented site classification in the Saguenay region, Québec”, *12th Canadian Conference on Earthquake Engineering,* Québec City, June 17-20, 2019. (conference)

CHAPTER 1

LITERATURE REVIEW

1.1. Site effect overview

A significant contribution to the observed damage during past destructive earthquakes was attributed to the phenomenon known as the site effect, e.g. 1985 M8.0 Mexico City, 1989 M6.9 Loma Prieta. Borcherdt and Glassmoyer (1992) and Borcherdt (1994) proposed the implementation of geotechnical and geological parameters as identification criteria to empirically delineate the effect of local site classes and associated spectral-frequency dependent amplification factors. The amplification factors account for the ratio of the ground motion intensity, for example, the response spectral acceleration, measured at the bedrock in comparison to the soil surface (Dobry et al., 2000). In general, there are two ways to evaluate the site effect and compute the site amplification (*A*), theoretically based on the wave propagation theory, and empirically by utilizing recordings of ground motion at various sites. The theoretical approach assumes that the seismic energy must be preserved during wave propagation and when a wave is totally transmitted from one material to another, the amplitude of the wave will vary inversely with square root of the impedance ($\rho \times V_s$) ratio (Shearer and Orcutt, 1987):

$$A \sim \left(\frac{\rho_{rock} \times V_{s,rock}}{\rho_{soil} \times V_{s,soil}}\right)^{1/2}, \tag{1-1}$$

where ρ_{rock} and ρ_{soil} are the average densities of bedrock and soil, respectively, and $V_{s,rock}$ and $V_{s,soil}$ are the shear-wave velocities of bedrock and the ground surface, respectively.

This broad-band amplification is true only when waves are totally transmitted between two media. An important amplification effect also occurs in association with large seismic impedance boundaries, known as resonance amplification. Multiplicative reflections within the surface layer result in modes with well-defined resonant frequencies. In this case, the amplitude at the surface of the layer will vary inversely with the impedance contrast. It should be noted that seismic energy dissipates as a consequence of inelastic attenuation (damping) and

spherical divergence (Kramer, 1996), and the effect of damping at high frequencies results in lower amplification. In fact, soil damping affects more high-frequency than low-frequency motion content. The value of amplification is controlled by two major factors, namely, the impedance ratio (I= $\frac{\rho_{rock} \times V_{s,rock}}{\rho_{soil} \times V_{s,soil}}$) and the internal damping β_s of the soft soil. The ratio of unit weight ($\frac{\rho_{rock}}{\rho_{soil}}$) ranges from 1.1 to 1.4 at most of the soft clay sites, and the shear-wave velocity of bedrock can be considered approximately constant. The damping ratio is principally dependent on the ground motion intensity at the site due to the nonlinear behavior of the soil and the plasticity index of the clay. Therefore, the amplification factor for a specific soil profile is approximately inversely proportional to the shear-wave velocity of the soft soil profile (Dobry et al., 2000).

Based on this theoretical framework, Borcherdt (1994) empirically concluded that the amplification factor is proportional to the time-averaged shear-wave velocity of the top 30 meters, $V_{s,30}$. The amplification factors were derived empirically by regression curves fitted to the average ratio of Fourier spectra computed in short periods (0.1 - 0.5 sec) and long periods (1 second and longer). This approach has been generally adopted in national seismic building codes to define site classification and determine potential amplification (CEN, 2004; BSSC, 2015; NRC, 2015).

1.2. Site effect in GMPEs

Ground motion prediction equations (GMPEs) are predictive relationships that indicate ground motion intensity (e.g. ground motion intensity) as a function of magnitude M, source-to-site distance R, local soil condition (site effect) S_i, fault mechanism F_i (Equation (1-2)).

$$Y = f(M, R, S_i, F_i) \quad (1\text{-}2)$$

$V_{s,30}$ has been widely used as a proxy for site effects in many GMPEs (Equation (1-3)). By developing empirical regression analysis, site amplification can be used for predicting the ground motion parameters (Boore and Atkinson, 2008; Campbell and Bozorgnia, 2008, 2014). The application of this parameter has been criticized because of its low performance in

reducing the standard deviation associated with GMPEs (Luzi et al., 2011), non-applicability in some regions away from the primary study area (California), and oversimplification of the site effect by considering the stiffness of the surface layers as the sole contributing factor (Castellaro et al., 2008; Gallipoli and Mucciarelli, 2009; Hassani and Atkinson, 2016; Braganza and Atkinson, 2017; Pitilakis et al., 2018).

Luzi et al. (2011) suggested and examined the performance of another site effect proxis known as fundamental site period (T_0), the period in which the first or maximum peak amplification occurs. They introduced T_0 as a complementary parameter to $V_{s,30}$ and showed that the standard deviation of residuals in the GMPE model decreased when both $V_{s,30}$ and T_0 were considered. To date, T_0 has been primarily applied in ground motion attenuation relations and site classifications developed for Japan (Yamazaki and Molas, 1995; Zhao et al., 2006). Yamazaki and Molas (1995) and Zhao et al. (Zhao et al., 2006) proposed a site classification scheme based on the soil natural period including four site classes approximately corresponding to the stiffness of the site profile. One of the advantages of this site classification is to demonstrate the relationship between the site period and site stiffness $V_{s,30}$. The seismic site parameters are commuted using the following Equations and the approximate relations are presented in Table 1-1.

$$V_{S,30} = \frac{30}{\left(\sum_{i=1}^{n}\left(\frac{h_i}{V_{s_i}}\right)+\frac{(30-\sum_{i=1}^{n} h_i)}{V_{s_{rock}}}\right)}, \tag{1-3}$$

$$V_{S,avg} = \frac{\mathrm{H}}{\left(\sum_{i=1}^{n}\left(\frac{h_i}{V_{s_i}}\right)\right)}, \tag{1-4}$$

$$T_0 = \frac{4H}{V_{S,avg}}, \tag{1-5}$$

where, h_i and V_{s_i} are the thickness and the interval shear-wave velocity of each layer *i*, respectively. *H* is the total soil thickness and the bedrock shear-wave velocity, $V_{s,rock}$, is included for deposit thickness lower than 30 m.

Table 1-1. Site classification based on fundamental site periods and corresponding $V_{s,30}$ site classes (Zhao et al., 2006)

Site class	Description	Natural period	$V_{s,30}$ Calculated from site period (m/s)
Hard rock			$V_{s,30} > 1100$
SC I	Rock	T < 0.2 sec	$V_{s,30} > 600$
SC II	Hard soil	$0.2 \leq T < 0.4\ sec$	$300 < V_{s,30} \leq 600$
SC III	Medium soil	$0.4 \leq T < 0.6\ sec$	$200 < V_{s,30} \leq 300$
SC IV	Soft soil	$T \geq 0.6\ sec$	$V_{s,30} \leq 200$

Luzi et al. (2011) proposed soil fundamental frequency as an alternative or complementary to $V_{s,30}$ for site classification, which resulted in a reduction of the standard deviation associated with GMPEs. Theoretically, the highest amplification occurs at the fundamental frequency and is proportional to the impedance ratio. Although they suggested that $V_{s,avg}$ can be a better proxy of the amplification value in comparison with $V_{s,30}$, the lack of information on depth to bedrock contended $V_{s,30}$ as a proxy of the soil amplification value. The authors concluded that the fundamental frequency can be determined by cost-effective measurements as well as ambient noise measurements or earthquake records; the site classification scheme can solely rely on this parameter.

1.3. Seismic code-oriented site classification

Several standard site classification methods are largely used in seismic engineering. Normally, a standard site classification scheme considers hard rock, moderately fractured and weathered rock, stiff and dense soil, loose sandy soil, and soft clayey soil. To differentiate among the different site classes for the construction of new buildings and other structures, building codes such as the current NBCC (NRC, 2015) and Eurocode 8 (CEN, 2004), rely mainly on $V_{S,30}$ and $V_{S,avg}$ values, and also include the standard penetration resistance (*SPT-N*) and the soil undrained shear strength (S_u). Other classification schemes utilize the fundamental site period T_0 (Zhao et al., 2006), or a combination of the soil thickness and

stiffness properties based on $V_{S,avg}$, $V_{S,30}$, T_0 and the thickness of the soil deposit, referred to the hybrid classification method (Pitilakis et al., 2018).

The NBCC seismic provisions, a modified version of NEHRP (Building Seismic Safety Council, 2009), recognize five site categories ranging from A (hard rock) to E (soft soil; Table 1-2). They are defined mainly through correlation with $V_{S,30}$, 30 m being the typical depth of geotechnical site investigations. An additional site class F (special soil) requiring site-specific geotechnical investigations includes liquefiable soils, sensitive or highly organic clays >3 m in thickness, or plastic clays >8 m thick. A similar approach for soil classification is suggested by Eurocode 8, since it is based on the same site parameters as NBCC. Eurocode 8 also contains five site classes from A through E though, with different $V_{S,30}$ ranges (Table 1-2). There is only one bedrock category, site class A, whereas site class E applies to soft soils with $V_{S,avg} < 360$ m/s and thickness $5 < H < 20$m overlying bedrock formations. Corresponding to the soil class F in NBCC, two soil types are defined, S1 and S2, for which site-specific studies have to be conducted.

Table 1-2. Standard site classifications schemes according to the NBCC and Eurocode 8

Code	Site class and $V_{S,30}$ (m/s)				
	A	B	C	D	E
NBCC (NEHRP)	>1500(*)	760–1500(*)	360–760	180–360	<180
Eurocode 8	>800(**)	360–800	180–360	<180	(***)

*Soft soil must be <3 m in thickness
**Surface weak materials must be <5 m
***$V_{S,avg}$<360 m/s and thickness 5<H<20 m

1.4. Seismic microzonation for hazard analysis

A standard site classification scheme considers site classes including hard rock, moderately fractured and weathered rock, stiff and dense unconsolidated soil, loose sandy soil, and soft clayey soil, each with its own range of $V_{s,30}, V_{s,avg}$ and T_0. Such classification provides a straightforward basis for mapping local site conditions in seismic microzonation studies (Bard and Riepl-Thomas, 1999). The results of seismic microzonation studies are usually presented on maps identifying and characterizing zones with seismically homogeneous behavior, e.g. zones susceptible to local seismic amplification or zones prone to instability, such as soil and rock sliding (Shano et al. 2020) and liquefaction (e.g. Huang et al., 2019). National and international guidelines propose a multistep approach to conduct seismic microzonation studies (e.g. TC4-ISSMGE, 1999; SM Working Group, 2015). The seismic microzonation at grades I and II addresses qualitative and semiquantitative evaluations of site classes and associated amplification. Here, surface and subsurface data are acquired from field tests and existing geological, geotechnical and geophysical maps as a basis to infer potential site amplification (Molnar et al., 2020). The grade III seismic microzonation complements results from grades I and II with detailed seismic site response analyses in terms of amplification of the ground motion using 1D and 2D numerical analyses (Licata et al., 2019).

Seismic microzonation and site categorization in Eastern Canada due to the characteristic geology of overlying soft postglacial sediments on hard crystalline bedrock cannot be compatible with regions where the soil mechanical properties of deposits increase

gradually and steadily with depth (Braganza and Atkinson, 2017). In Eastern Canada, geological modelling of subsurface layers plays a significant role in the determination of shear-wave velocity and thus site categorization. A number of seismic hazard studies have been carried out recently in southern Ontario and Quebec, and selected results are summarized in Table 1-3. Motazedian et al. (2011) identified three main geological layers for the city of Ottawa on the basis of their distinct shear-wave velocities, namely, postglacial, firm glacial and bedrock. The shear-wave velocity of the postglacial deposits, which are the surficial sediments in this region, presents gradually increasing values with depth, described as a representative V_s-depth profile (average and standard deviation defined by a regression model). Rosset et al. (2015) developed three different $\bar{V}_{s,30}$ models for Montreal using predictive equations for the V_s-depth profile: (1) a single-layer model based on the total thickness of soft soils, (2) a four-layer model based on geological and geotechnical information from borehole data, and (3) a composite model comprising all of the characteristics of the former two models. Nastev et al. (2016) in the Ottawa and St. Lawrence valleys implemented a similar approach to map the shear-wave velocity and the site fundamental period (T_0).

Due to the high variability of the V_s measurements and thickness of soil layers, the estimated value of $\bar{V}_{s,30}$ includes considerable uncertainty, which challenges the reliability of the averaging process. For example, considering $V_{s_{rock}}$ to be 2500 m/s causes a huge difference in $\overline{V_{s,30}}$ along with a site column where the total thickness of the soil layer range is less than 30 meters.

Table 1-3. Shear-wave velocity of major Quaternary deposits and bedrock outcrops of the Eastern Canada region

Authors	Location	Geological unit	Average shear-wave velocity of measurements (m/s)	Velocity-depth regression relationship	Remarks
Motazedian et al. (Motazedian et al., 2011)	City of Ottawa	postglacial sediments	~ 150	Vs = 123.86 + 0.88Z ± 20.3 m/s	For 10 < Z < 100 m
		firm glacial sediments	580 ± 174	-	Till
		Bedrock	2783 ± 504	-	Pre-Cambrian Migmatic and Metasedimentary
Rosset et al 2015	Montreal	Backfill and peat	~ 155	-	-
		Sand deposits	100 to 500	$V_s = 144.8 + 36.8\,Z^{0.57} \pm 54\ m/s$	-
		Leda clay	80 to 320	$V_s = 121.2 + 40.8\,Z^{0.43} \pm 43\ m/s$	Sensitive marine clay
		Till	565 ± 261	-	-
		Bedrock	2300 ± 590	-	Limestone and Shale
Nastev et al 2016a-b	Ottawa and St. Lawrence Valleys	Postglacial deposits (sand)	165 ± 49 (geometric mean: 158 m/s)	$V_s = 103.1 + 31.1\,Z^{0.5} \pm 52\ m/s$	Fluvial, aeolian, glaciofluvial, glaciolacustrine and deltaic sandy deposits
		Postglacial deposits (clay)	143 ± 46 (geometric mean: 137 m/s)	$V_s = 97.0 + 10.9\,Z^{0.5} \pm 41.6\ m/s$	Marin and glaciolacustrine clay, highly sensitive clay in some cases accompanied by organic sediments
		Till and sub-till sediments	400 ± 152 (geometric mean: 385 m/s)	-	-
		Bedrock	2500 ± 700	-	Precambrian and intrusive rocks
Foulon et al 2018	Saguenay Region	Sandy soils	80 to 260	$V_s = 40.9 + 53.7\,Z^{0.5} \pm 29.8\ m/s$	Postglacial deposits
		Clays	80 to 250	$V_s = 79.3 + 17.3\,Z^{0.5} \pm 45.3\ m/s$	Glaciomarine clay

1.5. Shear-wave velocity determination: Field Tests

Shear-wave velocity (V_s) is a fundamental property of soils, and in geotechnical problems, measuring this parameter provides the most reliable prediction of soil stiffness at small strains, $G_{max} = \rho V_s^2$, where ρ = mass density (Mayne and Rix, 1995; Robertson, 2009). Although V_s can be directly measured through geophysical methods, the relation between

shear-wave velocity and shear modulus facilitates the use of common conventional geotechnical field tests, such as standard penetration tests (SPTs) and cone penetration tests (CPTs), to estimate V_s and other useful geotechnical parameters (Table 1-4). A number of studies have proposed empirical correlations between SPT-N values and cone tip resistance with shear-wave velocity (Mayne and Rix, 1995; Hegazy and Mayne, 2006; Robertson, 2009; Anbazhagan et al., 2012; Hussien and Karray, 2015). Therefore, the selection of the appropriate empirical relationship requires particular attention to the soil type, the study region and the test methods.

Table 1-4. Important geotechnical parameters applied in soil classification

In situ test	Direct Parameter	Interpreted Parameter*
SCPT/CPTu	Cone resistance, q_c	Shear-wave velocity, V_s (CPTu)
	Sleeve friction, fs	Soil unit weight
	Pore Pressure, u	Over consolidation ratio
	Shear-wave velocity, Vs (SCPT)	Undrained shear strength
		Sensitivity
		Effective stress strength parameter
		Small strain shear modulus
		Constrained modulus
		Coefficient of consolidation
		hydraulic conductivity
SPT	SPT-N value	Shear-wave velocity, V_s
		Small strain shear modulus
		Undrained shear strength

* The reliability of interpretations depends on the soil type and the accuracy of the empirical relationships.

The standard penetration test (*SPT*) is one of the oldest methods for subsoil investigation. Due to the simplicity of the equipment and test procedure, it is popular for site response, liquefaction and seismic microzonation studies. Many empirical correlations have been developed initially in Japan between the shear modulus (and shear-wave velocity) and the *SPT-N* values. However, precautions must be followed for using these correlations because of differences in the procedures and equipment (Anbazhagan et al., 2012). A number of well-known empirical relationships for different soil types have been developed across the world (Table 1-5). Almost all of these empirical relationships use power-law equations to describe

the relationship between V_s and N, $V_s = aN^b$ where the constants a and b are determined using regression analysis (Hussien and Karray, 2015). It should be noted that the correction for hammer energy and overburden stress must be considered (Anbazhagan et al., 2012).

Table 1-5. V_s and N-SPT empirical correlations

Author (s)	Correlation (s)	Soil type
Ohta and Goto (1978)	$V_s = 62.14N^{0.22}D^{0.23}$ $V_s = 63.94N^{0.22}D^{0.23}$ $V_s = 71.52N^{0.22}D^{0.23}$ $V_s = 92.28N^{0.22}D^{0.23}$	Clay Medium sand Gravelly sand Gravel
Imai and Tonouchi (1982)	$V_s = 97N^{0.31}$	Sand – Alluvial sand
Seed et al. (1983)	$V_s = 56.4\ N^{0.50}$	Sand
Pitilakis et al. (1992)	$V_s = 162\ N^{0.17}$	Sand
Pitilakis et al. (1999)	$V_s = 145\ N_{60}^{0.178}$	General
Brandenberg et al. (2010)	$V_s = 57.11\ N_{60}^{0.096}\acute{\sigma}_{v0}^{0.236}$ $V_s = 43.81\ N_{60}^{0.178}\acute{\sigma}_{v0}^{0.231}$ $V_s = 54.05\ N_{60}^{0.230}\acute{\sigma}_{v0}^{0.164}$	Sand Silt Clay
Kishida and Tsai (2017)	$V_s = 62.8\ N_{60}^{0.172}\acute{\sigma}_{v0}^{0.167}$	Sand and silt

D, depth in m; V_s in m/s. $\acute{\sigma}_{v0}$, vertical effective stress in kPa. N_{60}, corrected *N*-values for hammer energy, rod length, and sampler inside diameter.

The CPT is the other useful and most common in situ test to determine the stiffness parameter of the subsoil, since it is fast, repeatable and economical. In addition, it provides near-continuous data and has a strong theoretical background (Robertson, 2009). This test can be incorporated in a seismic module that directly measures V_s. Numerous studies have evaluated the correlation between V_s and CPT data. The resulting correlations, based on the soil type, can be divided into three categories of cohesive, cohesionless soils and general correlations for undifferentiated types of soil (Cubrinovski et al., 2015). Some of the most cited correlations are presented in Table 1-6.

Table 1-6. Review of existing CPTu-V_s correlations

Author (s)	Correlation	Comment
Robertson (2009)	$V_s = \left[10^{0.55I_c+1.68}\left(\frac{q_t - \sigma_{v0}}{p_a}\right)\right]^{0.5}$ R^2 = n/a, N = 1035	General soil type, worldwide
Mayne and Rix (1995)	$V_s = 1.75q_c^{0.627}$, [R^2 = 0.74], N = 481	Clays, worldwide
Madiai and Simoni (2004)	$V_s = 155q_c^{0.29}f_s^{-0.10}$, [$R^2$ = 0.91], N: n/a (q_c and f_s are in MPa)	Holocene and Pleistocene fine-grained soils, Italy
	$V_s = 224q_c^{0.26}f_s^{-0.01}$, [$R^2$ = 0.81], N: n/a (q_c and f_s are in MPa)	Holocene and Pleistocene coarse-grained soils, Italy
Hegazy and Mayne (2006)	$V_s = 0.0831Q_{tn}e^{1.786I_c}\left(\frac{\acute{\sigma}_0}{p_a}\right)^{0.25}$ [R^2 = 0.85], N = 558	General soil type with $1.0 \leq I_c \leq 4.8$
Andrus et al. (2007)	$V_s = 2.27q_t^{0.412}I_c^{0.989}Z^{0.033}$ [R^2 = 0.78], N = 72	Holocene soils $1.19 \leq I_c \leq 4.0$, USA and Japan
	$V_s = 2.934q_t^{0.395}I_c^{0.912}Z^{0.124}$ [R^2 = 0.43], N = 113	Pleistocene soils $1.16 \leq I_c \leq 3.25$ USA and Japan
Long and Donohue (2010)	$V_s = 1.961q_t^{0.579}(1 + B_q)^{1.202}$ [R^2 = 0.77], N: n/a	Norwegian marine clay
Tonni and Simonini (2013)	$V_{s1} = 10^{(0.8I_c-1.17)}Q_{tn}$, [$R^2$ = 0.9], N = n/a	Holocene silt, silty sand and silty clay, Italy
McGann et al. (2015b)	$V_s = 18.4q_c^{0.144}f_s^{0.0832}Z^{0.278}$ [R^2 = 0.86], N = 513	Mainly for Holocene sands
Perret et al. (2016)	$V_s = 39q_t^{0.164}Z^{0.137}$ R^2: n/a, N = 1258	Pleistocene to Holocene, St. Lawrence River Valley sands, Eastern Canada
L'Heureux and Long (2017)	$V_s = 8.35(q_t - \sigma_{v0})^{0.22}\acute{\sigma}_{v0}{}^{0.357}$ [R^2 = 0.75], N = 115	Norwegian marine clay
Karray and Hussien (2017)	$V_{s1} = 43.7Q_{tn}{}^{0.25}/(D_{50})^{0.215}$, R^2 and N: n/a	Holocene worldwide fine-grained soils, $D_{50} < 0.2\ mm$
	$V_{s1} = 71Q_{tn}{}^{0.25}(D_{50})^{0.1}$, R^2 and N: n/a	Holocene worldwide coarse-grained soils, $D_{50} > 0.2\ mm$
Tong et al. (2018)	$V_s = 35.1q_t^{0.118}f_s^{0.102}Z^{0.139}$ [R^2 = 0.87], N:n/a	Silt and sand mixture, Yangtze delta, China

R^2 and *N* represent the coefficient of determination and number of data pairs, respectively.
V_s and V_{s1} are in m/s; q_t, q_c, f_s, σ_{v0} and $\acute{\sigma}_{v0}$ are in kPa; q_{c1} is in MPa; effective mean diameter D_{50} is in mm; p_a = 100 kPa; and Q_{tn}, B_q and I_c are dimensionless values.

Due to the unique environment, during and after the depositional process, using the global regression equations for specific soils of Eastern Canada would result in bias estimations; developing a specific CPTu-V_s correlation for this region will reduce the estimation uncertainty.

The geophysical methods to measure the share-wave velocity rely predominantly on the measurement of the travel time of the mechanical wave propagated through the medium. These surveys may be mainly categorized into two approaches, namely, invasive and non-invasive methods. Non-invasive methods are conducted from the ground surface and are more cost-efficient in comparison to invasive methods. However, they need more sophisticated

inversion analysis, especially for surface wave methods (Asten and Boore, 2006; Garofalo et al., 2016a).

The summarized in situ V_s profiling surveys proposed by Hunter and Crow (2012) for seismic site characterization are as follows:

a) Invasive Methods
    i) Borehole logging
        (1) Suspension Downhole Survey
        (2) Cross Hole surveying (CHT)
    ii) Seismic Cone Penetration Test (SCPT)
b) Non-Invasive Methods
    i) Shear-wave Refraction
    ii) Shear-wave Reflection
    iii) Surface wave dispersion
    iv) Ambient Noise (Microtremor)

The selection of an appropriate method is based on the geological conditions, the relative cost and the aim of the project. It should be mentioned that using microtremors to evaluate the wave velocity sometimes shows inconsistent results with invasive methods (Asten and Boore, 2006); however, this method can effectively evaluate the predominant frequency of a site and has been increasingly applied in various studies (Molnar et al., 2018).

1.6. Geological and geotechnical modelling

A 3D geological model can provide valuable information on the spatial distribution of sediments, soil properties, thickness of the geologic units, etc. As mentioned above, the local geologic characteristics can be used as a proxy for estimating the shear-wave velocity (Holzer et.al., 2005). The accuracy of the approximation may be enhanced by obtaining the correlation between shear-wave velocity, depth and considering also the geologic units (see Table 1-3) or using topographic slopes on a large regional scale (Heath et al., 2020; Thompson et al., 2014; Wald and Allen, 2007). A 3D geological model offers solutions to determine the geometrical

properties, it also provides a basis for the spatial prediction of geotechnical properties and the development of a geotechnical model (Lee et al., 2017).

The term “geotechnical model” takes different meanings of in the literature related to stability analysis (Phoon and Tang, 2019). For practical convenience, the geotechnical model considered herein is valid within the limits of elastoplastic behavior before ultimate failure. In this context, the geotechnical model is created similarly to the 3D geologic model in terms of engineering parameters, i.e., V_s in this case. A 3D geotechnical model helps to determine the seismic site parameters, including the average V_s value of the top 30 m of soil ($V_{s,30}$), the average V_s of all of the soil deposits ($V_{s,avg}$) and the fundamental site period (T_0) or frequency (f_0) (Hallal and Cox, 2021; Rohmer et al., 2020). Traditionally or commonly geomodels are generated deterministically (single user-interpreted solution) provide a deterministic model for the estimation of the shear-wave velocity and the thickness of deposits. However, fewer attempts have been made to consider the influence of soil geological uncertainty on the prediction of geotechnical properties (Zhang et al., 2021). A geostatistical approach is applied to provide quantitative spatial predictions of soil types (probabilistic geological model) prior to the estimation of geotechnical properties and provides an assessment of spatial uncertainty (e.g. Deutsch 2006). Assessment of uncertainty in geological modelling has been well elaborated in the approach of quantifying spatial variability as a source of spatial uncertainty (Chiles and Delfiner, 2009; Pyrcz and Deutsch, 2014).

Geostatistical modelling is applied to construct multiple realizations. For example, sequential indicator simulation (SIS) is a widely used geostatistical technique for modeling categorical variables (Deutsch, 2006). A set of alternative high-resolution models of the spatial distribution of the considered random variable is created during this process. Each equally probable realization reproduces the spatial statistics of the target variable (Deutsch, 2006). The method consists of three steps as follows:

i) Transformation of soil types to *K* indicator variables

$$i(u_\alpha; k) = \begin{cases} 1 & if\ category\ k\ prevails\ at\ location\ u\ , k = 1, \dots, K. \\ 0 & otherwise \end{cases} \quad (1\text{-}6)$$

Indicator transformation facilitates classical statistical analyses to infer representative proportions of the indicator variables;

ii) Determination of indicator variograms to model the spatial continuity of the indicator soil types;

iii) Simulation of the soil types honoring field observation at sampled locations (conditional simulation) in a sequential and reproducible manner.

1.7. Spatial variability

Soil properties vary from one location to another location. This variability is not a random process and involves some spatial dependency, which can be described by statistical tools such as the *autocovariance* and *semivariogram* (El-Ramly et al., 2002). Phoon and Kulhawy (1999) demonstrated that the spatial variation can be decomposed into a trend function t(z) and that a fluctuating component w(z) represents the inherent soil variability and can be modelled as a random field. The trend is evaluated using regression techniques and is usually a function of location (especially depth). The advantage of decomposition is that the residual w(z) may acquire stationary characteristics and can be modelled with a geostatistical approach. A random field is called *stationary* if the mean and variance remain constant at any location and the covariance function only depends on the distance *h*. In other words, knowing the *autocovariance* between known points Z(x) enables us to estimate the unknown value of Z(x+h) in addition to error variance using a regression model such as *kriging* (Chiles and Delfiner, 2009).

Modelling the spatial variation assists in predicting the soil attributes at unsampled locations. In the present study, the spatial variation is determined for continuous (soil thickness) and categorical (soil units) variables. An experimental variogram, $\hat{\gamma}(h)$, is used to statistically determine the average dissimilarity between data separated by vector *h* (Goovaerts, 1999) and is assumed as a measure of spatial variability.

$$\hat{\gamma}(h) = \frac{1}{2\,N(h)} \sum_{\alpha=1}^{N(h)} [z(u_\alpha) - z(u_\alpha + h)]^2, \qquad (1\text{-}7)$$

where $z(u_\alpha)$ and $N(h)$ are the values of the variable of interest at location u_α and the number of data pairs within distance *h* in the respective direction. In practice, the tolerance for distance *h* and its direction is specified. The direction of the separation vectors becomes irrelevant when the directional tolerance increases sufficiently. An omnidirectional variogram is a useful starting tool for structural analysis and provides the prerequisite information for calculating the directional variograms, whilst a directional variogram reveals the anisotropy pattern and the direction of the maximum and minimum spatial continuities (Isaaks and Srivastava, 1989). Equation (1-7) is applied for continuous variables, whilst an indicator variogram is calculated for categorical variables by substituting indicator data $i(u_\alpha; k)$ for K indicators as follows:

$$\hat{\gamma}_I(h;k) = \frac{1}{2\,N(h)} \sum_{\alpha=1}^{N(h)} [i(u_\alpha;k) - i(u_\alpha + h;k)]^2, \; k=1, \ldots, K. \tag{1-8}$$

With the determination of the standard variogram characteristics (i.e., range, sill and nugget effect), a theoretical model that best fits the experimental variogram is selected (e.g. spherical, exponential or Gaussian model).

The usual approach to model kriging uncertainty, the error variance of kriging is used (Isaaks and Srivastava, 1989):

$$\tilde{\sigma}_k^2 = \tilde{C}_{00} + \sum_{i=1}^{n} \sum_{j=1}^{n} w_i w_j \tilde{C}_{ij} - 2 \sum_{i=1}^{n} w_i \tilde{C}_{i0}, \tag{1-9}$$

where $w_i w_j$ represents the kriging weights, $\tilde{C}_{00}$ is the variance of point values, $\tilde{C}_{ij}$ is the covariance between measured samples and $\tilde{C}_{i0}$ is the covariance between measured and unknown values.

1.8. Integrating uncertainties

Geotechnical variability is the consequence of many distinct sources of uncertainties. The three main sources of uncertainty can be classified as *inherent soil variability*, *measurement error* and *transformation uncertainty* (Phoon and Kulhawy, 1999a). The first component corresponds to aleatory uncertainty, and the last two components are known as epistemic uncertainty. If the interest variable (design) is a function of the source variables with

known uncertainties, it is necessary to determine the uncertainty propagated to the interest variable (Phoon et al., 2006). Phoon and Kulhawy (1999b) defined the integrated uncertainty of a design variable (ξ_d) as a function of source uncertainties as follows:

$$\xi_d = T(t + w + e, \varepsilon) \tag{1-10}$$

where *t*, *w*, *e*, and ε are the deterministic trend functions of soil properties, inherent soil variability, measurement error and transformation uncertainty. The propagated uncertainty can be described using the second-moment approach, which provides an analytical approximation for the mean and standard deviation of the design variable as follows:

$$m_{\xi_d} \cong T(t, 0), \tag{1-11}$$

$$SD_{\xi_d}^2 \approx (\frac{\partial T}{\partial w})^2 SD_w^2 + (\frac{\partial T}{\partial e})^2 SD_e^2 + (\frac{\partial T}{\partial \varepsilon})^2 SD_\varepsilon^2, \tag{1-12}$$

where m_{ξ_d} and $SD_{\xi_d}^2$ are the mean and variance of the design variable (ξ_d), respectively; $SD_w{}^2$ is the variance of inherent soil variability; $SD_e{}^2$ is the variance of measurement error; and SD_ε^2 is the variance of transformation uncertainty. It should be noted that the mean of *w*, *e*, and ***ε*** is zero (the condition of unbiased approximation).

In seismic microzonation, Rosset et al. (2015) developed $V_{s,30}$ models to combine all various types of measured data into the appropriate multilayer model. The uncertainty (both epistemic and aleatory) involved in the determination of the design variable ($V_{s,30}$) was computed through the second-moment approach. The resulting uncertainty of $V_{s,30}$ in a four-layer model is defined as follows:

$$\sigma_{V_{s,30}}^2 = \left(\sum_{i=1}^4 \frac{30 Z_i}{V_{si}^2}\, \sigma_{V_{si}}^2 + \frac{30\,(30 - \sum_{i=1}^4 Z_i)}{V_{Srock}^2}\, \sigma_{V_{Srock}}^2\right) (\sum_{i=1}^4 \frac{Z_i}{V_{si}} + \frac{30 - \sum_{i=1}^4 Z_i}{V_{Srock}})^{-2}, \tag{1-13}$$

where $\sigma_{V_{s,30}}^2$, $\sigma_{V_{si}}^2$ and $\sigma_{V_{Srock}}^2$ are the variance of $V_{s,30}$, the variance of V_s of layer i and the variance of $V_{s,rock}$; V_{si} *and* V_{Srock} are the estimated shear-wave velocity of layer i and the bedrock, respectively; and Z_i is the thickness of layer i.

Talukder and Chouinard (2016) proposed a method known as conditional second-moment analysis to provide the $V_{s,30}$ maps and their related uncertainties since the various

types of information involved in producing the seismic microzonation maps and the related data are updating and evolving over time. This method was applied for the seismic microzonation of Montreal Island to produce probabilistic soil amplification factors.

As mentioned above, the uncertainty in shear-wave velocity can be classified as aleatory and epistemic. The aleatory uncertainty may be delineated by modeling the spatial variability. The epistemic uncertainty, which is related to the selected measurement methods, can be determined by multiple measurements at a single controlled location. Moss (2008) indicated the uncertainty of V_s measurement for a variety of commonly used geophysical methods (surface waves, P-S suspension logging, SCPT) by defining the coefficient of variation (COV= standard deviation/mean). He concluded that the COV varies from 1%-3%, 5%-6% and 20%-35% for borehole logging and SCPT, surface wave analysis and geological correlation, respectively. Although the uncertainty of shear-wave velocity measurements differs among geophysical methods, the inherent averaging effect in the determination of $V_{s,30}$ measurement results are similar to the value of $V_{s,30}$ for different methods (Garofalo et al., 2016a, 2016b).

CHAPTRE 2

SEISMIC MICROZONATION OF A REGION WITH COMPLEX SURFICIAL GEOLOGY BASED ON DIFFERENT SITE CLASSIFICATION APPROACHES

Mohammad Salsabili [1], Ali Saeidi [1], Alain Rouleau [1] and Miroslav Nastev [2]

[1]Département des Sciences Appliquées, Université du Québec à Chicoutimi, G7H 2B1 Saguenay, Canada; Mohammad.salsabili1@uqac.ca (M.S.); Alain_Rouleau@uqac.ca (A.R.)

[2]Geological Survey of Canada, G1K 9A9 Quebec City, QC, Canada; miroslav.nastev@canada.ca (M.N.)

Abstract

A seismic microzonation study was conducted to refine the seismic hazard model for the city of Saguenay, Canada. The Quaternary geology underlying Saguenay shows complex glacial and postglacial stratigraphy with a number of buried valleys filled with fluvioglacial and glaciomarine sediments. High impedance contrast between rock formations and surficial sediments is prone to seismic amplification. To evaluate their applicability, advantages and limitations in capturing the geological specificity of the study area, four site classification methods were applied: the current National Building Code of Canada (NBCC) and Eurocode 8, both mainly based on the average shear-wave velocity for the surficial sediments ($V_{S,avg}$) and for the top 30 m ($V_{S,30}$), a method based on the fundamental site period (T_0), and a hybrid method based on the combination of $V_{S,30}$, T_0 and $V_{S,avg}$. The study specifically aimed to evaluate the importance of the site classification parameters on the resulting microzonation maps. $V_{S,30}$ is capable to present the geological and geotechnical site conditions, however, the results may be further improved by considering $V_{s,avg}$ in shallow and T_0 in thick layers of soil sediments as secondary parameters. The T_0 method gives also satisfactory results with T_0 showing a better correlation to $V_{s,30}$ than to $V_{s,avg}$. The versatile hybrid method may be challenging to apply in certain cases with its nine different site categories and parameters.

Keywords: Seismic microzonation, building code, shear-wave velocity, fundamental site period

2.1. Introduction

An important aspect of geotechnical earthquake engineering is related to the evaluation of the expected intensity and the dominant period of the seismic ground motion at a given location. Knowledge of the geological and geotechnical properties of the surficial sediments is important in this respect since they tend to modify the amplitude and frequency content of the incoming seismic waves, a phenomenon known as the site effect (Seed et al., 1976). Significant damage to the built environment during the 1985 M8.0 Mexico City and 1989 M6.9 Loma Prieta earthquakes was attributed to the site effect (Borcherdt, 1994). To improve its understanding, Borcherdt (1994) proposed a simplified empirical procedure for delineation of local site categories and associated amplification factors in terms of the time-averaged shear-wave velocity of the top 30 meters, $V_{s,30}$. Ever since, $V_{s,30}$ has been adopted by building codes (e.g. BSSC, 2015) to determine the seismic lateral forces generated by the ground motion.

The capacity of $V_{S,30}$ as an efficient predictor of the local site amplification has also been criticized by several authors (e.g. Castellaro et al., 2008; Luzi et al., 2011; Braganza and Atkinson, 2017; Pitilakis et al., 2018). It can particularly be questioned in regions such as Eastern Canada, which are characterised with significant impedance contrasts, where thick surficial sediments with relatively low $V_{S,avg}$ overly stiff bedrock (Braganza et al., 2016; Braganza and Atkinson, 2017). Under such conditions, the impedance contrast contributes to shorten the incoming shear-wave wavelengths and increasing their amplitudes (Hunter and Crow, 2012). The amplification can further be increased when the shear-waves become trapped in low-velocity valleys filled with fluvioglacial and glaciomarine sediments contributing to a resonance effect at the fundamental period (T_0) until their energy is dissipated (Kramer, 1996; Hunter and Crow, 2012).

A standard site classification scheme considers site classes including hard rock, moderately fractured and weathered rock, stiff and dense unconsolidated soil, loose sandy soil, and soft clayey soil, each with its own range of $V_{s,30}, V_{s,avg}$ and T_0. Such classification provides a straightforward basis for mapping local site conditions in seismic microzonation studies (Bard

and Riepl-Thomas, 1999). The results of the seismic microzonation studies are usually presented on maps identifying and characterising zones with seismically homogeneous behaviour, e.g. zones susceptible to local seismic amplification or zones prone to instability, such as soil and rock sliding (Shano et al. 2020) and liquefaction (e.g. Huang et al., 2019). National and international guidelines propose a multi-step approach to conduct a seismic microzonation study (e.g. TC4-ISSMGE, 1999; SM Working Group, 2015). The seismic microzonation at grades I and II is dealing with qualitative and semi-quantitative evaluation of site classes and associated amplification. Here, surface and subsurface data are acquired from field tests and existing geological, geotechnical and geophysical maps as a basis to infer potential site amplification (Molnar et al., 2020). The grade III seismic microzonation complements results from grades I and II with detailed seismic site response analyses in terms of amplification of the ground motion using 1D and 2D numerical analyses (Licata et al., 2019). Within this framework, the seismic site classification based on building code provisions can be considered as a grade II seismic microzonation focusing on local amplification of seismic motion.

Some regions in the world, such as Eastern Canada, are characterized by significant impedance contrasts between the rock and soil deposits, and also show heterogeneous surficial geology units with variable thickness and stiffness properties (Braganza and Atkinson, 2017). In this context, the objective of the present study is to refine the seismic hazard model for the city of Saguenay, a region in Eastern Canada characterized by irregular topography (i.e., valleys and hills), with highly heterogeneous surficial geology of variable thickness and stiffness properties as well as with high impedance contrasts between the rock and overlying soils. It is aiming to determine the relative importance of the main site effect parameters, i.e., $V_{s,30}$, $V_{s,avg}$, and T_0, using 3D geological and geotechnical models. The specific objective is to determine the applicability of four site classification methods: the current NBCC (NRC, 2015), Eurocode 8 (CEN, 2004), the fundamental site period T_0 (Zhao et al., 2006) and the approach developed by Pitilakis et al. (2018). First, a review of the four site classification schemes and the geological settings of the study area are presented. Then, seismic microzonation maps are

generated applying each of the methods. The results of the comparative analysis are given at the end.

2.2. Site classification schemes

Several standard site classification methods are largely used in seismic engineering. Normally, a standard site classification scheme considers hard rock, moderately fractured and weathered rock, stiff and dense soil, loose sandy soil, and soft clayey soil. To differentiate among the different site classes for the construction of new buildings and other structures, building codes such as the current NBCC (NRC, 2015) and Eurocode 8 (CEN, 2004), rely mainly on $V_{S,30}$ and $V_{S,avg}$ values, and also include the standard penetration resistance (*SPT-N*) and the soil undrained shear strength (S_u). Other classification schemes utilize the fundamental site period T_0 (Zhao et al., 2006), or a combination of the soil thickness and stiffness properties based on $V_{S,avg}$, $V_{S,30}$, T_0 and the thickness of the soil deposit, referred to the hybrid classification method (Pitilakis et al., 2018).

The NBCC seismic provisions, basically a replica of NEHRP (Building Seismic Safety Council, 2009), recognize five site categories ranging from A (hard rock) to E (soft soil; Table 2-1). They are defined mainly through correlation with $V_{S,30}$, 30 m being the typical depth of geotechnical site investigations. Additional site class F (special soil) requiring site-specific geotechnical investigations includes liquefiable soils, sensitive or highly organic clays >3 m in thickness, or plastic clays >8 m thick.

A similar approach for soil classification is suggested by Eurocode 8, since it is based on the same site parameters as NBCC. Eurocode 8 also contains five site classes from A through E though with different $V_{S,30}$ ranges (Table 2-1). There is only one bedrock category, site class A, whereas site class E applies to soft soils with $V_{S,avg}$ < 360 m/s and thickness 5 < H < 20m overlying bedrock formations. Corresponding to the soil class F in NBCC, two soil types are defined, S1 and S2, for which site-specific studies have to be conducted.

Table 2-1. Standard site classifications schemes according to the NBCC and Eurocode 8

Code	Site class and $V_{S,30}$ (m/s)				
	A	B	C	D	E
NBCC (NEHRP)	>1500(*)	760–1500(*)	360–760	180–360	<180
Eurocode 8	>800(**)	360–800	180–360	<180	(***)

*Soft soil must be <3 m in thickness
**Surface weak materials must be <5 m
***$V_{S,avg}$<360 m/s and thickness 5<H<20 m

On the other hand, it has been demonstrated that the fundamental site period (T_0) can be a useful site parameter complementary to $V_{S,30}$, as it decreases the standard deviation of residuals in the modern ground motion prediction equations (e.g. Luzi et al. 2011). The fundamental site period has been applied explicitly in site classification studies in Japan (Molas and Yamazaki, 1995; Zhao et al., 2006). It can be measured in field conditions using the horizontal to the vertical spectral ratio of the ambient noise recordings (Nakamura, 1989). The site classification scheme proposed by Zhao et al. (2006) contains four site classes starting from short (SC I) to long periods (SC IV). They correspond approximately to the stiffness of the soil columns defined in NBCC and NEHRP (Table 2-2). It should be mentioned that the hard rock sites are rock outcrops where the assessment of T_0 is meaningless. SC I represents shallow deposit conditions with a resonance period <0.2 s and the site effect is similar to rock site.

Table 2-2. Site classification based on fundamental site period and corresponding NEHRP site classes (after Zhao et al. 2006)

Site class	Description	Site period	NEHRP site class
Hard rock			A
SC I	Rock	$T_0 < 0.2$ sec	A+B
SC II	Hard soil	$0.2 \leq T_0 < 0.4\ sec$	C
SC III	Medium soil	$0.4 \leq T_0 < 0.6\ sec$	D
SC IV	Soft soil	$T_0 \geq 0.6\ sec$	E+F

Likewise, as a part of the revision process of Eurocode 8, Pitilakis et al. (2018) proposed a novel, probably the most sophisticated classification scheme, as a combination of all main classification parameters: T_0, $V_{S,30}$, $V_{S,avg}$ and H (Table 2-3). The classification scheme comprises six main soil classes: from A referring to rock or near rock outcrop site conditions, to X associated to special soil profiles requiring site-specific investigations. Based on the definitions, the site classes A and E are similar to the classes A and E of Eurocode 8. The difference is in the introduction of sub-classes to the general soil categories B and C, which allows for more granular analyses of the site effect in the otherwise broad representations of different soil conditions.

Table 2-3. Site classifications scheme according to Pitilakis et al. (2018)

Site class	T_0	V_S (m/s)	Thickness	Description
A	≤0.2s	V_{S30} or $V_{s,avg}$ ≥ 800	Surface weathered layer H<5 m	Seismic bedrock
B_1	0.1-0.3s	$V_{s,avg}$: 350-600 $V_{S,30}$: 400-760	H<30 m	Very dense sand and/or stiff clay
B_2	0.3-0.6s	$V_{S,avg}$: 400-550 $V_{S,30}$: 350-500	30 m < H < 120 m	
C_1	0.6-1.0s	$V_{S,avg}$: 400-600 $V_{S,30}$: 350-450	H > 60 m	Medium dense sand and/or stiff clay
C_2	0.3-0.7s	$V_{S,avg}$: 250-450 V_{S30}: 250-400	20 m < H < 60 m	
C_3	0.7-1.4s	$V_{S,avg}$: 300-500 $V_{S,30}$: 200-350	H > 60 m	
D	≤1.4s	$V_{S,avg}$: 200-400 $V_{S,30}$: 150-300		Soft soil
E	0.1-0.5s	$V_{S,avg}$: 160-300	$5\text{ m} < H < 20\text{ m}$	Soft soils overlaying rock (or site class A)
X	Special soils requiring site-specific evaluations ($V_{S,avg} < 160\ m/s$)			

2.3. Materials and Methods

2.3.1. Geology of the study area

The presence of heterogeneous soil deposits including a soft clay layer with an important thickness and the proximity of the most active seismic zone in Eastern Canada, the Charlevoix seismic zone, prompted the selection of the city of Saguenay as a study area. Saguenay is the main urban center within the Saguenay-Lac-Saint-Jean region and covers an area of 1136 km² with a population of 147,100. It lies in the southern portion of the E-W trending Saguenay graben and is characterized by irregular topography (i.e., valleys and hills). The seismic activity of this region was reassessed following the 1988 M6.0 Saguenay earthquake. This intraplate earthquake, with a mid-crustal depth of 29 km and a moderate magnitude, occurred 35 km south of downtown Saguenay (Du Berger et al., 1991). The effects of the earthquake including soil liquefaction, rock falls, and landslides were observed as far as 200 km from the epicenter (Lamontagne, 2002; Wang, 2020).

The bedrock of this region is part of the Grenville province of the Canadian Shield and is mainly composed of crystalline Precambrian rocks (Davidson, 1998). It is generally covered by recent glacial and postglacial sediments. The different stratigraphic units can be grouped into five broad categories (from bottom to surface): 1) till, 2) glaciofluvial gravel and sand, 3) fine glaciomarine sediments (clay and silt), 4) coarse glaciomarine (sand and gravel), and 5) loose postglacial deposits consisting of alluvium, floodplain sediments, organic sediments, and landslide deposits. The regional surficial geology, the total thickness of unconsolidated sediments, and the areas covered by the various units are presented in Figure 2-1 and Table 2-4.

The glacial till at the base of the stratigraphic column is compact, semi-consolidated, and is considered continuous in the lowlands. There, the till thickness varies from a few meters to more than 10 m in certain locations. In the highlands, the till veneer is discontinuous and alternated with frequent rock outcrops (Foulon et al., 2018). The most widespread and thickest

deposits in the region are the fine postglacial sediments composed of silty clays. Bouchard and Tavenas (1983) proposed a pre-consolidation hypothesis for these clays due to the partial erosion following their deposition. These deposits are generally up to 10 m in thickness but can attain more than 100 m in certain areas in the lowlands. The remaining sedimentary units at the surface are considerably less frequent and are confined to sporadic areas in the lowlands.

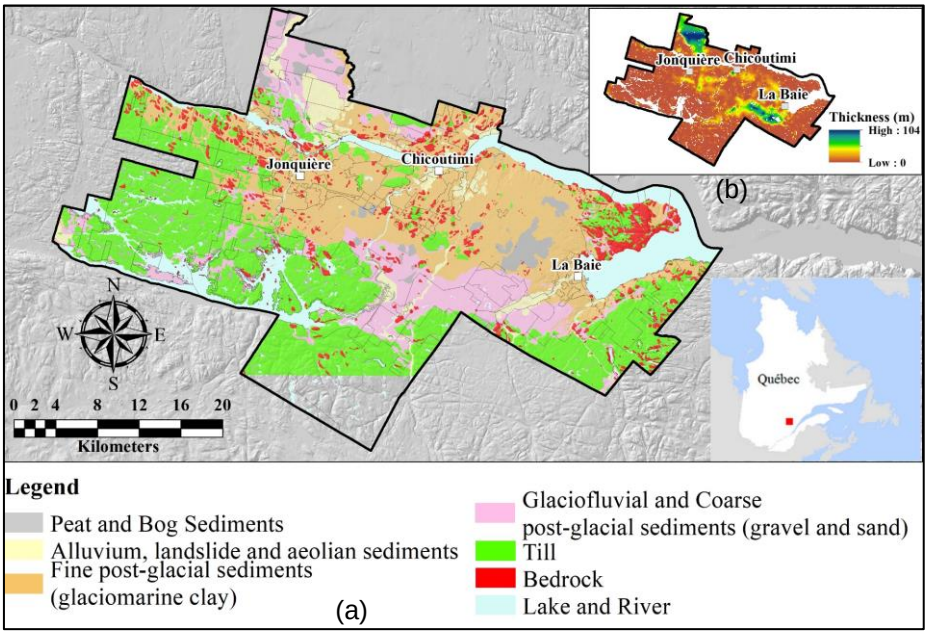

Figure 2-1. Study area; (a) simplified surface geology (modified from Daigneault et al. 2011); (b) thickness of surficial deposits (CERM-PACES, 2013). © Mohammad Salsabili, 2022

Table 2-4. Major Quaternary units and respective coverage of the study area

Geological unit	Area (km^2)	Area (%)
Alluvium	30	2.8
Eolian sediments	2	0.2
Landslide deposits	28	2.6
Peat and bog sediments	41	3.8
Coarse post-glacial sediments (sand and gravel)	149	13.9
Fine post-glacial sediments (glaciomarine clay)	317	29.6
Glaciofluvial sediments (gravel and sand)	16	1.5
Till	407	38.0
Bedrock	81	7.6
Total	1071	100.0

2.3.2. Mapping of $V_{S,30}$, $V_{S,avg}$ and T_0

As discussed above, the main parameters for seismic site classification are $V_{S,30}$, $V_{S,avg}$ and T_0. A 3D model of surficial geology was generated to provide valuable information on the spatial distribution of the soil units, their thickness and certain soil properties (Foulon et al. 2018). The local geologic characteristics can be used as a proxy for estimating the shear-wave velocity (Holzer et.al., 2005). The accuracy of the approximation may be enhanced by obtaining the correlation between shear-wave velocity and depth based on each soil type (e.g. clay, sand etc.). A 3D model provides valuable information on critical factors such as the spatial distribution of sediments, the soil properties, the thickness of the geologic units, and others. This information contributes to generating an enhanced approximation of the shear-wave velocity especially for the region with sparse measured V_s data. Leapfrog Geo (ARANZ Geo Limited 2014) software was used herein to model the 3D stratigraphy (Figure 2-2). This software uses an implicit modelling method by applying polylines (segments that define the sedimentary interfaces) and polygons representing the interfaces interpolated from the polylines. The spatial and vertical heterogeneity of the surficial sediments was modelled with five soil units based on the existing Quaternary geology maps and subsurface data interpreted from 3,342 borehole logs (Lasalle and Tremblay, 1978; Daigneault et al., 2011; CERM-PACES, 2013).

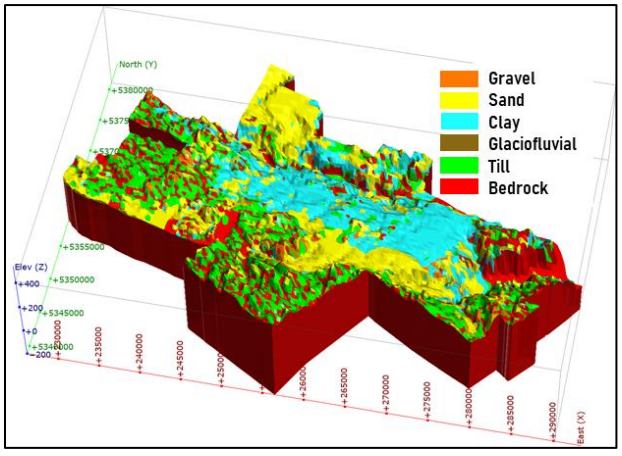

Figure 2-2. 3D geological model of the study area (modified from Foulon et al. 2018). © Mohammad Salsabili, 2022

The adequacy of having V_S measurements from geophysical or geotechnical tests is hardly achievable for all parts of the region. By developing a *V*s-depth profile for the study area (Table 2-5), the shear-wave velocity variation with depth of the soil column was determined. Hence, at a location with no direct *V*S measurement, an approximate V_s-value is assigned based on the V_s-depth profile. Such correlations will be combined with the 3D geological model to determine the variation of V_s for each site column through the region.

To obtain representative interval V_s and V_s-depth profiles, results of 64 standard penetration tests (SPTs) and 122 cone penetration tests (CPTs) for the Saguenay region were acquired from the Quebec Ministry of Transport (Figure 2-3a). The SPT data were converted to V_s applying the empirical relationship of Ohta and Goto (1978) for medium sandy soils since the medium-sized sand is prevailing in the study area (Dion, 1986). Meanwhile, the CPT data associated with clay deposits were converted using the empirical relationship of Mayne and Rix (1995) consistent with glaciomarine clay deposits. Due to the lack of V_s measurements in till deposits and bedrock, regional V_s estimates valid within the larger Ottawa - St. Lawrence region were applied herein (Nastev et al., 2016). The ranges of retained shear-wave velocities and standard deviations for selected Quaternary deposits are given in Table 2-5.

Table 2-5. Representative shear-wave velocity of bedrock and surficial sediments (after Nastev et al., 2016 and Foulon et al., 2018)

Location	Geological unit	Average shear-wave velocity of measurements (m/s)	Velocity-depth relationship	Remarks
Saguenay region	Sandy soils	80 ~ 260	$V_s = 40.9 + 53.7\ Z^{0.5} \pm 29.8$ m/s	Postglacial deposits
	Clayey soils	80 ~ 250	$V_s = 79.3 + 17.3\ Z^{0.5} \pm 45.3$ m/s	Glaciomarine clay
Ottawa and St. Lawrence Valley	Till	400 ± 152	-	Glacial deposits
	Bedrock	2500 ± 700	-	Precambrian rocks

The mapping of $V_{S,30}$, $V_{S,avg}$ and T_0 was performed using the 3D geological model and the representative *Vs*-depth functions (Figure 2-3b, c and d). Appropriate V_s was assigned to each unit based on the depth and the soil type. Then, the averaged values were calculated on a 2D raster with a cell size of 250×250 m. The $V_{S,30}$ and $V_{S,avg}$ values for each cell were calculated using the following equations,

$$V_{S,30} = \frac{30}{\left(\sum_{i=1}^{n}(\frac{h_i}{V_{s_i}})+\frac{(30-\sum_{i=1}^{n} h_i)}{V_{s_{rock}}}\right)}, \quad (2\text{-}1)$$

$$V_{S,avg} = \frac{\mathrm{H}}{\left(\sum_{i=1}^{n}(\frac{h_i}{V_{s_i}})\right)}, \quad (2\text{-}2)$$

where, h_i and V_{s_i} are the thickness and the interval shear-wave velocity of each layer *i*, respectively. The bedrock shear-wave velocity, $V_{s,rock}$, was included for deposit thickness lower than 30 m. The exception was cells where the soft soil thickness was more than 3m and the $V_{S,30}$ calculated initially was higher than 760 m/s. In this case $V_{S,30}$ was substituted with $V_{S,avg}$ of soils. Alternatively, T_0 and subsequent harmonics were approximately estimated with the theoretical solution for a vertically propagating horizontal shear-wave in elastic homogeneous soils given with the following equation (Kramer, 1996):

$$T_{\mathrm{n}} = \frac{4\times H}{V_{S,avg}\times(1+2n)}, \; for \; n = 0, 1, 2 \ldots, \quad (2\text{-}3)$$

where, H is the total soil thickness and n ≥ 1 indicates higher harmonics.

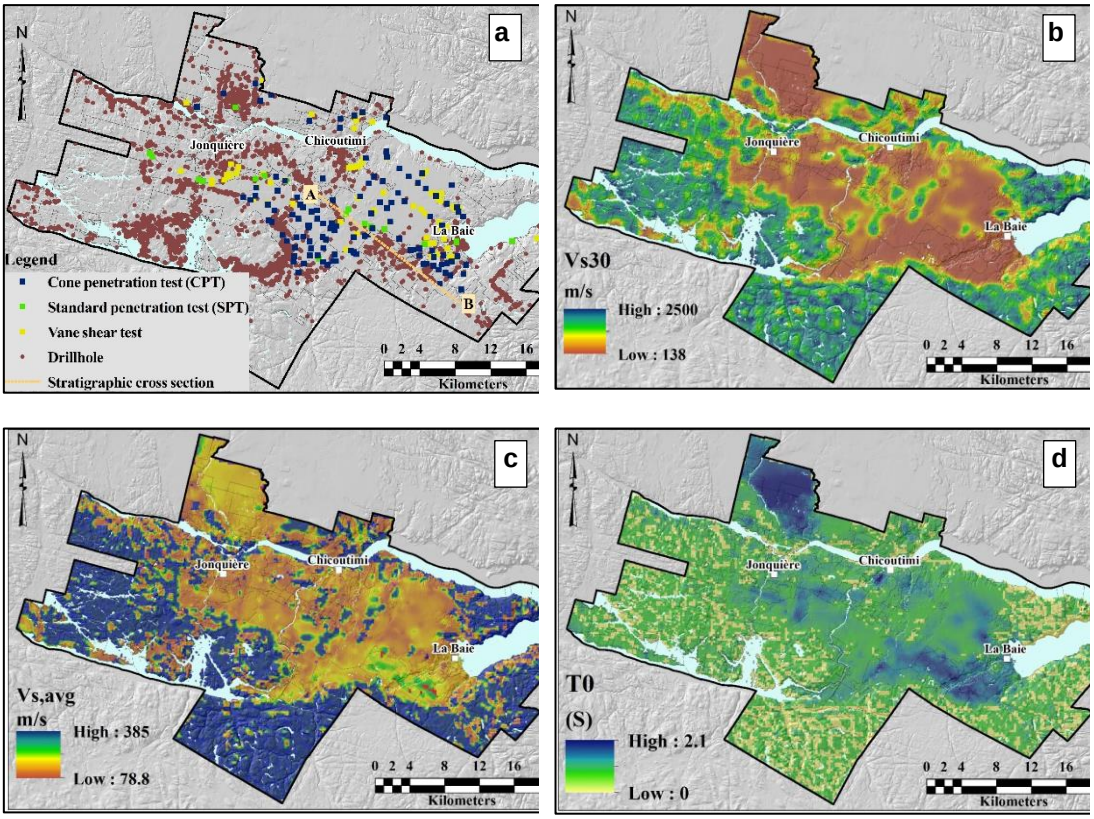

Figure 2-3. Spatial distribution of: (a) geotechnical tests and boreholes, (b) $V_{s,30}$, (c) $V_{s,avg}$ and (d) T_0 . © Mohammad Salsabili, 2022

2.4. Results and Discussion

2.4.1. Site classification results

The regional seismic site classification was conducted based on the NBCC, Eurocode 8, the fundamental site period (Zhao et al., 2006), and the hybrid approach (Pitilakis et al., 2018). The results of the site classifications are given in Figure 2-4. General observations are discussed below for each of the applied site classification methods.

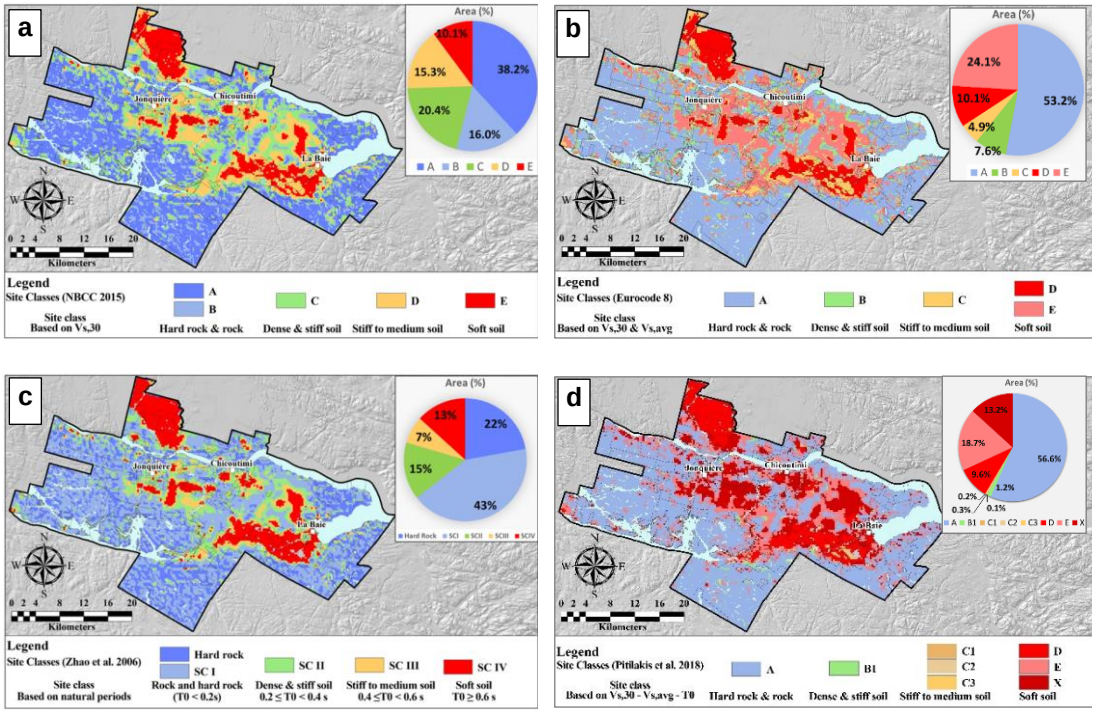

Figure 2-4. Spatial distribution of seismic site classes and relative coverage of the study area based on site classification methods: (a) NBCC, (b) Eurocode 8, (c) fundamental periods of soil (T_0) and (d) hybrid approach. © Mohammad Salsabili, 2022

NBCC (Figure 2-4a): rock site conditions A and B cover 38.2% and 16.0 % of the study area, respectively, which is actually more than 50% of the mapped area. These site classes are found in rock outcrops and areas where bedrock is covered with till veneer or with soft sediments less than 3m thick. There, the ground surface practically replicates the bedrock surface. Site classes C and D share 20.4% and 15.3% of the study area, respectively, whereas only 10.1% of the study area is classified as soft soil, site class E. Due to the predominantly shallow sediments conditions in the region and the addition of the high V_{Srock} in the $V_{S,30}$ assessment, site classification based on NBCC ends up in about 90% of the area being classified as rock and dense stiff soil. To evaluate the effect of averaging the $V_{S,30}$ across geologic units with significantly different V_s, the contribution of the individual units in each site class is calculated from the 3D geological model. The influence of the contributing thicknesses

in terms of percentage can then be considered as representative of the regional impact of a given geologic unit to each site class (Table 2-6).

Table 2-6. Contribution of the different geologic units to the NBCC site classes.

Site class	% of total area	Bedrock	Till	Glaciofluvial sediments	Clay	Sand and gravel	Total
A	38.2%	97.5%	2.5%	0.0%	0.0%	0.0%	100.0%
B	16.0%	86.4%	11.0%	0.0%	1.4%	1.1%	100.0%
C	20.4%	76.3%	7.4%	0.4%	8.4%	7.5%	100.0%
D	15.3%	39.7%	8.6%	3.6%	28.2%	20.0%	100.0%
E	10.1%	2.4%	3.5%	2.2%	69.9%	21.9%	100.0%

It can be observed in Table 2-6 that bedrock is the dominant unit in site classes A to D in absolute or relative terms, with contributions varying from 39.7% for site class D to 97.5% for site class A. Of particular concern is the significant contribution of V_{Srock} in site classes C and D. This occurs in areas with relatively shallow unconsolidated sediments, where clayey soils are the second most important unit. There, the high impedance contrast may lead to seismic amplification considerably higher than otherwise predicted by NBCC. The thick clay sediments are by far the major contributor to the site class E with practically negligible participation of the bedrock, 2.4%.

Eurocode 8 (Figure 2-4b): in this site classification, 53.2 % of the area is delineated as rock, site class A. Similar to the NBCC classification, rock sites cover more than half of the study area comprising bedrock or shallow till outcrops. The spatial coverage of site classes C and B, stiff to very stiff soils, corresponding to NBCC site classes C and D, decreases considerably to 7.6% and 4.9%, respectively. Soft soil, ground type D, covers 10.1% of the study area, whereas 24.1% was delineated as ground type E, which represents less than 20m thick soil column overlying bedrock. Again, the influence of the contributing thickness of each geologic unit was considered in the estimation of V_{s30} and $V_{s,avg}$ (Table 2-7). The contribution of the bedrock thickness is limited practically to site classes A and B only, whereas sands and gravels dominate in the site class C and clayey sediments in the site class D. Based on the

definition of soil type E, the bedrock impacts are excluded in areas with shallow surficial sediments.

Table 2-7. Contribution of the different geologic units to the Eurocode 8 site classes.

Site class	% of total area	Bedrock	Till	Glaciofluvial sediments	Clay	Sand and gravel	Total
A	53.2%	94.5%	4.8%	0.0%	0.4%	0.3%	100.0%
B	7.6%	81.6%	7.4%	0.1%	6.2%	4.7%	100.0%
C	4.9%	14.4%	11.6%	8.4%	22.6%	43.1%	100.0%
D	10.1%	2.4%	3.5%	2.2%	69.9%	21.9%	100.0%
E*	24.1%	-	21.5%	2.4%	51.7%	24.4%	100.0%

* $V_{S,avg}$ estimated

Fundamental site period (Figure 2-4c): the main portion of the region is identified as rock outcrop (22%) and site class *SCI* (43%) with an average vibration period less than 0.1 s (Table 2-8). The site response there will coincide with the seismic energy content at high frequencies. Site class *SCII* covers 15% of the study area and corresponds to relatively softer, $V_{S,avg}$=142 m/s, and shallower soils, H=10.3m. The site classes *SCIII* and *SCIV*, on the other hand, are with similar $V_{s,avg}$, but with significantly higher average thickness confirming that the thickness is more important for the determination of T_0 than $V_{S,avg}$ (the denominator in equation 1). It can also be observed in Table 2-8 that $V_{S,30}$ is inversely proportional and correlates better to T_0 values than the $V_{S,avg}$ values.

Table 2-8. Descriptive statistical parameters of site classes based on fundamental periods

Site class	% of total area	Mean T_0 (s)	Mean $V_{S,avg}$ (m/s)	Mean $V_{S,30}$ (m/s)	Mean thickness (m)
Bedrock	22%	-	-	2500	-
SCI	43%	0.07	274	1304	3.6
SCII	15%	0.29	142	400	10.3
SCIII	7%	0.49	151	245	18.6
SCIV	13%	1.03	176	165	46.3

Hybrid approach (Figure 2-4d): as expected, most of the study area is delineated as rock or near rock outcrop conditions, site class A. Note that the influence of the bedrock is excluded herein due to the application of $V_{s,avg}$ and T_0 in the site classification. The spatial coverage of stiff and dense soils, site classes B_1 and C_1, C_2 and C_3 combined is almost negligible with only about 2% (Table 2-9). For comparison, the corresponding NBCC classes C and D have significantly higher coverage, 35.8%, as a consequence of adding V_{Srock} in the $V_{S,30}$ estimates. Softer soils are considerably more represented: site classes D and E cover 9.6% and 18.7% of the study area, respectively, whereas about 13.2% are classified as special soils which require site-specific evaluation, site class X. Till is the main geological unit in the determination of site classes A and B, sands and gravels are dominant in the site class C, whereas site classes D, E and X consist predominantly of clayey soils.

Table 2-9. Total thickness percentage of geological units contributing to the estimation of site classes based on the hybrid classification approach

Site Class	% of total area	Bedrock	Till	Glaciofluvial sediments	Clay	Sand and gravel	Total
A	56.6%	-	73.31%	0.14%	13.82%	12.73%	100.00%
B1	1.2%	-	99.96%	0.00%	0.00%	0.04%	100.00%
C1	0.1%	-	20.16%	11.87%	0.20%	67.78%	100.00%
C2	0.3%	-	33.99%	2.32%	3.22%	60.47%	100.00%
C3	0.2%	-	14.63%	4.61%	21.45%	59.31%	100.00%
D	9.6%	-	12.37%	7.37%	55.76%	24.51%	100.00%
E	18.7%	-	28.03%	3.07%	31.92%	36.98%	100.00%
X	13.2%	-	10.65%	0.94%	79.37%	9.05%	100.00%

2.4.2. Comparative analysis

The correlations between the site parameters are analyzed in this chapter to better understand the causes for eventual discrepancies.

2.4.2.1. Statistical comparison

The simplified geology of the study area comprises Precambrian bedrock, stiff dense glacial till, and postglacial sandy, soft clayey soils and other soft soils which require site-specific study. Each of these four main geological units and the special soils has its own range of $V_{s,30}, V_{s,avg}$ and T_0, which result in different site categories depending on the applied site classification method. In order to assess the efficiency of the seismic microzonation methods to recognize these geologic conditions, the resulting site classes are compared statistically and differences are quantified in percentages (Figure 2-5).

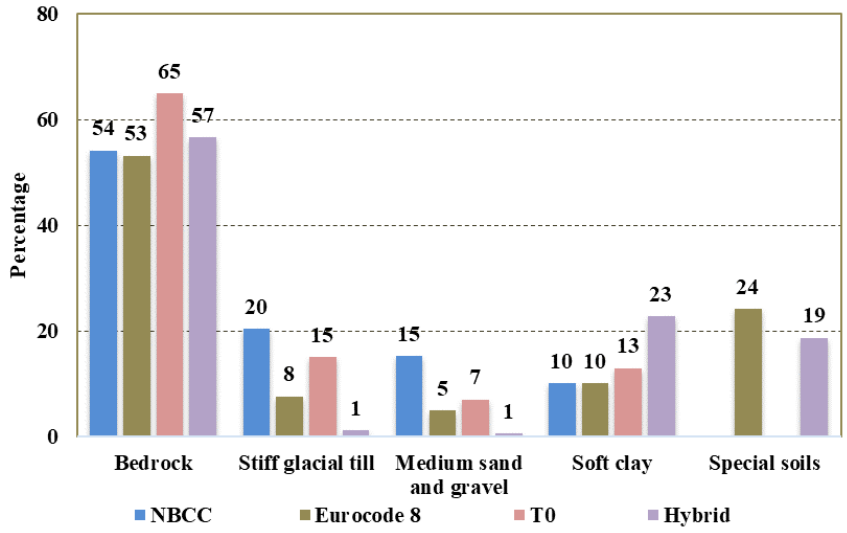

Figure 2-5. Relative surface area coverage by each soil type based on the four site classification schemes: Eurocode 8, NBCC, the fundamental site period and the hybrid method. © Mohammad Salsabili, 2022

Figure 4 shows that all four microzonation methods appear to be in relatively good agreement for bedrock and sites with dominant soft clayey soils. For mainly stiff and soils with medium stiffness, the NBCC and T_0 methods are well correlated with each other. On the other hand, the Eurocode 8 and the hybrid classifications underestimate the stiff and medium soils conditions sorting them either as soft or special soils (site class E). The areas covered with

these soil types produce the main site classification difference between the NBCC and T_0 methods on one side and Eurocode and the hybrid method on the other.

2.4.2.2. Geological cross-section

Another comparison was conducted over a representative 20 km long cross-section taken as an example of the geological setting in the study area together with four typical stratigraphic columns indicated with i through iv in Figure 2-6. As can be observed, the thickness and soil types vary laterally and vertically suggesting different site class evaluations. Thanks to the geological and geotechnical profiles, the similarities and differences of each site classification scheme are better compared:

iv) Medium thickness sediments, 5<H<30m: The site evaluations are different in this stratigraphic column. NBCC and T_0 site classification methods identify rock and stiff soil conditions. On the other hand, for Eurocode 8 and the hybrid method these site conditions are soft soils since they both take into account $V_{S,avg}$ of the surficial sediments instead of $V_{S,30}$ and T_0 by the former two methods.

v) Thick sediments, H>30m: the observed evaluations of site conditions are in fair agreement, soft soils, by all four classification methods.

vi) Thick sediments, H>30m: the $V_{S,30}$ based site classifications, NBCC and Eurocode 8, evaluate this soil column with medium stiffness, whereas T_0 and the hybrid method identify rather soft soil conditions. This is because, in the two former schemes, the soil thickness has more weight in the final results than the stiffness (V_s). A typical example is the differences in site classification of stratigraphic columns ii and iii due to the presence of thick stiff sandy soils.

vii) Shallow sediments, H<5m: this geological setting is probably the least challenging and all site classification methods are in agreement evaluating rock or shallow rock site conditions with a short fundamental period (T_0 <0.2s).

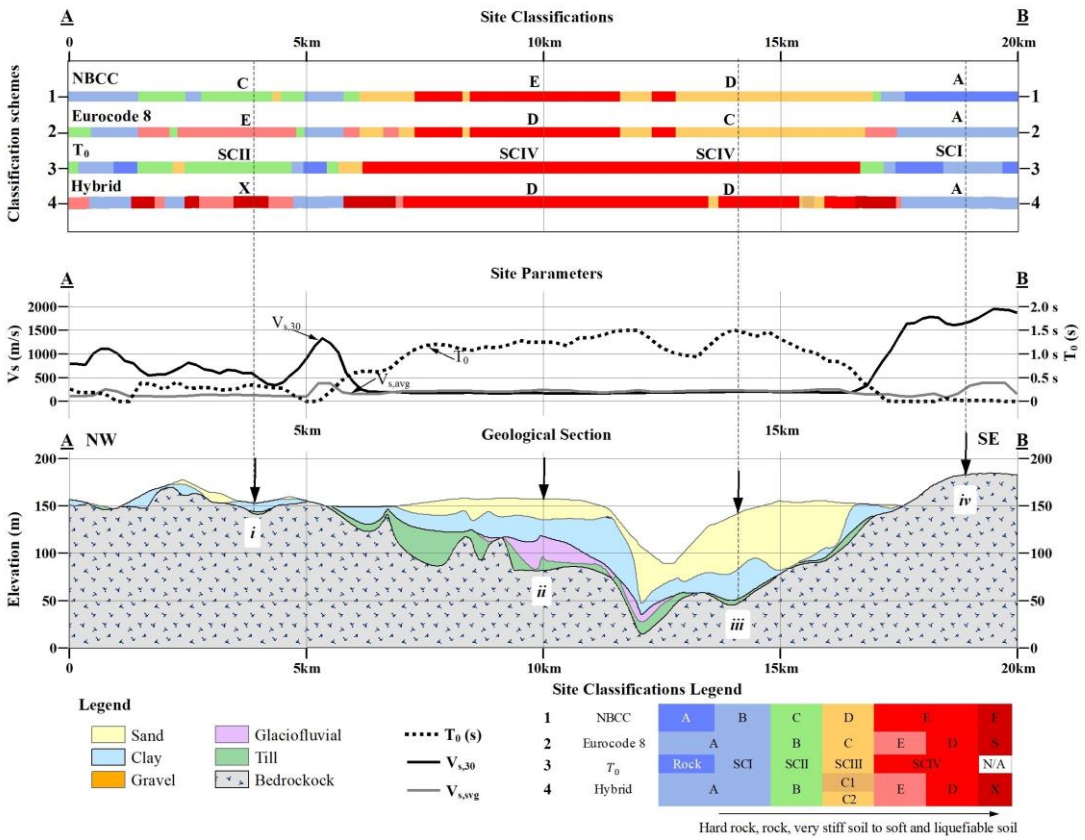

Figure 2-6. Representative cross-section (from below): local geology with the four stratigraphic columns (i through iv), variation of the three main seismic parameters ($V_{s,30}$, T_0, $V_{s,avg}$), and the seismic site classification based on the four different schemes. The location of the cross-section is indicated in Figure 2-3a. © Mohammad Salsabili, 2022

2.4.2.3. Correlations of seismic site parameters

Of particular interest are the mutual relationships between the main site parameters. Understanding the correlations between the site parameters helps identify the similarity and differences in the respective site classification results. It can also help to eliminate well-correlated parameters and retain those that represent best the local site conditions, thus reducing the complexity of the site classification without omitting valuable information. In this respect, regression analyses are conducted between $V_{S,30}$, $V_{S,avg}$ and the fundamental site frequency, f_0=1/T_0 (Figure 2-7). The results reveal a strong correlation, R^2=0.95, between $V_{S,30}$ and f_0 for 9,246 measurement sites (Figure 2-7a). Simple linear regression is applied for

frequencies of up to 12Hz, since data are sparse beyond this limit. To better understand the influence of the $V_{s,rock}$ on the correlation, data for surficial soil with H<30m are represented with yellow dots. At these sites, the $V_{S,30}$ is estimated as a combination of $V_{s,rock}$ and V_s of soils. Elsewhere, $V_{S,30}$ corresponds to deeper soil sediments with H>30m, indicated with black dots (left hand side of Figure 7a). On the other hand, it can be observed in Figure 2-7b that the correlation between $V_{S,avg}$ and f_0 is practically inexistent. This suggests that the addition of $V_{S,rock}$ to the soil V_s in the top 30m actually improves the correlation with f_0. A similar conclusion on the relationship between $V_{S,30}$ and f_0 was obtained in site amplification studies by Ghofrani et al. (2013) and Finn and Ruz (2015). These studies showed a strong $V_{S,30}$ vs. f_0 correlation in shallow soils, which was not necessarily observed in deep soil sediments characterised with low frequencies.

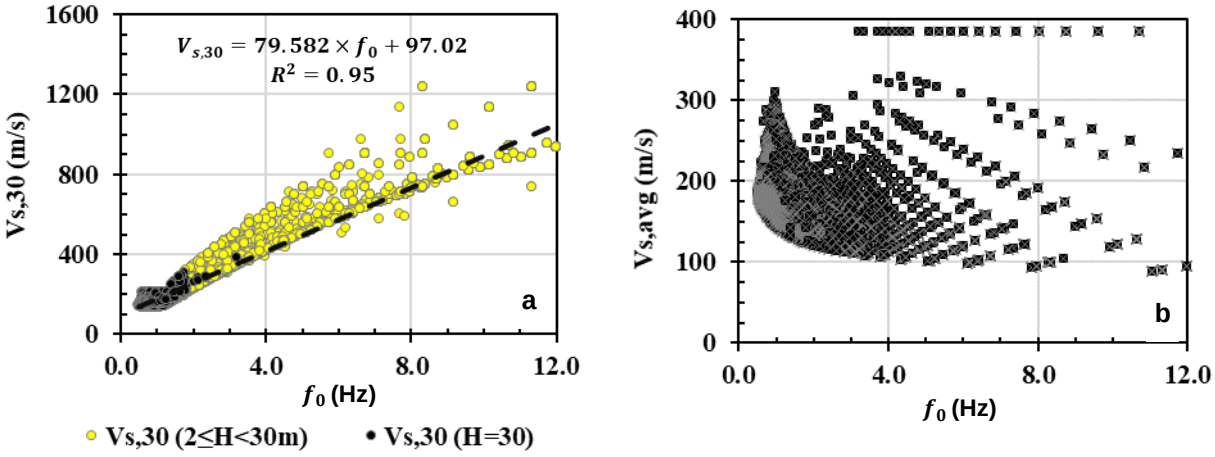

Figure 2-7. Correlation of the fundamental site frequency f_0 with (a) $V_{S,30}$, and (b) $V_{S,avg}$. © Mohammad Salsabili, 2022

2.5. Conclusion

A seismic microzonation study was conducted in the complex geologic environment underlying the city of Saguenay. The main seismic site classification parameters considered in the analyses were: average shear-wave velocity of the top 30 m ($V_{s,30}$), average shear-wave velocity for the total thickness of the surficial sediments ($V_{s,avg}$) and the fundamental site period

(T_0). Four different classification schemes were applied and compared: NBCC, Eurocode 8, fundamental site period and the hybrid approach based on all main site parameters. All of the classification methods have their own advantages and limitations with respect to the local geological and geotechnical conditions. The following are the major conclusions drawn from this study:

- The site classifications based on $V_{S,30}$, NBCC and Eurocode 8, appear the most consistent with the local conditions. The results could be further improved considering secondary parameters, e.g. $V_{S,avg}$ in shallow (H<30 m) and T_0 in deeper soil sediments (H>30 m). In such a case, the impact of the stiffness and thickness of the surficial sediments will be better accounted for.

- Site class E in Eurocode 8 and the hybrid method refers to medium to soft soils, 5<H<20 m, on top of bedrock. In NBCC, the V_S of these soils is combined with V_{Srock} yielding $V_{S,30}$ considerably higher than V_S. Since such site conditions cover a significant portion of the study area, their dynamic response should be analysed more in detail.

- Eurocode 8 doesn't include the hard-rock site condition as is the case with the site class A in NBCC. Classification of rock sites into two categories helps distinguish the site effect in crystalline hard rocks and more fractured sedimentary rocks formations.

- A strong correlation between $V_{S,30}$ and T_0 was observed in shallow sediments (H<30 m) and a relatively weaker correlation in deeper sediments (H>30 m), whereas the correlation between $V_{s,avg}$ and T_0 is practically inexistent. This suggests that the addition of $V_{s,rock}$ to the V_s soil in the top 30 m improves the correlation between $V_{s,30}$ and T_0. Due to this strong correlation, NBCC site classification yields similar patterns as the T_0 scheme.

- The site classification based on T_0 is affected considerably more by the thickness of the overlying sediments than by $V_{S,avg}$. Therefore, most of the shallow deposit conditions have a resonance period <0.4 s, which highlights the potential for seismic amplification in the short period range.

- The hybrid site classification proposes a multitude of classification parameters, which, in certain cases, may lead to confusion in selecting the appropriate site class. However, the results arrange the site conditions mainly into two major groups: rock and soft soils. Stiff and medium stiffness soils share only a limited part of the study area as opposed to the NBCC site classification.

As an overall conclusion, this study demonstrates that site classification based on $V_{s,30}$ is in general consistent with the geological and geotechnical conditions of the study area. However, the results may be further improved considering $V_{s,avg}$ in shallow (H<30 m) and T_0 in

deeper soil sediments (H>30 m) as secondary parameters. In such a case, the impact of the stiffness and thickness of the surficial sediments will be better accounted for.

Acknowledgments

The authors would like to thank the members of the CERM-PACES project at UQAC for their cooperation in conducting the field tests and providing access to various datasets.

Authors' contributions

Funding acquisition, A.S.; Methodology, M.S. and A.S.; Project administration, A.S.; Software, M.S.; Supervision, A.S., A.R. and M.N.; Writing – original draft, M.S.; Review & editing, A.S., A.R. and M.N.

Funding

This research was partially funded by the Natural Sciences and Engineering Research Council of Canada (NSERC) and Hydro-Quebec under project funding no. RDCPJ 521771 – 17.

Availability of data and materials

All the datasets that have been used and analyzed during the current study is available from the corresponding author on reasonable request.

Competing interests

I have declare that there is no any competing interests.

CHAPTER 3

3D PROBABILISTIC MODELLING AND UNCERTAINTY ANALYSIS OF GLACIAL AND POSTGLACIAL DEPOSITS OF THE CITY OF SAGUENAY, CANADA

Mohammad Salsabili [1], Ali Saeidi [1], Alain Rouleau [1] and Miroslav Nastev [2]

[1] Département des Sciences Appliquées, Université du Québec à Chicoutimi, G7H 2B1 Saguenay, Canada; ali_saeidi@uqac.ca (A.S.); Alain_Rouleau@uqac.ca (A.R.)

[2] Geological Survey of Canada, G1K 9A9 Quebec City, QC, Canada; miroslav.nastev@canada.ca

Abstract

Knowledge of the stratigraphic architecture and geotechnical properties of surficial soil sediments is essential for geotechnical risk assessment. In the Saguenay study area, the Quaternary deposits consist of a basal till layer and heterogeneous postglacial deposits. Considering the stratigraphic setting and soil type heterogeneity, a multistep stochastic methodology is developed for 3D geological modelling and quantification of the associated uncertainties. This methodology is adopted for regional studies and involves geostatistical interpolation and simulation methods. Empirical Bayesian kriging (EBK) is applied to generate the bedrock topography map and determine the thickness of the till sediments and their uncertainties. The locally varying mean and variance of the EBK method enable accounting for data complexity and moderate nonstationarity. Sequential indicator simulation is then performed to determine the occurrence probability of the discontinuous postglacial sediments (clay, sand and gravel) on top of the basal till layer. The individual thickness maps of the discontinuous soil layers and uncertainties are generated in a probabilistic manner. The proposed stochastic framework is suitable for heterogeneous soil deposits characterized with complex surface and subsurface datasets.

Keywords: soil variability; 3D modelling; kriging; geostatistical simulation

3.1. Introduction

The soil stratigraphy and geotechnical characteristics are important factors in geotechnical risk evaluations over a region. The two factors and their uncertainties are key elements, especially for probabilistic seismic risk assessment. The regional properties of soil deposits are heterogeneous due to the differences in deposition geometry and process. Soil heterogeneity is attributed to two main sources: one is rooted in the lithology and the other is the inherent spatial soil variability (Elkateb et al., 2003). The so-called lithological (soil type) heterogeneity is related to the substantial differences in the mineralogy, grain size and others, within a relatively uniform soil mass. This heterogeneity is qualified using descriptive terms (i.e., soil types), such as sand, clay and stiff/soft soil layers. The second source of heterogeneity is rooted in the inherent spatial soil variability, which modifies the spatial variation of soil properties due to different deposition conditions and different loading histories (Elkateb et al., 2003).

The spatial variation of soil properties has been modelled using random field theory, where the spatial variation of a given soil unit is decomposed into a deterministic trend function and residuals (Fenton, 1999; Fenton and Griffiths, 2003; Phoon and Kulhawy, 1999a; Uzielli et al., 2005). Residuals represent the inherent spatial soil variability described by the coefficient of variation and the scale of fluctuation (Phoon and Kulhawy, 1999a). Using this approach, predictions are made separately for the trend and the residuals of geotechnical quantitative parameters (shear strength, cone resistance, shear modulus, etc.). Recently, some methods have been developed to model the random field directly from sparse and nonstationary data (Wang et al., 2018; Zhao and Wang, 2020). In soil and rock engineering practices, investigations use geostatistical techniques to estimate soil (or rock) geotechnical/geomechanical properties and capture the heterogeneity (Ferrari et al., 2014; Kring and Chatterjee, 2020; Pinheiro et al., 2016; Vessia et al., 2020).

In seismic hazard assessment, local soil conditions tend to modify the amplitude and frequency content of the incoming seismic waves. This condition is known as the site effect, which depends on geotechnical (soil type, shear modulus, damping ratio, etc.) and geometrical

(3D stratigraphy, basin topography, soil thickness, etc.) properties of the soil deposits. A 3D geological model offers solutions to determine the geometrical properties and provides a basis for the spatial prediction of geotechnical properties, particularly the soil shear-wave velocity (*Vs*) (Lee et al., 2017). A 3D model helps determine the seismic site parameters, including the average V_s value of the top 30 m of soil ($V_{s,30}$), the average V_s of all of the soil deposits ($V_{s,avg}$) and the fundamental site period (T_0) or frequency (f_0) (Hallal and Cox, 2021; Rohmer et al., 2020). In Eastern Canada, Rosset et al. (2015) developed three different models for the Montreal region using predictive equations for V_s as a function of depth: a single-layer model based on the total thickness of soft soils, a four-layer model based on geological and geotechnical information from borehole data and a composite model that included the characteristics of the two former models. Nastev et al. (2016) in the Ottawa and St. Lawrence Valleys and Foulon et al. (2018) in the Saguenay City region assigned a typical *V*s depth function for postglacial sediments and a single V_s value to glacial sediments and bedrock units. These studies used a deterministic 3D geological model for mapping the spatial distribution of $V_{s,avg}$ and T_0. They analysed the uncertainty propagated to site parameters using the first-order, second-moment approach, and they considered only the statistical uncertainty related to the V_s of soil deposits. This approach ignores the spatial uncertainties related to the 3D geological model. Considering the uncertainties related to the type and thickness of the soil layers certainly helps the development of reliable seismic hazard maps.

This study aims to develop a methodology for probabilistic regional 3D modelling of soil deposits by considering soil type heterogeneity as the main source of uncertainty. This methodology is adopted for regional studies and involves stochastic interpolation and simulation methods. The capacities and advantages of the interpolation and geostatistical methods applied in each step are discussed. The territory of Saguenay City is used as a case study for the application of the methodology. Firstly, empirical Bayesian kriging (EBK) is tested and validated to determine the bedrock topography map in terms of the total soil thickness and the thickness of the till layer, that is, the basal glacial sediments. Available surficial geological maps, borehole logs, rock outcrops (zero soil thickness) and shallow till data are used in the

interpolation processes. Secondly, sequential indicator simulation (SIS) is conducted to predict the occurrence probability of the discontinuous postglacial soil layers on top of the till layer (e.g. clay, sand and gravel). Finally, the estimated probabilities are applied to determine the consistent spatial distribution of discontinuous soil units, the thickness maps and the associated uncertainties.

3.2. Methodology

With the rapid development of computational power and probabilistic methods, developing 3D geological models from borehole data and providing valuable insights into many engineering problems that traditionally rely on 1D and 2D assumptions, such as continuous stratigraphic layers simplified in the geological sections, are possible. The proposed methodology is adopted for regional study areas with variable soil thickness of more than 100 m in which a basal layer overlies the bedrock. The methodology is implemented in three phases (Figure 3-1): (I) data preparation, (II) mapping of bedrock and basal soil topography and (III) developing the probabilistic 3D geological model.

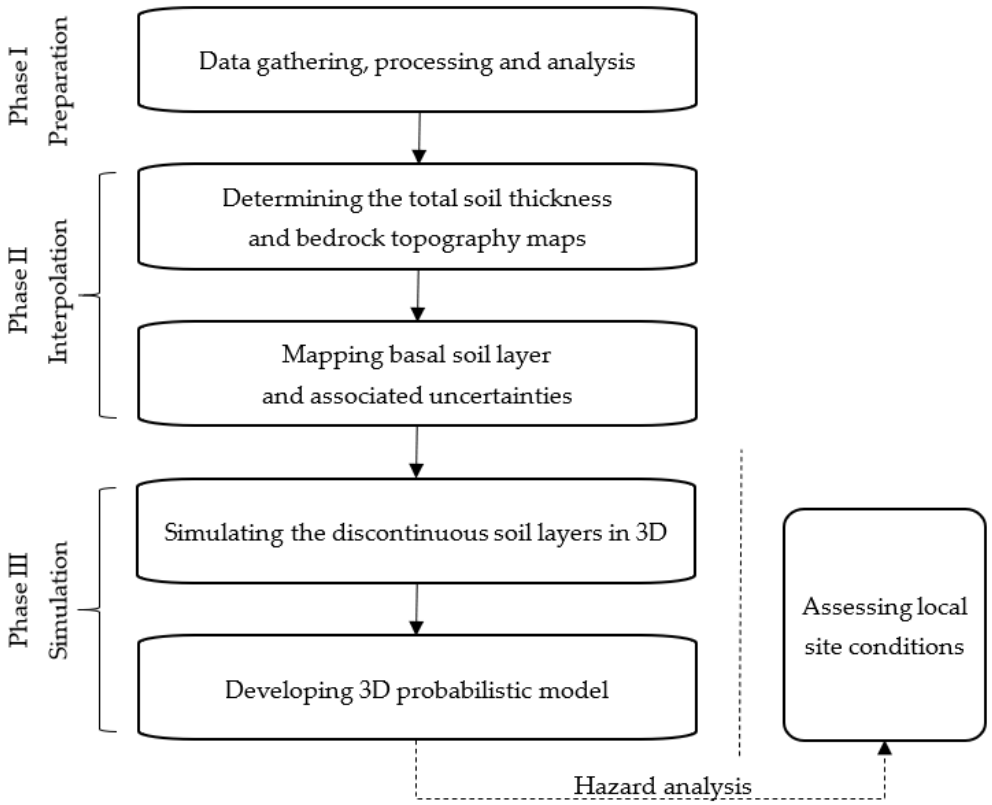

Figure 3-1. Methodology for developing a regional 3D probabilistic geological model. © Mohammad Salsabili, 2022

The data preparation step (Figure 3-2) relies on the acquisition of available data from various sources of information, as discussed below. Following the integration of the available data, the next step in this phase is data verification. It is performed by examining the consistency between borehole logs and geological maps and cross-sections, and between borehole collars and topographic maps. The observation data are then divided into two groups: the soil thickness data represented with points (x, y and thickness) and the soil type data represented with 3D borehole data (x, y, z and soil units).

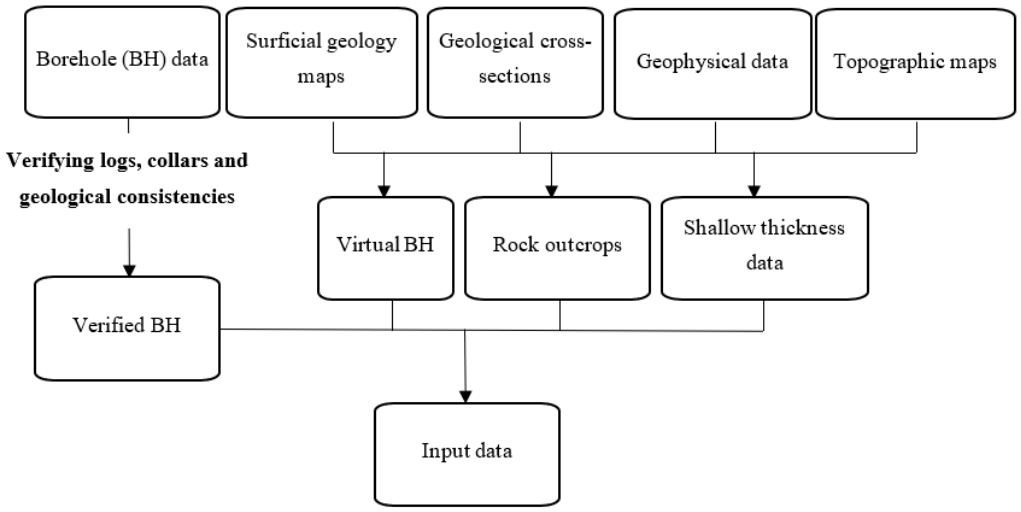

Figure 3-2. Phase I: workflow of data preparation. © Mohammad Salsabili, 2022

Next, a decision has to be made on the type of predictive model. For a stratigraphic soil unit that extends as a continuous layer, the thicknesses distribution can be modelled using spatial interpolation methods (Figure 3-3). In the study region described below, the till layer at the base of the Quaternary sequence is in contact with the bedrock and is assumed to be spread all over the territory underneath the recent soil layers. An appropriate spatial interpolation method should be selected in this phase corresponding to the preprocessing results. The trend and parameters, such as skewness or asymmetry of the probability distribution, and high or peak values, affect the stationarity and must be considered in choosing the appropriate geostatistical method (details can be found in Sections 3.3 and 3.4). For a soil layer that is discontinuous laterally but maintains a vertical relationship with other layers, a random function approach using *geostatistical simulation* is used; this condition is the case for the sand and clay layers in the study region described below.

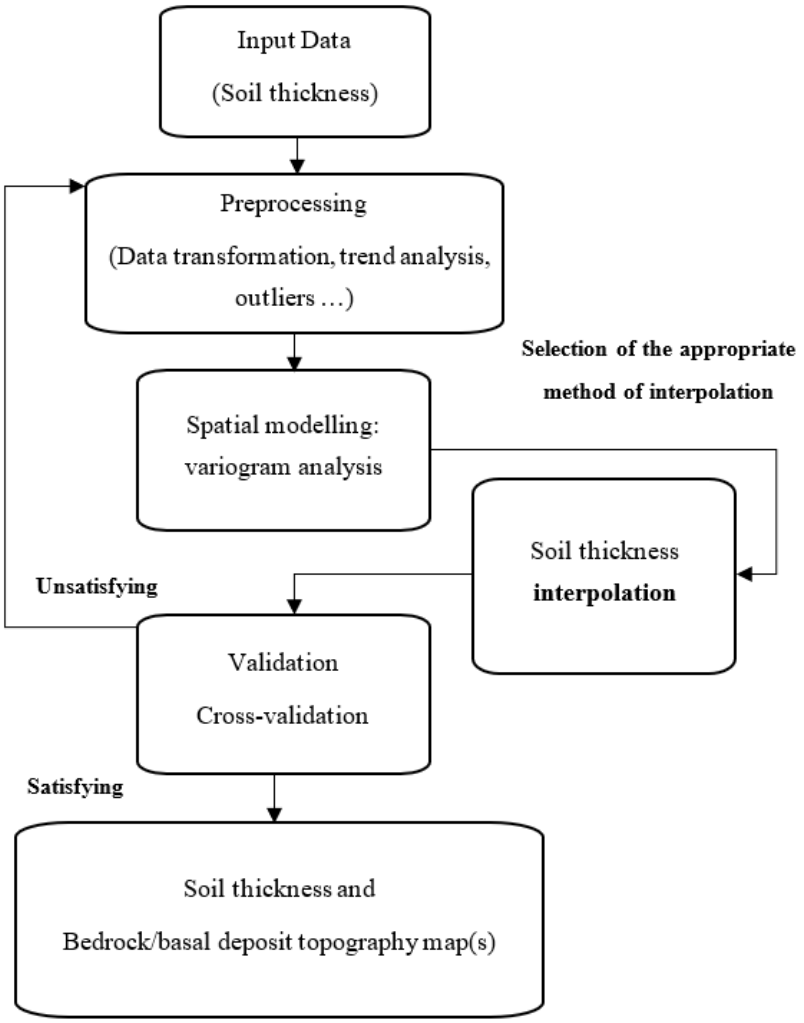

Figure 3-3. Phase II: workflow of the spatial interpolation of total soil thickness and thickness of the continuous basal layer. © Mohammad Salsabili, 2022

Multiple realizations of discontinuous soil types are generated using geostatistical simulation. These realizations can then provide the occurrence probability of discontinuous soil layers. The resulting probability values are used to create thickness maps of discontinuous soil layers and their associated uncertainties at unsampled locations (Figure 3-4).

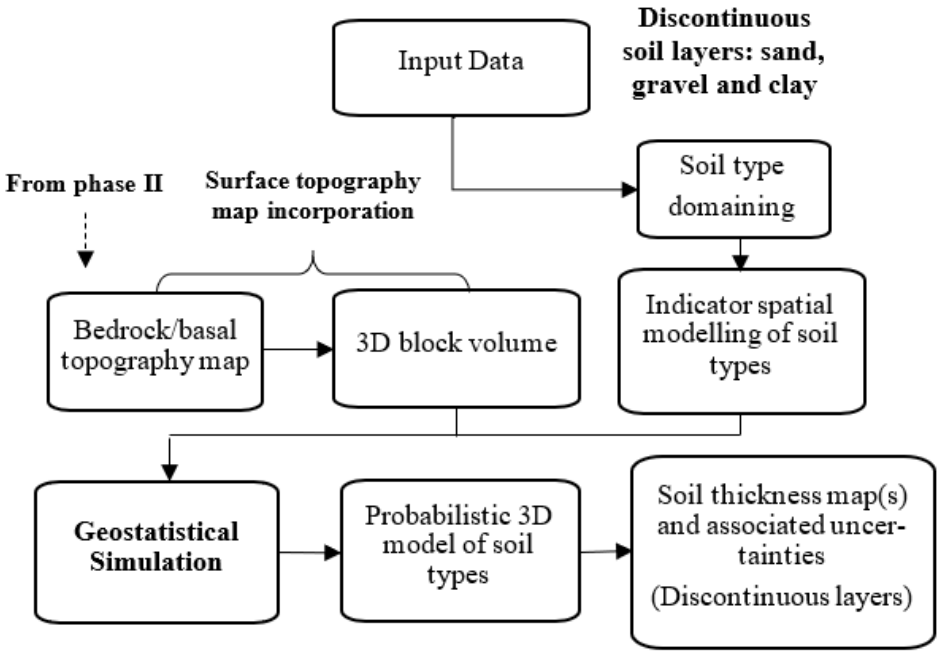

Figure 3-4. Phase III: methodology for determining soil thickness map(s) and associated uncertainties of discontinuous soil layers using geostatistical simulation. © Mohammad Salsabili, 2022

The development of a probabilistic 3D geological model must use a spatial prediction approach that considers the uncertainties in the spatial variation models and in the ensuing stochastic simulation. This interpolation approach uses a geostatistical method that is presented in the following section.

3.3. Applied Geostatistical Methods

3.3.1. Spatial Interpolation

Appropriate prediction methods are required for a realistic reconstruction of the soil heterogeneity over a region with a complex 3D soil deposit architecture, relatively sparse field observations and datasets with clustered sampling patterns. The prediction methods for computing spatial data fall into two broad categories: deterministic and stochastic (Myers,

1994). Deterministic predictions are obtained by using mathematical functions with known sample points. Stochastic methods associate the distribution of unknown values with a similar known distribution and can quantify the uncertainty associated with the interpolated values; this capability makes them superior to the deterministic approaches. Stochastic methods include those based on geostatistics and hybrid methods that consider machine learning (Li and Heap, 2008). In geostatistical methods, the principal concept of statistical inference is based on stationarity and requires the independency of the univariate and bivariate probability laws from the location; this concept is called *second-order stationarity*: the mean is constant and the variance only depends on separation *h* (Chiles and Delfiner, 2009; Isaaks and Srivastava, 1989). Given the data complexity of a study on a regional scale, the EBK method is selected to overcome the potential of the nonstationarity of data, automate the fitting of variograms and solve the kriging models. The process consists of: (i) estimation of a semivariogram model on the basis of the input data, (ii) simulation of a new set of data from the semivariogram model, (iii) estimation of a new semivariogram model on the basis of the simulated dataset and (iv) calculation of a weight for the new model using Bayes' rule. The repetition of the process results in a spectrum of semivariograms rather than a single one. Hence, the uncertainty introduced in the variogram arises from using a series of semivariogram models rather than a single one (Krivoruchko and Gribov, 2019). The automated simulation process facilitates the subsetting of data into large datasets typical for regional studies and helps achieve local stationarity in subareas where the dataset is a mixture distribution of high and low values. The EBK method is particularly efficient for spatial interpolation in large-scale studies and/or datasets with complexities (Giustini et al., 2019; Krivoruchko and Gribov, 2019; Mirzaei and Sakizadeh, 2016).

In addition to the EBK method, the results are compared with the conventional deterministic interpolation method, triangulated irregular network (TIN). For an area in the same region of Eastern Canada as the present study, Chesnaux et al. (Chesnaux et al., 2017) concluded that the expected values predicted with the TIN method are more accurate than the ordinary kriging method.

3.3.2. Spatial Variation

Spatial variation refers to the dissimilarity of the pairs of values of a random variable as a function of their distance (Isaaks and Srivastava, 1989). Modelling the spatial variation assists in predicting the soil attributes at unsampled locations. In the present study, the spatial variation is determined for continuous (soil thickness) and categorical (soil units) variables. An experimental variogram, $\hat{\gamma}(h)$, is used to statistically determine the average dissimilarity between data separated by vector *h* (Goovaerts, 1999) and is assumed as a measure of spatial variability.

$$\hat{\gamma}(h) = \frac{1}{2\,N(h)} \sum_{\alpha=1}^{N(h)} [z(u_\alpha) - z(u_\alpha + h)]^2, \tag{3-1}$$

where $z(u_\alpha)$ and $N(h)$ are the values of the variable of interest at location u_α and the number of data pairs within distance *h* in the respective direction. In practice, the tolerance for distance *h* and its direction is specified. The direction of the separation vectors becomes irrelevant when the directional tolerance increases sufficiently. An omnidirectional variogram is a useful starting tool for structural analysis and provides the prerequisite information for calculating the directional variograms, whilst a directional variogram reveals the anisotropy pattern and the direction of the maximum and minimum spatial continuities (Isaaks and Srivastava, 1989). Equation (3-1) is applied for continuous variables, whilst an indicator variogram is calculated for categorical variables by substituting indicator data $i(u_\alpha; k)$ for K indicators as follows:

$$\hat{\gamma}_I(h; k) = \frac{1}{2\,N(h)} \sum_{\alpha=1}^{N(h)} [i(u_\alpha; k) - i(u_\alpha + h; k)]^2, \; k=1, \ldots, K. \tag{3-2}$$

With the determination of the standard variogram characteristics (i.e., range, sill and nugget effect), a theoretical model that best fits the experimental variogram is selected (e.g. spherical, exponential or Gaussian model).

3.3.3. Uncertainty of Spatial Interpolation

The usual approach to modelling kriging uncertainty applies the error variance of kriging as follows (Isaaks and Srivastava, 1989):

$$\tilde{\sigma}_k^2 = \tilde{C}_{00} + \sum_{i=1}^{n}\sum_{j=1}^{n} w_i w_j \tilde{C}_{ij} - 2\sum_{i=1}^{n} w_i \tilde{C}_{i0}, \quad (3\text{-}3)$$

where $w_i w_j$ represents the kriging weights, $\tilde{C}_{00}$ is the variance of point values, $\tilde{C}_{ij}$ is the covariance between measured samples and $\tilde{C}_{i0}$ is the covariance between measured and unknown values.

3.3.4. Stochastic Simulation

The 3D model of categorical variables is constructed by applying *deterministic* or *stochastic* approaches. Deterministic modelling is highly dependent on expert judgment and is conducted by delineating the boundaries of geological units and verifying and interpreting the borehole logs in successive cross-sections. In most cases, field observations are insufficient to provide reliable modelling. Thus, stochastic modelling algorithms are applied to construct multiple realizations. For example, SIS is a widely used technique for categorical variable models (Deutsch, 2006). A set of alternative high-resolution models of the spatial distribution of the considered random variable is created during this process. Each equally probable realization reproduces the spatial statistics of the target variable (Deutsch, 2006). The method consists of three steps as follows:

viii) Transformation of soil types to *K* indicator variables

$$i(u_\alpha; k) = \begin{cases} 1 & if\ category\ k\ prevails\ at\ location\ u\ , k = 1, \dots, K. \\ 0 & otherwise \end{cases} \quad (3\text{-}4)$$

Indicator transformation facilitates classical statistical analyses to infer representative proportions of the indicator variables;

ix) Determination of indicator variograms to model the spatial continuity of the indicator soil types;

x) Simulation of the soil types honoring field observation at sampled locations (conditional simulation) in a sequential and reproducible manner.

3.4. Saguenay City Data Preparation and Analysis

3.4.1. Geologic Framework of the Study Area

The territory of Saguenay City located in Eastern Canada was selected as the study area due to its relatively high seismic hazard (https://earthquakescanada.nrcan.gc.ca/ (accessed on: 29 April 2021)) and the presence of layered soil deposits with complex and variable spatial and vertical distributions. This city is the main municipality within the Saguenay–Lac-Saint-Jean region, and its territory covers 1136 km^2, with a population of 147,100. It has a hilly topography and lies in the southern portion of the E–W-trending Saguenay graben. The regional seismic activity of this region was reassessed following the 1988 M6.0 Saguenay earthquake. The epicenter of this intraplate earthquake with a midcrustal depth of 29 km was 35 km south of the downtown area (Du Berger et al., 1991). The earthquake's secondary effects included liquefaction, rock falls and landslides observed within a distance of 200 km from the epicenter (Lamontagne, 2002).

The bedrock of the Saguenay region is part of the Grenville Province of the Canadian Shield and is mainly composed of crystalline Precambrian rocks (Davidson, 1998). On the basis of the geological sections (Daigneault et al., 2011; LaSalle and Tremblay, 1978) and subsurface data (CERM-PACES, 2013), the soil deposits are grouped into two major geological classes: glacial and postglacial sediments (Walter et al., 2018). They can be further subdivided into five categories: till, gravel, clay, sand and other recent sediments (Figure 3-5).

i) Till: This glacial sediment is located at the base of the stratigraphic soil column; it is compact and semi-consolidated. Till is the most widespread soil unit in the study area and ranges in thickness from a few meters to >10 m at certain locations. In the highlands, the till veneer is frequently discontinuous and results in areas of rock outcrops. Most of the till outcrops are assumed to be less than 1 m thick on the geological map (Daigneault et al., 2011). With the exception of rock outcrops, till

continuously covers the bedrock elsewhere, representing an important assumption in the 3D modelling approach.

ii) Gravel: This coarse sediment is mainly of glaciofluvial and alluvial origin; it consists of gravel, sand and sometimes till. This unit is occasional in the region, often in contact with till or sand units.

iii) Clays: These fine postglacial sediments are the most present soil type by volume in the study area. They are composed mainly of silt, silty clays and clay. They have a thickness of up to 10 m and may attain a maximum thickness of >100 m in the lowlands.

iv) Sand: This group consists mainly of coarse glaciomarine deltaic and prodeltaic sediments and alluvial sands composed of sand and gravely sands.

v) Other sediments: This extremely heterogeneous category comprises all the remaining sediments; it mainly includes loose postglacial sediments consisting of alluvium, floodplain sediments, organic sediments and occasional landslide colluvium that can be classified into sand, clay and gravel on the basis of grain size distribution.

The surficial deposit map in Figure 3-5 shows that till is the most widespread soil type at the surface, followed by clay and sand sediments.

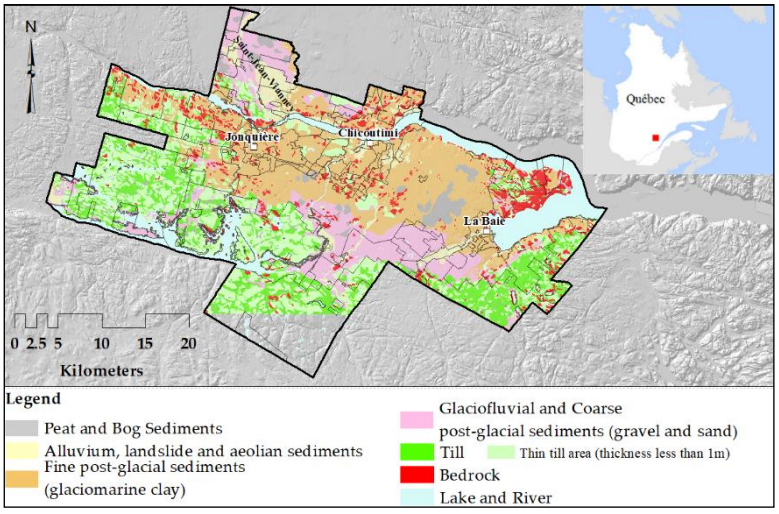

Figure 3-5. Saguenay study area: surficial geology map (modified from Daigneault et al. (Daigneault et al., 2011)) (CERM-PACES, 2013). © Mohammad Salsabili, 2022

3.4.2. Input Data and Analysis

Subsurface and surface data were collected from various sources of information (Figure 3-6). Borehole logs are the main subsurface data where the soil thickness data and soil types are obtained. The other invaluable sources of data are rock outcrops with zero soil thickness value; the virtual data derived from geological cross-sections and thin till data (thickness ≤ 1 m) interpreted from the surficial geological map (CERM-PACES, 2013). Borehole data were obtained from groundwater wells, exploration boreholes and geotechnical drilling logs. The brief descriptions of the input data stored in the database are as follows:

i) Borehole logs: The database contains 3524 borehole logs distributed over the study area (CERM-PACES, 2013). A total of 2402 boreholes are sufficiently deep to reach the bedrock. The remaining 1122 boreholes that do not reach the bedrock indicate that the bedrock is deeper than the borehole depth, and a groundwater-bearing layer is possibly encountered in the coarse soil deposits.

ii) Virtual logs: A total of 26 geological cross-sections distributed over the region were developed on the basis of expert opinion in previous geological studies (CERM-PACES, 2013). These cross-sections include 973 virtual logs distributed in a regular spatial pattern at a distance of ~500 m to improve the data coverage mainly in the lowland areas (Figure 3-6).

iii) Rock outcrops: During the geographic information system processing of the surficial geology map, additional 1033 data points were introduced to indicate rock outcrops. Located within the bedrock polygons, they improve the realistic spatial variability of the sediment thickness.

iv) Till veneer: Till sediments cover most of the study area. Till outcropping areas, with a thickness equal to or less than 1.0 m, are located in the highlands and are referred to as a till veneer. In these areas, the till thickness is fixed to 1 m, and the till outcrop polygons are modelled with a mesh of 75 m, generating an additional 42,649 points with a known thickness.

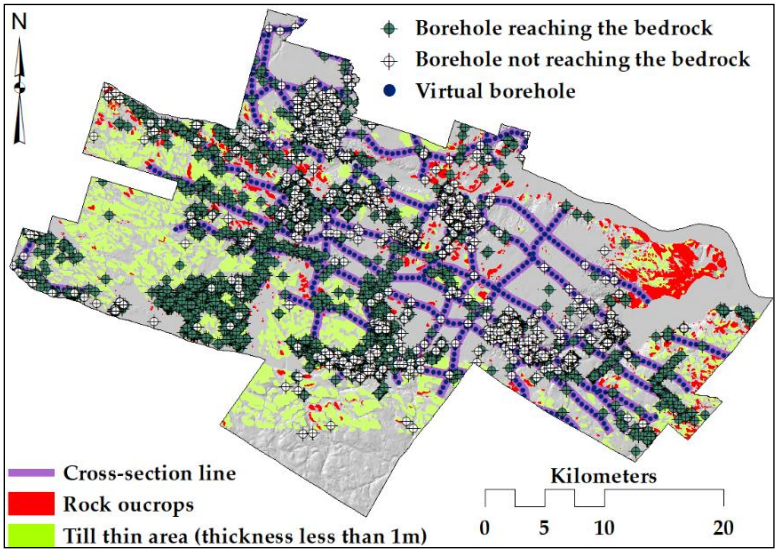

Figure 3-6. Complete set of the available observation points, including borehole logs, rock outcrops and shallow till data. © Mohammad Salsabili, 2022.

Rock outcrops (zero soil thickness) and shallow till data (1 m soil thickness) are valuable sources of complementary information, mainly in the highlands where they improve the accuracy of the geological model (Figure 3-6). However, the rock outcrops and till veneer points are observed over large areas of the region, in comparison with other data, which are limited to the borehole locations (Liang et al., 2014). The resulting bias in the simulation of the soil types is avoided by using the rock and till outcrop data only to generate the bedrock and till topography maps and then excluding these later data for the simulation of other soil units. The till veneer data are only applied to create the thickness map of till deposits.

Figure 3-7 shows the histograms of the total soil thickness and thickness of glacial deposits. A total of 2745 soil thickness values are selected comprising the boreholes that reach the bedrock and virtual logs located in areas with sand, clay or gravel soil units. The average thickness of sediments over these areas is approximately 17 m with a positive skewness and a relatively high standard deviation of 18.7 m, indicating high thickness variability (Figure 3-7a). Important thicker parts are located in two areas: La Baie and Saint-Jean-Vianney (Figure 3-5). The incorporation of rock outcrops with zero soil thickness value decreases the average thickness (12.89 m), but the effects on the other parameters are minor (Figure 3-7b). A total of

1007 data points are selected from the virtual logs and boreholes reaching the bedrock at the location where the till sediments are exposed. Figure 3-7c illustrates that the average thickness of till is approximately 5 m in the borehole data, whilst the maximum nearly reaches 50 m. Attention must be given to the presence of outliers because they have a major influence on the interpolated surfaces (Wu et al., 2011). Given that the expected thickness of till rarely exceeds 20 m, higher thickness values are most probably a consequence of poor logging of other soil units considered as outliers. The exact values of the outliers are determined using a box plot and are cases with values more than 1.5 times the interquartile range. Here, these values are replaced by a maximum of 13.85 m (Figure 3-7d). Following the replacement of the outliers of till thickness, the 1007 points are merged with till veneer and rock outcrop data in the database.

On the basis of the statistical summary, we can perceive existing high or low values, and the asymmetry of the probability distribution questions the stationarity. The asymmetry is evident in Figure 3-7 by comparing the observed thickness histograms and theoretical normal distributions of the different soil properties. In this context, traditional kriging methods (e.g. ordinary or transformed Gaussian kriging) do not perform well, whereas the EBK method is particularly helpful to overcome the nonstationarity by defining subsets (subareas) and automated variography analysis.

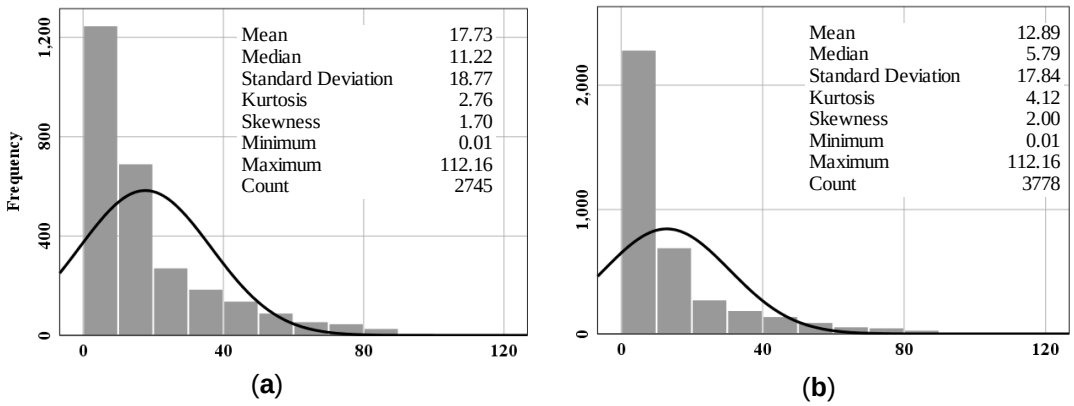

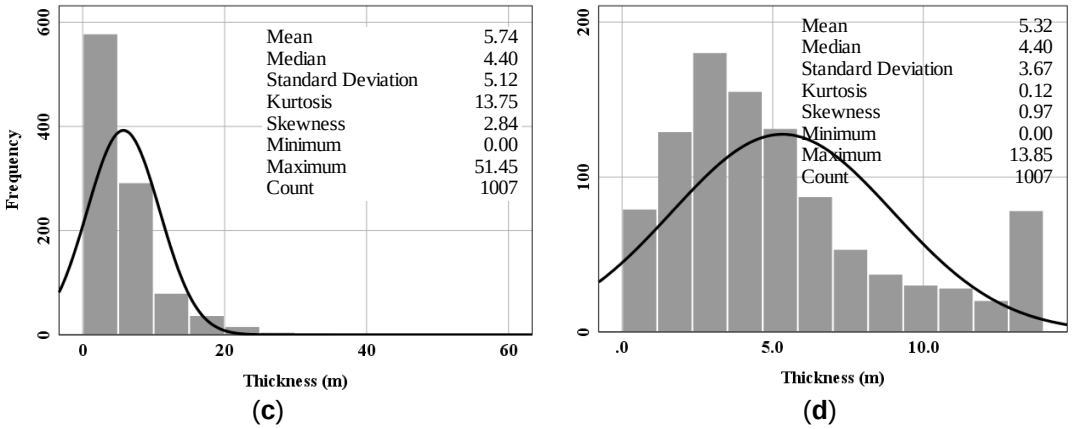

Figure 3-7. Thickness distributions of soil deposits as observed in borehole logs: (**a**) total soil thickness, depth to rock; (**b**) total soil thickness, including rock outcrops; (**c**) till sediments; (**d**) till sediments following replacement of outliers. The black line represents the normal distribution curve. © Mohammad Salsabili, 2022.

Table 3-1 provides the proportions of each soil unit based either on real or on virtual borehole logs. One of the main reasons for the differences in percentages is the clustered drilling pattern of the real boreholes drilled mainly in coarse sandy soils for drinking water supply. Given that virtual boreholes are designed in a systematic pattern, the percentages of virtual data are deemed reliable estimates for the layer thickness. The percentage values indicated in Table 3-1 denote the marginal probabilities that are applied in the geostatistical simulation using the Stanford Geostatistical Modelling Software (Remy et al., 2009).

Table 3-1 Percentage of each soil type based on real and virtual borehole logs.

Geological Unit	Real Borehole Data (%)	Virtual Logs (%)
Clay	53.60%	58.54%
Gravel	6.80%	2.06%
Sand	35.66%	18.37%
Till	3.94%	21.03%

3.4.3. Modelling Spatial Variation: Variogram Analysis

Two sets of directional variograms (not shown here) are calculated to determine the anisotropy axis and describe the spatial variation of soil types and their thickness. The first set

uses a 2D coordinate system for the soil thicknesses, and the second set applies a 3D coordinate system for the soil types. Using the EBK method automates the fitting of variograms by simulating variograms per subset of data and then weighting the models using Bayes' rule. The subsequent repetition of the process results in a spectrum of semivariograms rather than in a single one (Krivoruchko, 2012; Pilz and Spöck, 2008).

In the case of categorical variables, soil types, an indicator transformation is first performed. Indicator variograms are then computed to describe their spatial variability. The directional experimental variograms are computed using different lag sizes to capture the short- and long-scale variabilities. The experimental variograms show nested structures (e.g. Figure 3-8) and can be interpreted as a short- and a long-scale variability. The short-scale structure captures the variability over a distance of hundreds of meters and can be referred to as local soil variability. The long-scale structure captures the variability over a distance of thousands of meters and can be referred to as geological (stratigraphic) variability. In all the anisotropic models, the anisotropy is interpreted as geometric, in which the range changes with the direction, whereas the sill is constant. Detailed discussion on variogram modelling can be found in (Isaaks and Srivastava, 1989).

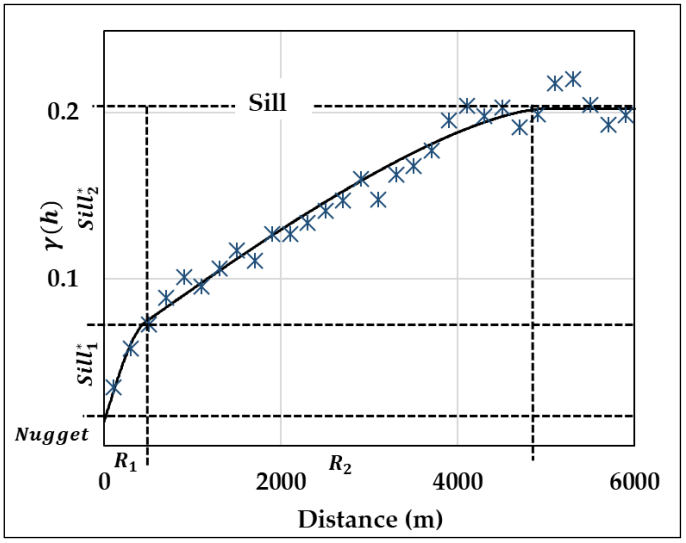

Figure 3-8. Example of variogram modelling: a nugget and two spherical nested structures are fitted on an experimental sample variogram. R_1 and R_2 refer to the ranges of the two nested models. © Mohammad Salsabili, 2022.

Directional and omnidirectional variograms are analyzed using a lag size of 25 m to model the variability at the short scale of all soil units. Lag sizes of 300 and 750 m are adopted to capture the variability at the long scale for gravel, sand and clay layers. The selected bandwidth is three times larger than the lag size to limit eventual deviation around the direction of the azimuth vector. The range of short-scale variability can be measured within hundreds of meters, as indicated in Table 2, whilst that of long-scale variability is within thousands of meters. Significant spatial variances are captured in short-scale variability, and the geometrical anisotropy with an azimuth angle of 135° corresponds to the geological continuity in the study area (Figure 3-5). As expected, the vertical range in all of the considered models is considerably lower than the horizontal ranges. The anisotropy consequently refers to the high density and the remarkable variation in data in the vertical direction compared with the horizontal.

Table 3-2. Variogram model parameters of the soil type indicators.

Variables	Number of Structures	Model Properties Structure 1			Model Properties Structure 2		
		Model Type	Anisotropy Axis (a_{max}, a_{med}, a_{min})	Model Parameters	Model Type	Anisotropy Axis (a_{max}, a_{med}, a_{min})	Model Parameters
Clay	2	Sp.	(135°,45°,90°)	Nugget: 0.01 R_1: (375,212.5,75) $Sill_1$ *: 0.18	Ex.	(135°,45°,90°)	R_2: (12825,4275,75) $Sill_2$ *: 0.05
Sand	2	Sp.	(135°,45°,90°)	Nugget: 0.02 R_1: (412.5187.5,62.5) $Sill_1$ *: 0.17	Sp.	(0°,0°,90°)	R_2: (12375,12375,62.5) $Sill_2$ *: 0.03
Gravel	2	Sp.	-	Nugget: 0.01 R_1: (150,150,150) $Sill_1$ *: 0.026	Ga.	(0°,0°,90°)	R_2: (4600,4600,150) $Sill_2$ *: 0.015

* Partial sill, R: range (meter), Sp.: spherical, Ex.: exponential, Ga.: Gaussian. a_{max}, a_{med} and a_{min} refer to the azimuths of the three principal axes of the anisotropy.

3.5. Results

3.5.1. Construction of the Total Soil Thickness Map (Depth to Bedrock)

3.5.1.1. Spatial Interpolation

The spatial interpolation of the total soil thickness that represents the depth to bedrock map is performed by using the EBK method in addition to TIN. The study area is discretized into a regular grid of 902 × 637 cells with 75-m spacing. Figure 3-9a,b illustrate the resulting depth to bedrock maps. The estimated thickness of the deposits varies from zero to approximately 100 m, with similar variability patterns modelled by the two methods. The areas covered by till veneers and rock outcrops are excluded; they are indicated by the white background on the maps.

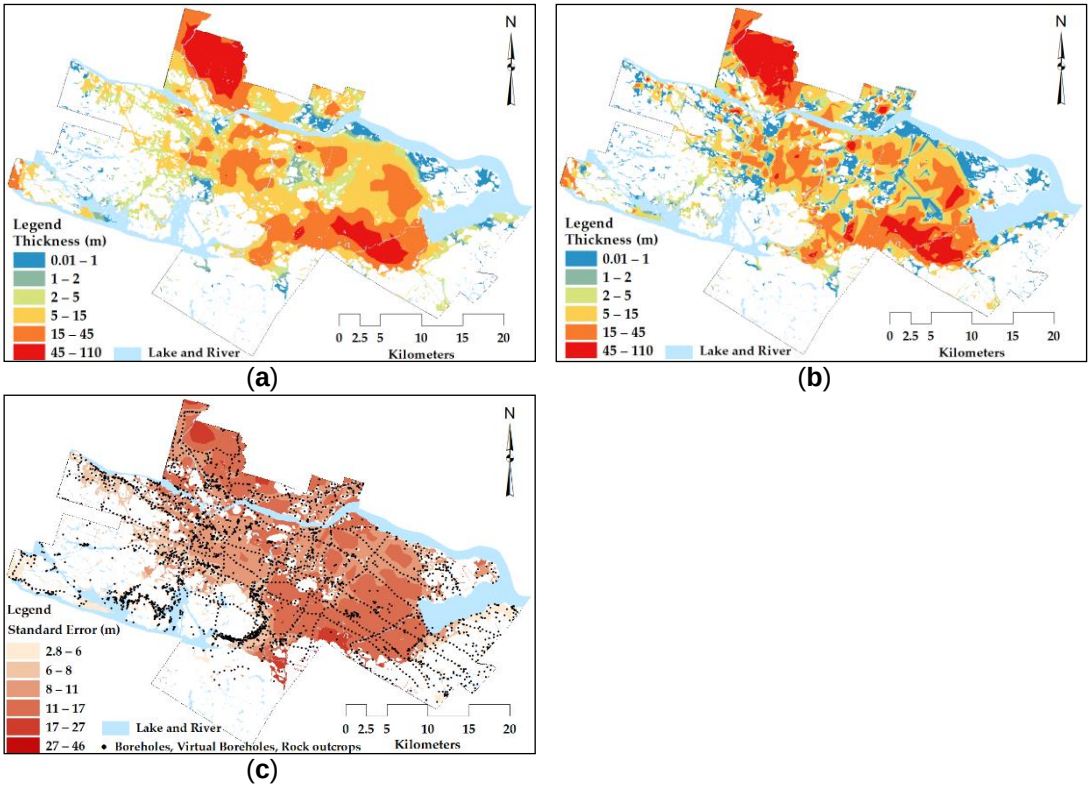

Figure 3-9. Total soil thickness maps obtained with: (**a**) EBK, (**b**) TIN; and (**c**) the map of the kriging standard deviation ($\tilde{\sigma}_k$) EBK. The areas with till or rock outcrops are excluded and indicated with white background. © Mohammad Salsabili, 2022.

Figure 3-9c shows the spatial distribution of the standard deviation of the kriging with EBK ($\tilde{\sigma}_k$). As expected, lower uncertainties are associated with locations in the proximity of the existing data. However, relatively higher $\tilde{\sigma}_k$ values are also observed, where the depth to rock is the highest. This phenomenon is a consequence of the locally varying mean and variance of the EBK method assumed as reliable results. TIN is a deterministic interpolation method and does not allow for the uncertainty of estimation.

3.5.1.2. Validation

Two approaches are applied to validate the estimation of soil thickness. The first approach is the routine cross-validation procedure in which the measured data are removed individually and re-estimated from the remaining dataset, referred to as the “leave-one-out

method". The second approach is based on a subset of data that is held back from the estimation process. In this case, the boreholes not reaching the bedrock are used as the validation dataset.

Cross-validation: The cross-validation procedure is used to optimize the estimation parameters. The optimized parameters include the lag size, the minimum and maximum numbers of participant data and the subset size in the EBK method. Four parameters are used to check the performance of the kriging methods: mean error (ME), root mean square error (RMSE), mean standardized error (MSE) and mean square standardized error (MSSE). The standardized values consider the kriging variance and are dimensionless. They provide an accurate comparison in addition to the statistical ME and RMSE values. The MSE values should be close to zero and can be obtained as follows (details can be found in (Chiles and Delfiner, 2009)):

$$MSE = \frac{1}{N}\sum_{\alpha=1}^{n}\frac{(Z^*(u_\alpha)-Z(u_\alpha)}{\tilde{\sigma}_k(u_\alpha)}, \quad (3\text{-}5)$$

where *N* is the number of measured data, and $Z^*(u_\alpha)$ and $Z(u_\alpha)$ are the estimated and measured values of random variable *Z* at the location of u_α, respectively. $\tilde{\sigma}_k(u_\alpha)$ and $\tilde{\sigma}_k^2(u_\alpha)$ are the kriging standard deviation and variance of the random variable *Z*, respectively.

The MSSE value should be close to one. For an MSSE greater than one, the variability in the estimated values is underestimated. Otherwise, the variability is overestimated. The parameter can be obtained with the following equation (Chiles and Delfiner, 2009).

$$MSSE = \frac{1}{N}\sum_{\alpha=1}^{n}\frac{\left((Z^*(u_\alpha)-Z(u_\alpha)\right)^2}{\tilde{\sigma}_k^2(u_\alpha)}. \quad (3\text{-}6)$$

Chiles and Delfiner (Chiles and Delfiner, 2009) recommended a tolerance of $1 \pm 3\sqrt{(2/N)}$ for the accepted MSSE. A total of 3778 measurements are used for estimating the total soil thickness in which the accepted tolerance is within the [0.93–1.07] range.

The cross-validation results reveal that (Table 3-3) the EBK method provides accurate and unbiased estimates with low ME and MSE values close to zero. The EBK method also gives relatively low values of RMSE and MSSE that vary within the acceptable tolerance range.

Table 3-3. Cross-validation results for the total soil thickness estimates using EBK methods.

ME (m)	RMSE (m)	MSE	MSSE
0.05	8.94	0.01	0.94

Validation using a test set: The 1122 boreholes that do not reach the bedrock, shown in Figure 3-6, were used as a test set for the soil thickness predictions. The depth of the observed point is underestimated when the total soil thickness estimates at these locations are lower than the observed borehole depths. Accordingly, the "*thickness error*" is considered the difference between the measured and estimated thicknesses, and only the positive errors are considered. Table 4 provides the statistical results of the thickness errors with respect to the different interpolation methods. The EBK method yields a lower number of underestimated soil thickness values at 313 boreholes, suggesting that this method provides better overall spatial predictions. When the mean error values and the sum of the errors are compared, EBK appears to provide slightly better predictions.

Table 3-4. Thickness error results at the locations of 1122 boreholes known not to reach the bedrock.

Thickness error	TIN	EBK
Mean (m)	12.2	11.8
Sum (m)	3889.8	3682.6
Error count (boreholes)	318	313

Figure 3-10 represents the distributions of the thickness error estimated by EBK in addition to the TIN methods. The thickness error is less than 10 m in approximately 60% of the

underestimated borehole values. Overall, the results of the validation procedures indicate that the EBK method respects the observed values and provides accurate spatial predictions. This method provides a reliable measure of uncertainty at the estimation points.

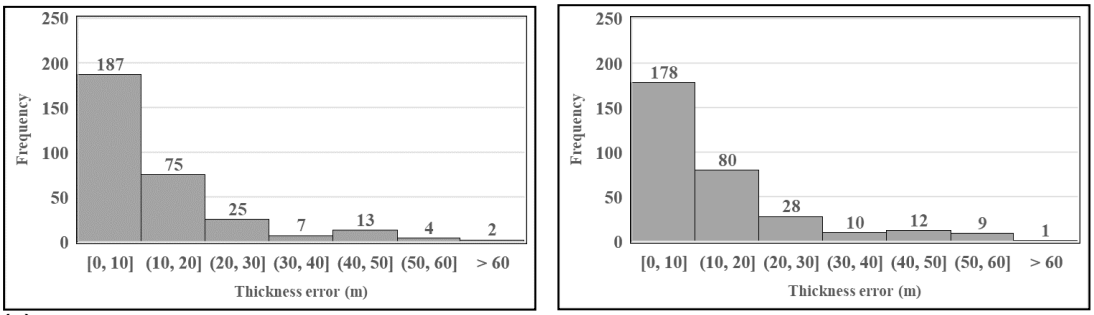

Figure 3-10. Thickness error distributions for the test set of 1122 boreholes not reaching the bedrock estimated by (**a**) EBK and (**b**) TIN. © Mohammad Salsabili, 2022.

3.5.2. Determination of the Till Thickness Map

The spatial distribution of the till thickness as a continuous soil layer at the base of the Quaternary sequence is estimated with a similar procedure to the one applied for interpolation of the total soil thickness using the EBK method. The difference is that the outliers are replaced because the till deposits cannot be easily distinguished from the other soil types due to difficulties related to the presence of drilling mud. Thus, replacing the outliers of the till thickness data can be considered a conservative approach to estimate the thickness of other postglacial deposits. Replacement is also an effective method for stabilising the variance. A complete set of observation points, including 2402 real and 973 virtual boreholes, 1033 rock outcrops and 42,649 points of thin till thickness (1 m), is incorporated to create the till thickness map. The thin thickness data dictate the highly skewed distribution of the 1 m data. Therefore, subsetting the data is a great advantage in using the EBK method. Figure 3-11 presents the resulting spatial distribution of the till thickness and the associated kriging standard deviation. Replacement of outliers combined with the use of shallow till data prevents potential soil

thickness overestimation and generates conservative estimates for the future evaluation of the geotechnical soil parameters.

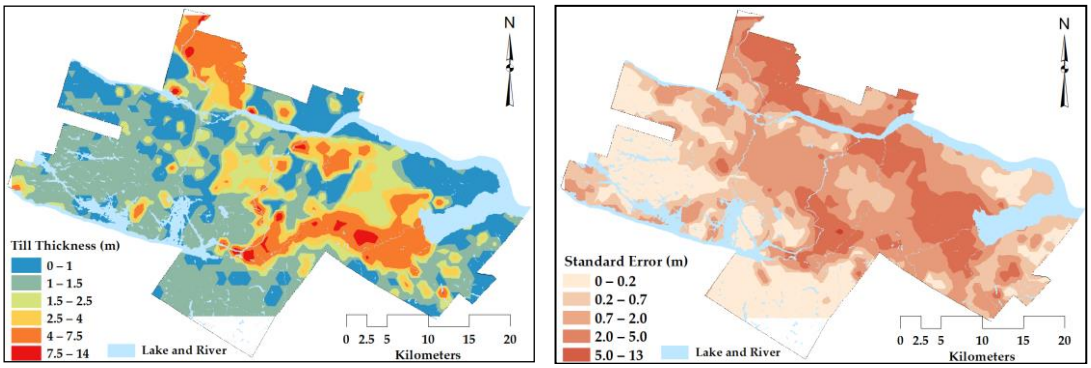

Figure 3-11. (a) Till thickness map and (b) kriging standard deviation, $\tilde{\sigma}_k$. © Mohammad Salsabili, 2022.

3.5.3. 3D Modelling of Discontinuous Soil Layers

A full 3D volume is required to determine the soil type of discontinuous soil layers. The block model fills this volume, and each block represents the smallest unit of soil type using geostatistical simulation. For this purpose, the maps of bedrock and till topography are created by using digital elevation modelling, and total soil thickness and till thickness maps. When the bedrock and till topography maps are created, the space between the top and bottom of each surface is filled with 75 × 75 × 2 m blocks. Overall, 100 realizations are generated using the conditional SIS method to determine the probability of occurrence for each of the postglacial deposits: clay, sand and gravel. Figure 3-12 shows a plan and cross-section through one of the SIS realizations in an area where all four surficial soil units are present.

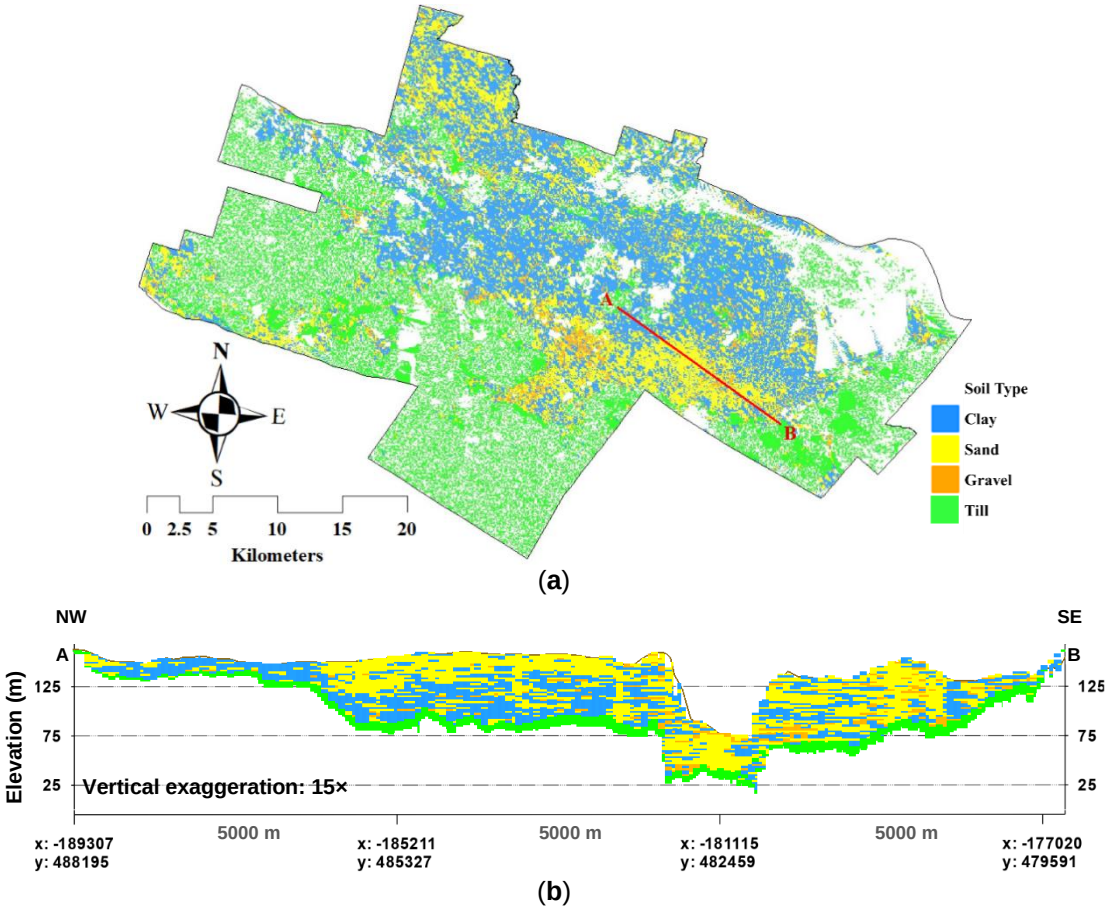

Figure 3-12. (a) Plan and (b) cross-section of one SIS realization of sand, clay and gravel. The thickness of the till unit shown in the cross-section is determined in Section 5.2. © Mohammad Salsabili, 2022.

The results of the SIS simulation are visually compared with the deterministic geological cross-section (Figure 3-13). Figure 13a represents a part of the main cross-section of the study area (Figure 3-12a). Figure 3-13b shows the soil units with the highest probability of occurrence resulting from 100 realizations. The comparison of Figure 3-13a,b shows that the probabilistic model is consistent with the interpretations of expert geologists; however, it yields a realistic soil variability prediction corresponding to the real borehole data. This observation is particularly true when comparing the individual borehole logs or the entire right-hand portion of the cross-section extending from borehole F1161. This condition is mainly due to the nature of the probabilistic estimates that consider the entire set of input data and the extent of the geological units in 3D. Figure 13c–e present the probabilities of occurrence of the

individual soil units. The 3D simulation of the discontinuous soil units quantifies the uncertainty of the predictions (Figure 3-13f) using the total standard deviation of the soil thickness computed from the probability of a categorical distribution for each block. The thickness standard deviation represents the total uncertainty that reaches its maximum in locations where the probabilities tend to be average, such as 0.5. The average probabilities are generated in two types of location: in the areas of contact between sand and clay or gravel and the areas with a high variability of soil types (locations near boreholes F11611 and SIH1340). This variability can be a result of errors in geological logging or from the inherent soil variability. The detailed computations of the thickness maps of postglacial deposits and the associated uncertainty are discussed next.

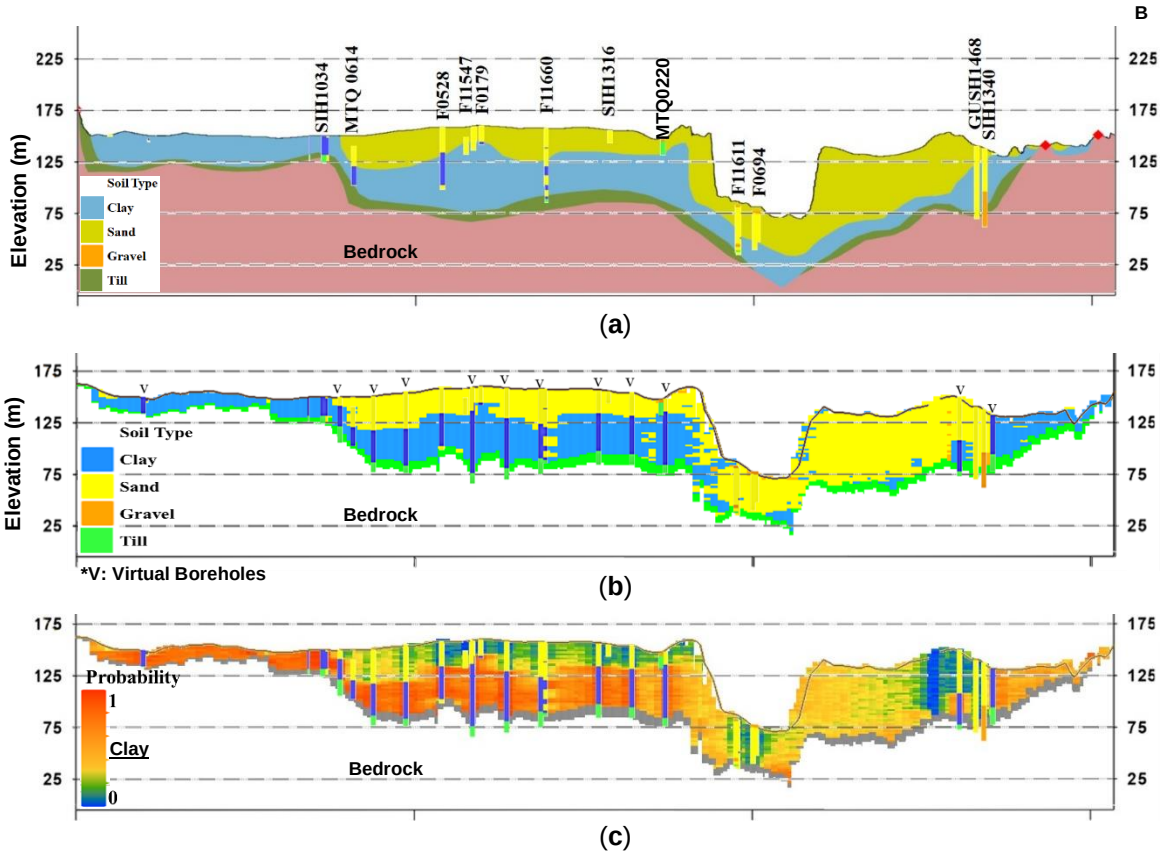

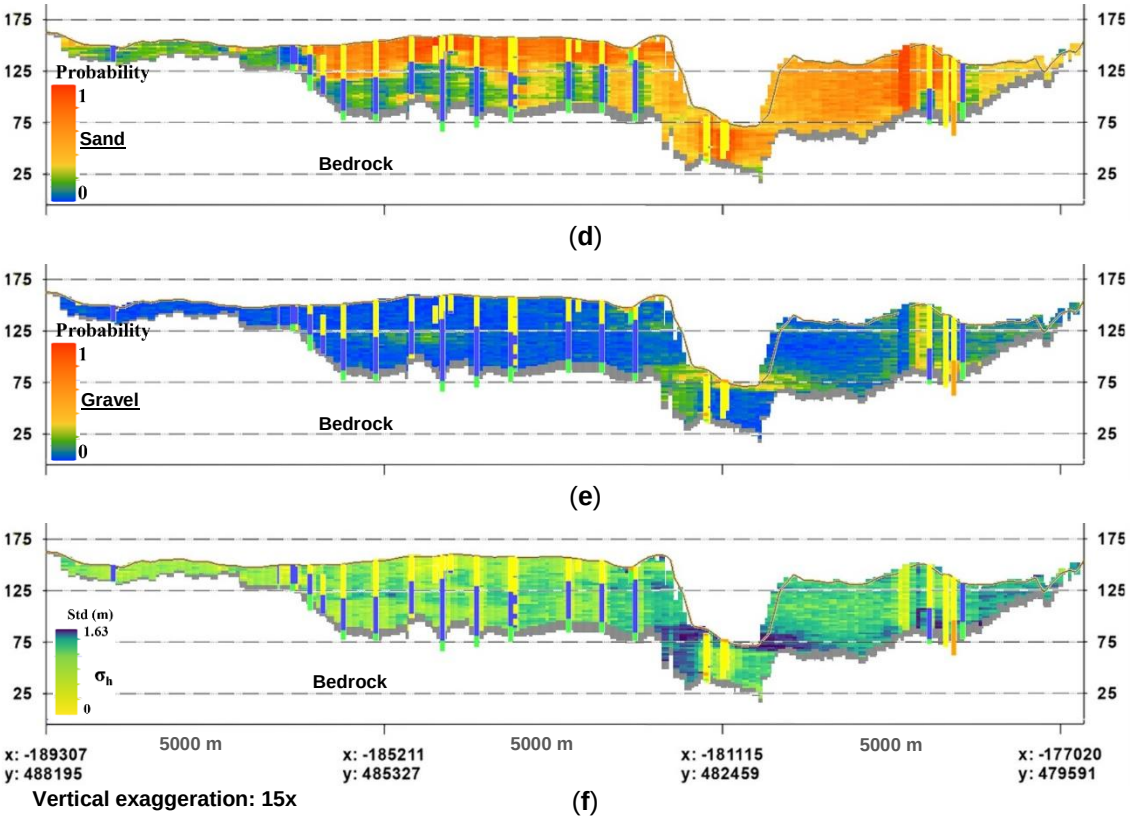

Figure 3-13. Stratigraphic cross-sections: (**a**) deterministic based on expert opinion (modified from CERM-PACES (CERM-PACES, 2013)); (**b**) soil units with the highest probability of occurrence based on conditional SIS; individual probabilities of occurrence for (**c**) clay, (**d**) sand and (**e**) gravel obtained from a set of 100 conditional SIS; and (**f**) total standard deviation (σ_h) of the thickness computed by using the probability of categorical distribution. © Mohammad Salsabili, 2022.

3.5.4. Thickness Maps of Discontinuous Soil Layers

The above 3D probabilistic model provides the spatial distribution of the discontinuous soil units and their probability of occurrence within the regular 75 × 75 × 2 m blocks. In the determination of seismic parameters at a site (e.g. $V_{s,30}$ and T_0), the geometry (soil thickness) and shear-wave velocity (V_{s_i}) of each soil layer are important variables. Therefore, the 3D model must be transformed into a set of 2D thickness maps to obtain the thickness of the individual discontinuous soil units. Thus, the thickness mean and variance of each block are computed

on the basis of the discrete probability distribution of the random categorical variable (X_i) with an event probability p_i as follows:

$$E(X_i) = p_i, Var(X_i) = p_i(1 - p_i), \tag{3-7}$$

where $E(X_i)$ is the mean, $Var(X_i)$ is the variance and $x_i \in \{0,1\}$, $i \in \{1, \dots, k\}$. The thickness mean and the variance are scaled at the 2 m height of the blocks, *h*, as follows:

$$E(hX) = hE(X), \tag{3-8}$$

$$Var(hX) = h^2 Var(X). \tag{3-9}$$

The thickness maps and the associated variances are obtained by computing the sum of the mean thickness and the variance of the blocks in a vertical column. In other words, the probabilities of occurrence are considered the weighting factors (Equation (3-8)) for the calculation of the soil thickness. In this case, the resulting thickness maps consider all the probabilities of occurrence for each soil type (not only the most probable one). The total variance for an individual soil unit (e.g. clay) is computed by summing up the block variance for each variable (Equation (3-9)) in a vertical column. The standard deviation is then computed as the square root of the total variance.

Figure 3-14 represents the weighted thickness maps based on the probability of discontinuous postglacial deposits (clay, sand and gravel units) and the associated standard deviations of the thickness. A single pixel on these maps represents the weighted sum of the 2-m-high blocks in a vertical column for the same individual soil unit. The comparison of the standard deviation and thickness maps reveals that the local thickness uncertainty depends mainly on the following factors: differences between the presence of the discontinuous soil units in the neighboring boreholes, the soil thickness values and the distances to the

observation points. In other words, the greater the differences in the thickness or the distance, the greater the standard deviation.

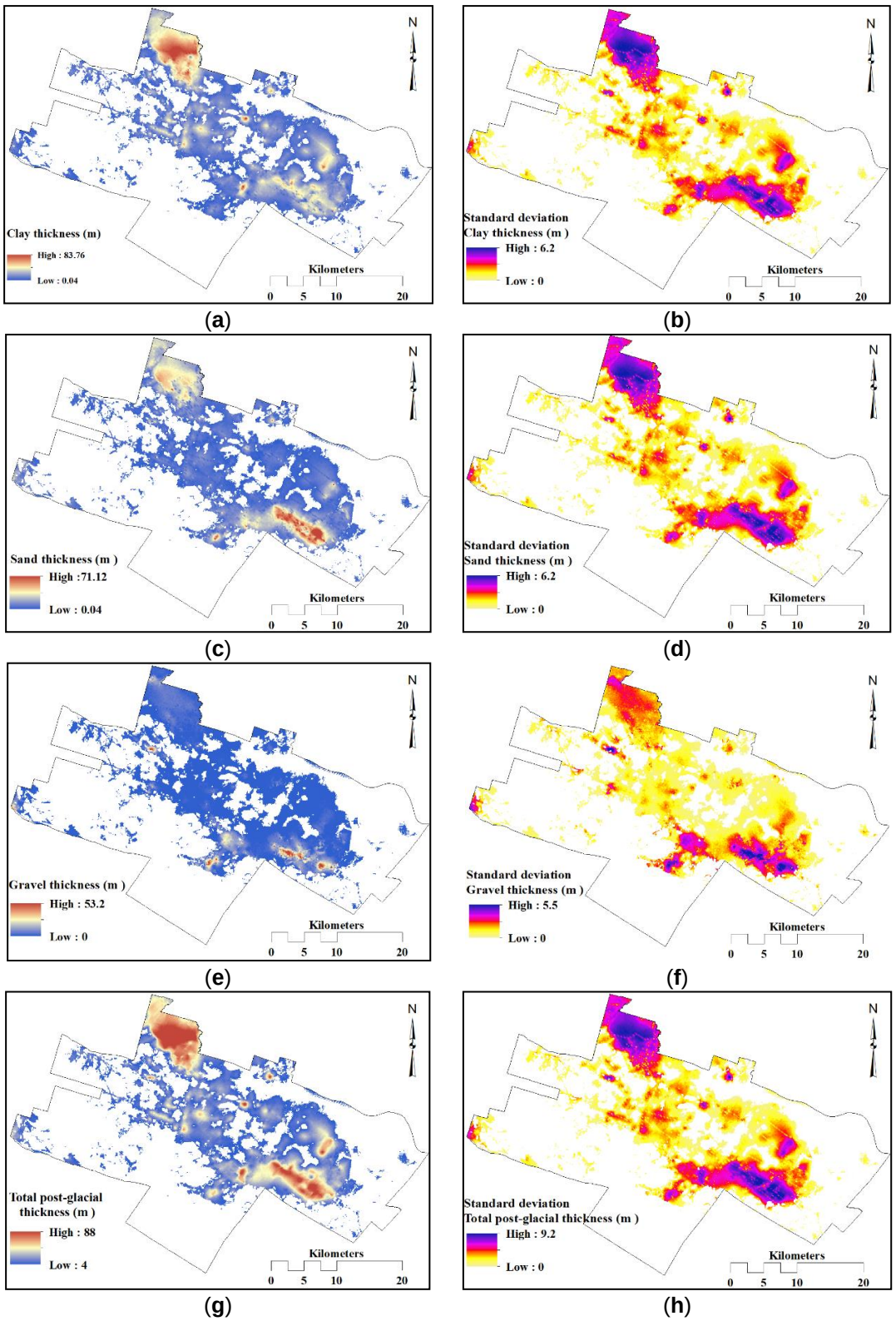

Figure 3-14. Spatial distribution of the weighted thickness and associated spatial standard deviation (σ_h) for (**a**,**b**) clay, (**c**,**d**) sand, (**e**,**f**) gravel and (**g**,**h**) total postglacial deposits. © Mohammad Salsabili, 2022.

3.6. Conclusions

This study adopted a combined multistep methodology of interpolation and simulation to develop a 3D geological model for geotechnical and seismic hazard evaluation at a regional scale. This approach focuses on considering geologic rules of stratification, reducing the effect of skewness of the observation points, and realistically predicting soil variability.

The interpolation procedure incorporates boreholes logs, in addition to the rock outcrop and shallow till data; these sources of data result in being invaluable in soil thickness mapping. Providing bedrock and till deposit maps allows considering the geologic rule of stratification of the basal till and the exclusion of low and zero thickness data from the simulation process of the discontinuous layers (i.e., clay, sand and gravel). The results of the validation and cross-validation verify that EBK is an appropriate interpolation method, producing an accurate outcome in regional studies involving extensive data with complexity.

SIS predicts the occurrence probability of discontinuous soil layers, as a representation of the soil type variability. The results indicate that the assumption of a continuous stratigraphic layer for the clay and for the sand and gravel units as drawn in the geological sections does not correspond to the real spatial variability of these layers. This observation is supported by the abrupt discontinuity and repetition of the deposits in the 3D model. The simulation of the soil type shows the benefit of considering the spatial soil variability and its associated uncertainty. The advantage is that the areas identified with increased uncertainty are characterised with considerable stratigraphic inconsistency and require further field measurements.

The proposed approach provides the basis for developing a reliable 3D shear-wave velocity model including its uncertainties. The 3D geological and velocity models can enhance the mapping of seismic site parameters (e.g. $V_{s,30}$ and T_0), which are important factors in seismic hazard assessment.

Author Contributions

Funding acquisition, A.S.; Methodology, M.S. and A.S.; Project administration, A.S.; Software, M.S.; Supervision, A.S., A.R. and M.N.; Writing – original draft, M.S.; Review & editing, A.S., A.R. and M.N.

Funding

This research was partially funded by the Natural Sciences and Engineering Research Council of Canada (NSERC) and Hydro-Quebec under project funding no. RDCPJ 521771 – 17.

Acknowledgments

The authors would like to thank the members of the CERM-PACES project for their cooperation and for providing access to the database.

Conflicts of Interest

The authors declare no conflict of interest

CHAPTER 4

DEVELOPMENT OF EMPIRICAL CPTU-V_S CORRELATIONS FOR POSTGLACIAL SEDIMENTS IN SOUTHERN QUEBEC, CANADA, IN CONSIDERATION OF SOIL TYPE AND GEOLOGICAL SETTING

Mohammad Salsabili [1], Ali Saeidi [1], Alain Rouleau [1] and Miroslav Nastev [2]

[1] Département des Sciences Appliquées, Université du Québec à Chicoutimi, G7H 2B1 Saguenay, Canada; mohammad.salsabili1@uqac.ca; alain_rouleau@uqac.ca

[2] Geological Survey of Canada, G1K 9A9 Quebec City, QC, Canada; miroslav.nastev@canada.ca

Abstract

The correlation of shear wave velocity (V_S) with piezocone penetration test (CPTu) parameters is investigated in postglacial sediments along the St. Lawrence and Saguenay rivers, Southern Quebec, Canada. The compiled database includes 991 CPTu-V_S measurements at 40 sites. The objectives are to examine the applicability of existing CPTu-V_S correlations, identify the main CPTu parameters and develop specific CPTu-V_S correlations that account for the effects of soil type (sandy or clayey) and geological setting (Champlain or Laflamme sea sediments). Results reveal that the application of existing correlations is biased in varying degrees, denoting a need for site-specific correlations for the study area. Multivariate regression analyses confirm the importance of cone tip resistance and depth as V_S predictors assisted by normalized pore pressure and soil behavior type index. Consideration of soil type and geological setting helps reduce uncertainties in CPTu-*Vs* correlations for fine-grained soils.

Keywords: Piezocone penetration test (CPTu); shear-wave velocity; seismic piezocone (SCPTu); multiple nonlinear regression; empirical correlation; soil behavior type (SBT)

4.1. Introduction

Shear-wave velocity (V_s) is among the key parameters in geotechnical investigations and dynamic site characterizations. This parameter defines the shear modulus (G_{max}) and behavior of soils at a small strain amplitude (Clayton, 2011). The V_s of the top 30 m is recommended in building code provisions for seismic site classification,(e.g. NRC (2015)) and used in microzonation studies at urban and regional scales (e.g. (SM Working Group, 2015; TC4-ISSMGE, 1999)). Accordingly, seismic site characterization requires sufficient V_s measurements that are obtained by performing in situ and/or laboratory tests.

In situ V_s measurements can be conducted with invasive methods, such as cross-hole or down-hole tests, or with non-invasive methods, e.g. refraction or surface wave methods (Garofalo et al., 2016a, 2016b; Hunter and Crow, 2012). The invasive seismic piezocone test (SCPTu) provides continuous subsurface profiling allowing the development of accurate empirical correlations between V_s and soil strength-based parameters. Interpretations of the soil stratigraphy (Vessia et al., 2020; Wang et al., 2019) are based on the CPTu parameters, such as cone tip resistance (q_t), sleeve friction (f_s) and friction ratio ($R_f = f_s/q_t$ in percent) in early studies (Robertson and Campanella, 1983) and normalized cone resistance (Q_{tn}) and friction (F_r) in recent studies (Robertson, 1990, 2009, 2016). The stress exponent (Zhang et al., 2002) and normalized pore pressure B_q (Schneider et al., 2008) are additional parameters used in defining soil behavior type index I_c. The classification of soil types is determined using either normalized SBT charts or indexes, such as B_q and I_c (Robertson and Wride, 1998), relating the normalized cone parameters to SBT.

CPTu-V_s correlations are traditionally developed through regression analysis using the CPTu parameters as a series of predictor variables and the measured V_s as a response variable. The V_s depends on in situ environmental factors, effective stress state, void ratio, water content (in saturated clay), cementation and aging (Mayne and Rix, 1995; Robertson, 2009). These parameters are regarded as potential sources of uncertainty for the development of CPTu-V_s correlations and limit the application of existing correlations that consider soil type, geological age and database locality (region-specific correlations) (McGann et al., 2015a).

Numerous CPT-V_s correlations have been reported in the literature using direct (q_t, f_s and Z), computed indirect (Q_{tn}, I_c and B_q) and/or other laboratory index parameters (e.g. OCR, e_0 and w) in literature (Table 1-6). The resulting equations are based on a limited data set and from different soil types with different geological structures and geotechnical conditions. Their applicability to regions with different soil structures, especially with sensitive clay, is questionable. Meanwhile, Southern Quebec clay layers have been deposited in at least two different invading paleo sea-water bodies, namely, Laflamme and Champlain Seas, with various source rocks and geological conditions for sea-bottom soil deposits, thereby pointing out the need for region-specific CPTu-V_s correlations.

The primary objective of the present study is to develop a region-specific CPTu-V_s correlation for postglacial soil deposits of Southern Quebec, Canada. These surficial sediments were deposited following the Wisconsinan glacial period, during the invading Laflamme and Champlain sea episodes and their retreat. In addition to the fine marine (clay) and coarser littoral and alluvial (sand and gravel) sediments, they often contain soft and sensitive clays (Locat and St-Gelais, 2014). A field testing program is implemented, and a comprehensive dataset of acquired geotechnical parameters is created. Next, the applicability of existing equations for predicting measured V_s values is evaluated. Nonlinear regression analyses are then performed to develop CPTu-V_s correlation equations on the basis of the specific soil type and postglacial sedimentation basins of the ancient Laflamme (Saguenay River) and Champlain (St. Lawrence River) Seas.

4.2. Study area

The study area covers several of the most populated regions in Southern Quebec along the St. Lawrence and Saguenay rivers, including Trois-Rivières, Quebec City and Saguenay City.

4.2.1.Bedrock and surficial geology

The postglacial sediments consist of Champlain and Laflamme sea sediments originating from glacial abrasion of the surrounding bedrock lithology around 14,000 BP to 8,000 BP. The source rocks of the sediments in this region can be generally divided into three main geological provinces (Fulton et al., 1986; Locat and St-Gelais, 2014): (1) the Canadian Shield to the north (Precambrian crystalline metamorphic rocks), (2) St. Lawrence Platform (Palaeozoic sedimentary rocks, mainly sandstone and limestone) and (3) the Appalachians to the south (Palaeozoic sedimentary rocks, mainly shales, sandstones, volcanic and minor carbonates). The deposit layers in the paleo-sea bottoms are characterized by various sedimentation mechanisms and grain-size distributions, such as fine marine sediments and coarse littoral, sublittoral, alluvial and even deltaic sands. After deposition, these sediments were topographically uplifted due to glacial melting and exposed to subsequent erosion and occasional leaching of salts from the initial pore water. The latter process affects the sensitivity of fine silty–clayey sediments. Locat and St-Gelais (Locat and St-Gelais, 2014) reported that the primary mineral (non-clay) content is from 62% and 80%, whereas the amount of clay minerals ranges from 9% to 34 % in sensitive fine-grained sediments. According to the grain size composition, soil deposits can be regrouped into four major categories, namely, clay, sand, gravel and other recent sediments (Daigneault et al., 2011; LaSalle and Tremblay, 1978).

- Clay: These fine-grain postglacial sediments are composed mainly of silt, silty clays and clay. They have a general thickness of up to 10 m and may attain a maximum thickness of >100 m in lowlands.
- Sand: This group consists mainly of coarse glaciomarine deltaic and prodeltaic sediments and alluvial sands composed of sand and gravely sands.
- Gravel: This coarse sediment is mainly of glaciofluvial and alluvial origin; it consists of gravel, sand and sometimes till.
- Other sediments: This highly heterogeneous category comprises all remaining sediments; it mainly includes loose postglacial sediments consisting of alluvium, floodplain sediments, organic sediments and occasional landslide colluvium.

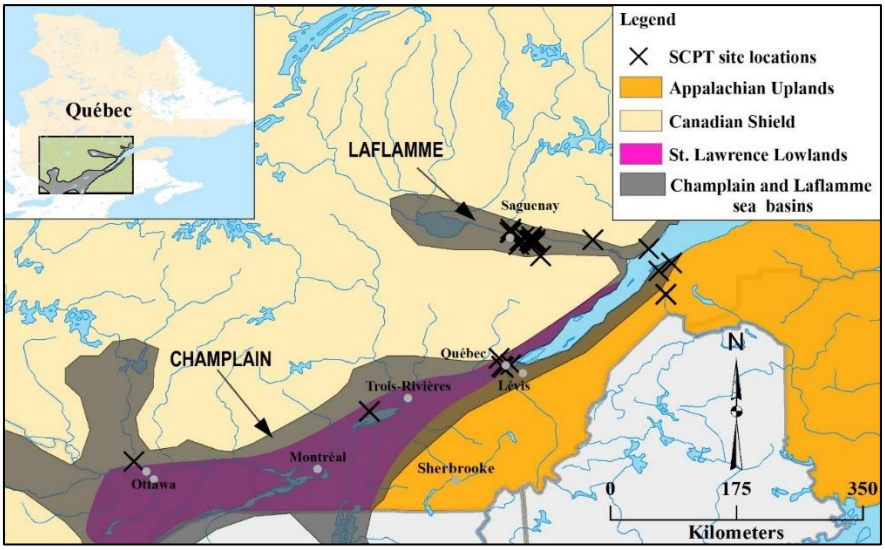

Figure 4-1. Geological provinces and distribution of SCPTu site locations. The grey area represents the spread of marine clays (modified from Locat and St-Gelais (Locat and St-Gelais, 2014)). © Mohammad Salsabili, 2022.

4.2.2.Field testing

Field SCPTu testing was conducted in this study to improve the data coverage in the territory of Saguenay City (Figure 1). SCPTu soundings were carried out using a standard type 2 piezocone with the following specifications: 60° apex angle, 10 cm^2 base area of the conical tip and 150 cm^2 sleeve area with the filter located at the shoulder. A dual-array seismic cone was mounted on the top of the piezocone. The addition of seismic sensors (usual geophones) allows the measurement of the arrival of vertically propagating seismic body waves generated from a source on the ground surface. For a given depth, the SCPTu method generates four types of data, namely, V_s, raw cone tip resistance q_c, frictional cone resistance f_s and penetration pore pressure u_2. Notably, q_c and f_s are soil characteristics in large strains (Mayne and Rix, 1995). All SCPTu soundings were performed at a penetration rate of 2 cm/s. High-resolution CPTu data were collected every 1 cm, and V_s values were recorded at each 50 cm depth interval. Shear-wave velocities were determined from seismic signals by applying the cross-correlation algorithm (Campanella and Stewart, 1992).

4.2.3.Database

The final soil database includes 27 recent SCPTu soundings conducted by the Quebec Ministry of Transportation (MTQ) and 13 SCPTu soundings conducted by the Université du Québec à Chicoutimi (UQAC) research group as described above. The data contained a complete set of direct measurements: q_c, f_s, $u_{2,}$ depth and V_s. For a comparison between V_s and CPTu data pairs, the average of the CPTu data was calculated based on the same intervals as those of the V_s measurements: 50 cm for UQAC and 100 cm for MTQ tests. High variability of in situ V_s at shallow depth is observed due to the presence of surface noise and 'freeze–thaw cycles' of surficial soil deposits (Motazedian et al., 2011). After data processing, 991 CPTu-V_s data pairs were retained for the analyses. Figure 4-2a shows a histogram of V_s values, which varied from 92 m/s to 445 m/s with an approximate normal distribution. The V_s values were assumed to be consistent over the interval between two measurements, and the midpoint of each interval (Z) was assumed to be the depth of the measured V_s (Figure 4-2b). In contrast to the relatively symmetrical distribution of V_s, the penetration values (q_t, f_s and u_2) show skewed distributions mainly due to the mixture of different soil types (Figures 2c–2e).

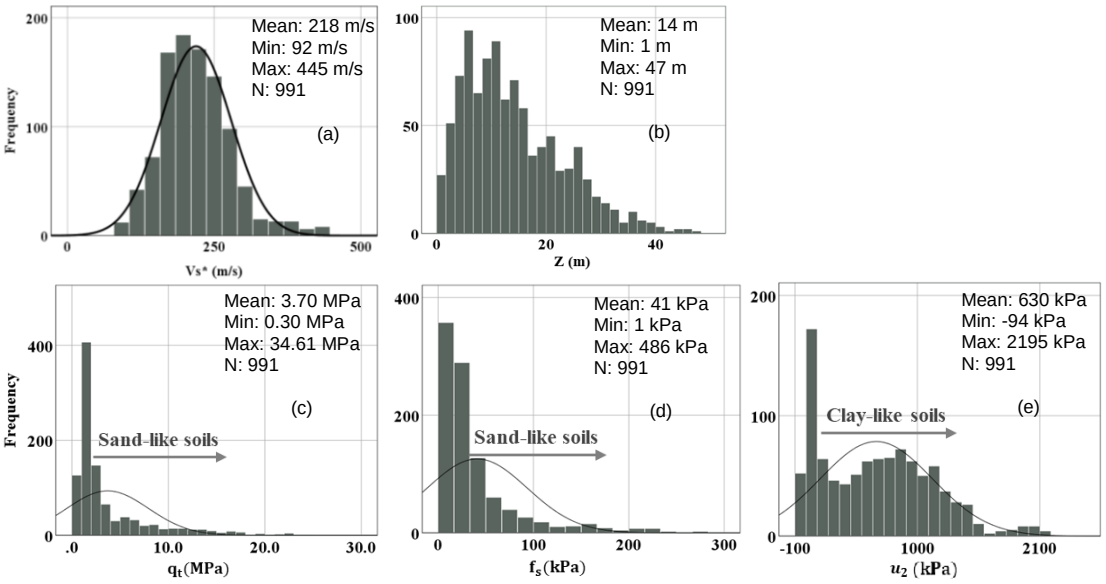

Figure 4-2. Distributions of (a) measured shear-wave velocity V_s, (b) midpoint depth Z, (c) cone tip resistance q_t, (d) sleeve friction f_s and (e) pore pressure measured behind the cone u_2. The black line represents the normal distribution. © Mohammad Salsabili, 2022.

4.3. Soil classification

The collected test results include data from various depositional environments and a wide range of soils, such as glaciofluvial deposits, marine clays, littoral, sublittoral deposits and in some parts deltaic sand. Under such conditions, the soil physical characteristics (e.g. grain size and plasticity) vary significantly in vertical and horizontal directions, thus introducing heterogeneity in soil types from fine silty clay soils to coarse gravelly sands. Soil classifications were performed using widely accepted CPTu-based charts and indexes (shown below) to determine the soil stratigraphy in the study area, particularly in locations with transitional soil types.

i) Soil behavior index (I_c) is a function of normalized cone measurements Q_{tn} and F_r (Robertson, 2009). It applies textural-based descriptions for interpretation of the soil type, such as sand or clay. I_c increases with increasing apparent fine content, and soil plasticity with I_c=2.6 is accepted as a rough threshold between sand-like or clay-like

behavior for normally consolidated soils. However, a problem may arise in the classification of transitional soils with I_c around 2.6.

ii) Normalized soil behavior type (SBTn) charts proposed by Robertson (2009) and then updated (Robertson, 2016). The charts link Q_{tn} and F_r to soil types, and the latest chart (Robertson, 2016) delineates the in situ behavior of soils, such as being sensitive, contractive or dilative.

iii) Soil classification based on the normalized cone tip resistance (Q_{t1}) and normalized excess pore pressure (B_q) proposed by Schneider et al. (Schneider et al., 2008). It uses normalized parameters, and the resulting classification is based on textural descriptions.

The analysis of the postglacial soil type behavior revealed the presence of two major soil groups: silt mixtures, clayey silt or silty clay ($2.6 < I_c < 2.95$) and clean to silty sand ($1.31 < I_c < 2.05$). Clays ($2.95 < I_c < 3.6$) and sand mixtures ($2.05 < I_c < 2.60$) are encountered less frequently (Figure 4-3a). The recently developed SBTn plot, shown in Figure 4-3b, can predict soil behavior in a detailed manner. The major part of the tested fine soils in the St. Lawrence Lowlands includes sensitive clays (CCS type) and transitional contractive soils (TC type), which are generally loose and potentially liquefiable. Clean sands make up the other soil group recognized as a dilative behavior type (SD). An important part of the results was identified as transitional soils, for which the interpretation of CPT measurements becomes challenging when soil-specific correlations for sands or clays are used.

Drainage conditions during CPTu measurements provide useful information for the classification of transitional soils. The method developed by Schneider et al. (Schneider et al., 2008) applies B_q to the delineation of CPTu penetration conditions (drained, undrained or partially drained). Through this approach, the soils in the current study were classified into three distinct groups: sand, silt and clay (some clays are sensitive), as shown in Figure 4-3c.

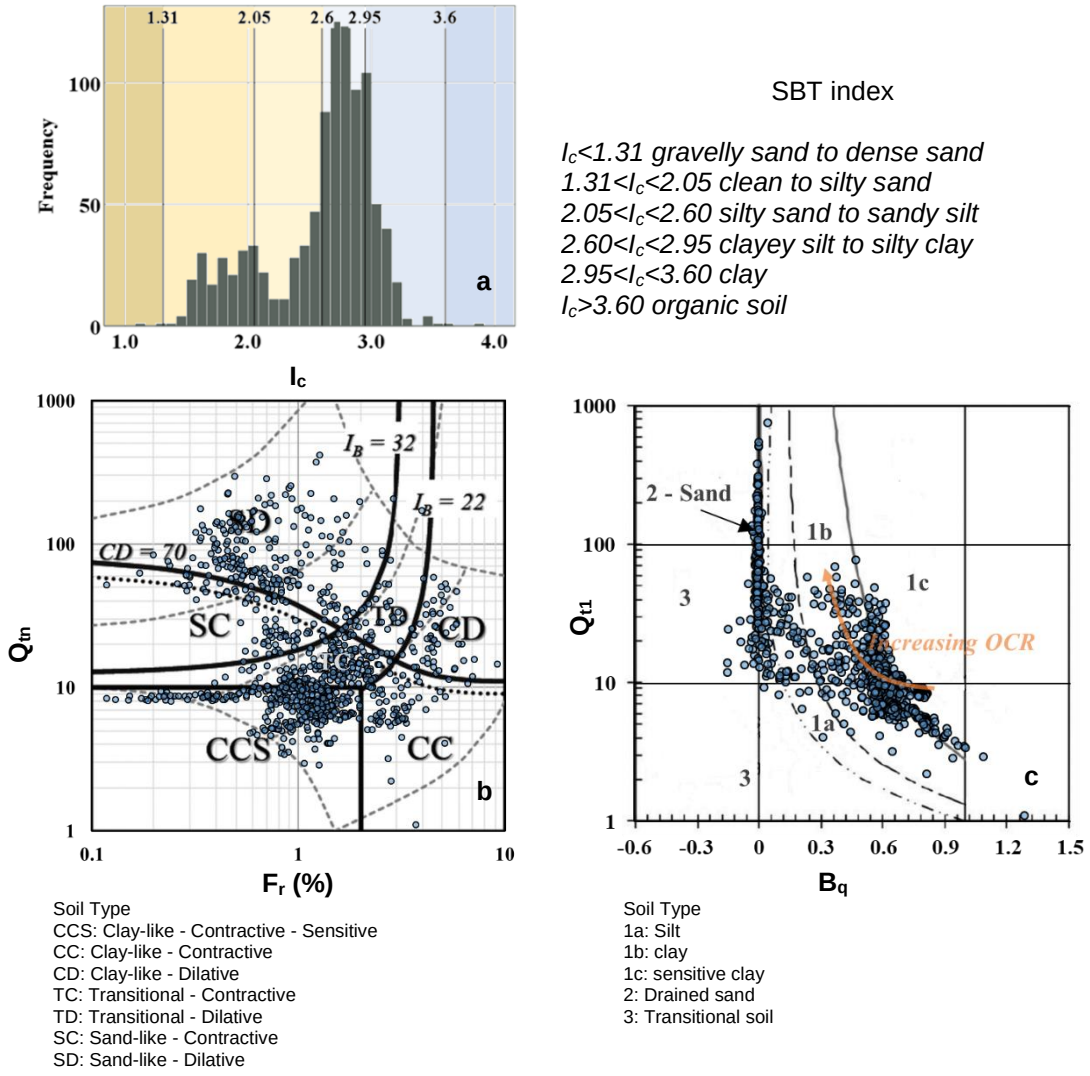

Figure 4-3. Soil behavior types based on three different approaches: (a) soil behavior type index I_c (Robertson, 2009), (b) Q_{tn}–F_r (Robertson, 2016) and (c) Q_{t1}–B_q (Schneider et al., 2008). © Mohammad Salsabili, 2022.

Figure 4-4 shows an example of a SCPTu profile in transitional soils. Here, B_q can be used to interpret the behavior of transitional soils and distinguish between clay- and sand-like materials. Specifically, transitional soils with B_q > 0.1 can be classified as clay or silt soils, and this is more informative than the classification based on Robertson's approach (Robertson, 2016) with TC type and more accurate in parts with SC soil behavior types.

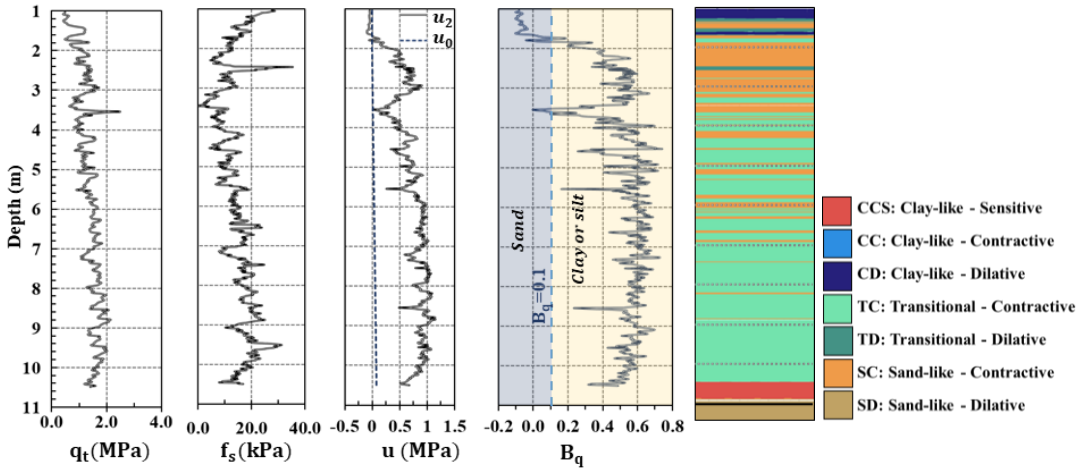

Figure 4-4. Example of SCPTu sounding (SCPT-C37-19) in a site exposed to transitional soil layers, soil classification based on Robertson (2016). © Mohammad Salsabili, 2022.

The main challenge in using the pore water pressure-related parameters is the unsaturated zones, where interpretations may be unreliable. Scholars recommend the application of a combination of CPTu-based results to reduce the soil classification bias (Robertson, 2016). In this study, I_c and B_q were regarded as the main criteria for soil classification.

4.4. Evaluation of the applicability of selected CPTu–V_s correlations

Many studies have analyzed the correlations between measured V_s values and CPTu parameters (Table 1-6). The applicability of these correlations to postglacial deposits in Southern Quebec was assessed in this work. The important characteristics of these correlations are described by the following points.

- Cone tip resistance is recognized as the governing variable in all correlations. It is applied as a direct (q_c or q_t), net ($q_n = q_t - \sigma_{v0}$) or normalized (Q_{tn}) parameter.
- CPTu-V_s correlations are developed using direct, indirect or normalized parameters. Stress-normalized quantities for both V_s and CPTu parameters are suggested to remove the effect of overburden pressure (Hussien and Karray, 2015; Karray and Hussien, 2017), however, some studies prefer direct parameters over computed or normalized parameters due to the potential uncertainty involved in their calculation (McGann et al., 2015b; Tong et al., 2018).

- CPTu-V_s correlations are developed with or without consideration of the soil behavior type (e.g. (Mayne and Rix, 1995; Perret et al., 2016)). For soil type-specific correlations, challenges are encountered in transitional soils wherein differentiation of soil types is difficult (Karray and Hussien, 2017).

- Aging and local specific depositional environment significantly affect the correlations (Andrus et al., 2007).

- Laboratory index soil parameters improve the predictive accuracy of regression functions (Karray and Hussien, 2017; L'Heureux and Long, 2017). However, the obtainment of undisturbed continuous samples is not performed in all geotechnical studies; the applicability of the equations is limited to a specific site or region where laboratory tests are available (Cai et al., 2014).

- Stress state is recognized as a governing factor and can be identified by the initial effective stress for both V_s (Brandenberg et al., 2010; Motalleb Nejad et al., 2017) and CPTu parameters (Hussien and Karray, 2015).

- Theoretically, effective stress is preferred to depth, but due to the uncertainty in the determination of the unit weight and water level, using Z as an indicator of the stress state results in better correlation coefficients (Tong et al., 2018; Zhang and Tong, 2017).

- The CPTu-V_s relationships are modelled by applying logarithmic transformations or nonlinear regression analysis.

Amongst the V_s prediction equations presented in Table 1-6, the six most widespread equations were developed by Mayne and Rix (1995), Andrus et al. (2007) for Pleistocene soils, Robertson (2009), Long and Donohue (2010), McGann et al.(2015b) and Perret et al. (2016) are tested for the soil dataset. These equations apply different CPTu parameters for specific or general soil type, and a comparative analysis helps understand their significance and reliability in the study area.

The selected CPTu-V_s correlations were applied to the 40 SCPTu profiles in this study, and the predicted V_s values were compared with the measured V_s. Three parameters were used to evaluate and compare the individual performance.

- Mean bias error: $\mathrm{MBE} \cong \frac{1}{n}\sum(measured\ V_s - predicted\ V_s)$, where n is the number of samples;

- Root mean squared error: $\mathrm{RMSE} \cong \sqrt[2]{\frac{1}{n}\sum(measured\ V_s - predicted\ V_s)^2}$;
- R^2: coefficient of determination.

Figure 4-5 illustrates the overall scatter plots of the measured and predicted V_s values applying the six existing correlations. MBE or the bias indicates the systematic error of a prediction model to underestimation (positive values) or overestimation (negative values). Herein, all the models were biased in varying degrees. The models of Andrus et al. (2007) and Perret et al. (2016) had the least bias with MBE = 11 and 13 m/s, respectively, whereas those of Robertson (2009) and McGann et al. (2015b) showed the highest bias with 50 and 72 m/s, respectively. The RMSE of the two latter models was also high (64 and 82 m/s), and their R^2 was <0.5, making them the two most poorly predictive models. In terms of R^2, the models of Andrus et al. (2007) and Mayne and Rix (1995) had the highest R^2 value of 0.64. All the models presented an underestimation of V_s, particularly for V_s > 270 m/s in the soil database, except for the model of Long and Donohue (2010) in which MBE was negative (−29 m/s). Overall, Andrus et al.'s (2007) prediction model that was developed for Pleistocene soils appeared to be the best model with lower MBE and RMSE and higher R^2 than the others. An interesting feature of the model is that the model was developed for general soil types and is independent of u_2 parameters (applicable for non-piezocone data).

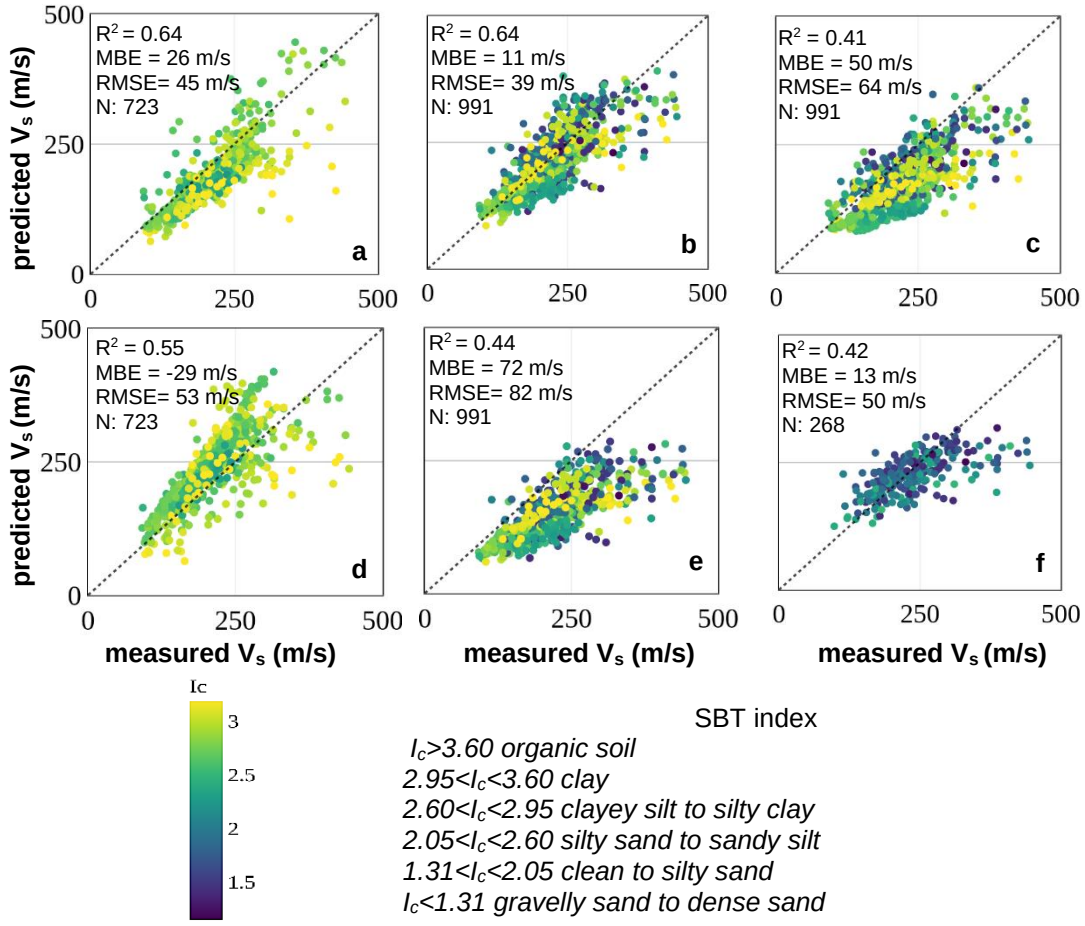

Figure 4-5. Performance of selected existing CPT–V_s correlations in Quebec soil deposits. (a) Mayne and Rix (1995), (b) Andrus et al. (2007) for Pleistocene, (c) Robertson (2009), (d) Long and Donohue (2010), (e) McGann et al. (2015b) and (f) Perret et al. (2016). © Mohammad Salsabili, 2022.

To compare the predicted values with the measured V_s values, an example is given for a site with two distinct soil layers (sandy to silty layer) that are approximately 11 m thick with overlying deep clayey soils (Figure 4-6). The V_s values at shallow depth (< 4 m) shows high variability due to the surficial noise (e.g. freeze and thaw cycles and human activities). The V_s values gradually increased in the sandy layer in correlation with q_t, f_s and depth until it approached the value for clay soils. Then, the values began to decrease, and after experiencing a reduction, they became practically constant in the clayey layer. The comparison suggests that in most of the predicted profiles, the V_s values were underestimated to various

degrees. The only model that overestimated the clay V_s values was that of Long and Donohue (2010) for Norwegian clays. However, the prediction results of the models of Perret et al. (2016) and Andrus et al. (2007) had better correlations. Similar observations were obtained for the other profiles, suggesting the necessity for the development of region-specific V_s prediction models.

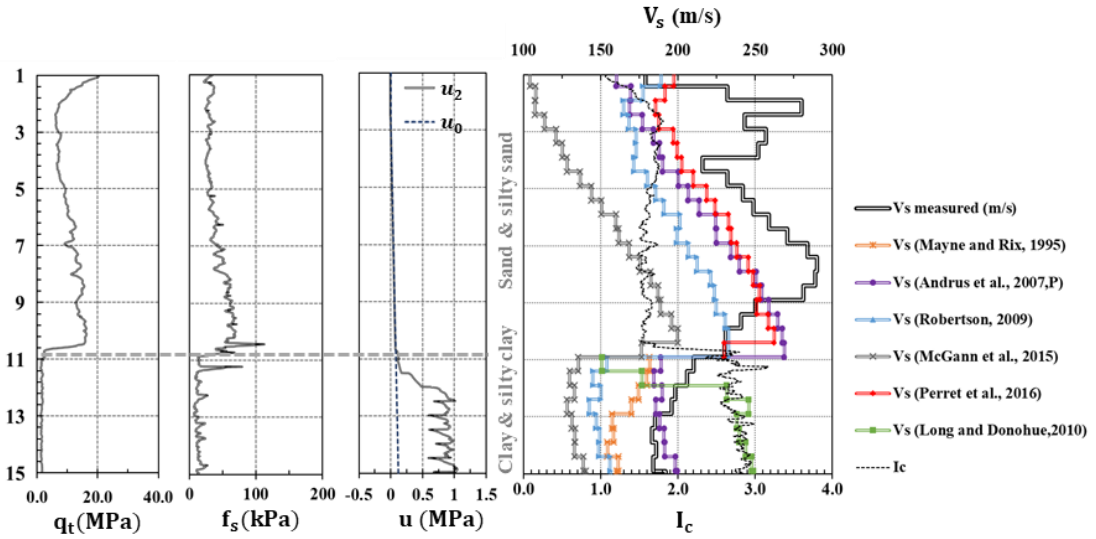

Figure 4-6. Example of SCPTu profiling (SCPT-23F) in a site exposed to two distinct soil layers: comparison of in-situ measured and predicted V_s profiles. © Mohammad Salsabili, 2022.

4.5. Development of empirical CPTu-V_s and -V_{s1} correlations

In light of the results shown above, we developed region-specific CPTu-V_s correlations for postglacial soil deposits in Southern Quebec. We conducted the analysis for the general soil dataset first, followed by the analysis for clay-like and sand-like soil types.

4.5.1. Correlations for the general soil database

To perform the regression analysis, the relationships between the CPTu-based variable and V_s were visually investigated to determine the effect of individual predictors on response variables V_s and V_{s1} (Figure 4-7). V_s is in m/s; q_t, q_c, f_s, σ_{v0} and $\acute{\sigma}_{v0}$ are in kPa; p_a =

100 kPa; and Z is depth in meters. A positive correlation was observed between the direct CPTu measurements and V_s, and it was attributed to the soil's stiffness properties and overburden pressure (Figure 4-7a). The stress dependency between the predictors and response variables affects the calibration of the regression parameters (Kishida and Tsai, 2017; Tsai et al., 2019). To eliminate this effect, the overburden pressure is accounted for in the parameters *Vs,* q_t, f_s and u_2. *Vs* and q_t are generally normalized for vertical effective stress, whereas sleeve friction (f_s) and excess pore pressure ($\Delta u = u_2 - u_0$) are normalized with respect to the corrected net tip resistance ($q_t - \sigma_{v0}$) known as stress-normalized parameters (V_{s1}, Q_{tn}, F_r and B_q) (Robertson, 2009). The linear V_{s1}–Q_{tn} correlations in sand-like soils (Figure 4-7b) and the V_{s1}–depth correlations (Figure 4-7c) in clay-like soils should be considered. Applying stress-normalized parameters for clay models appears to be questionable due to the V_{s1}–depth correlation (the depth remaining dependency). The data pairs are colored with respect to I_c, demonstrating that the correlation between CPTu parameters and V_s is strongly affected by the soil types and essentially nonlinear.

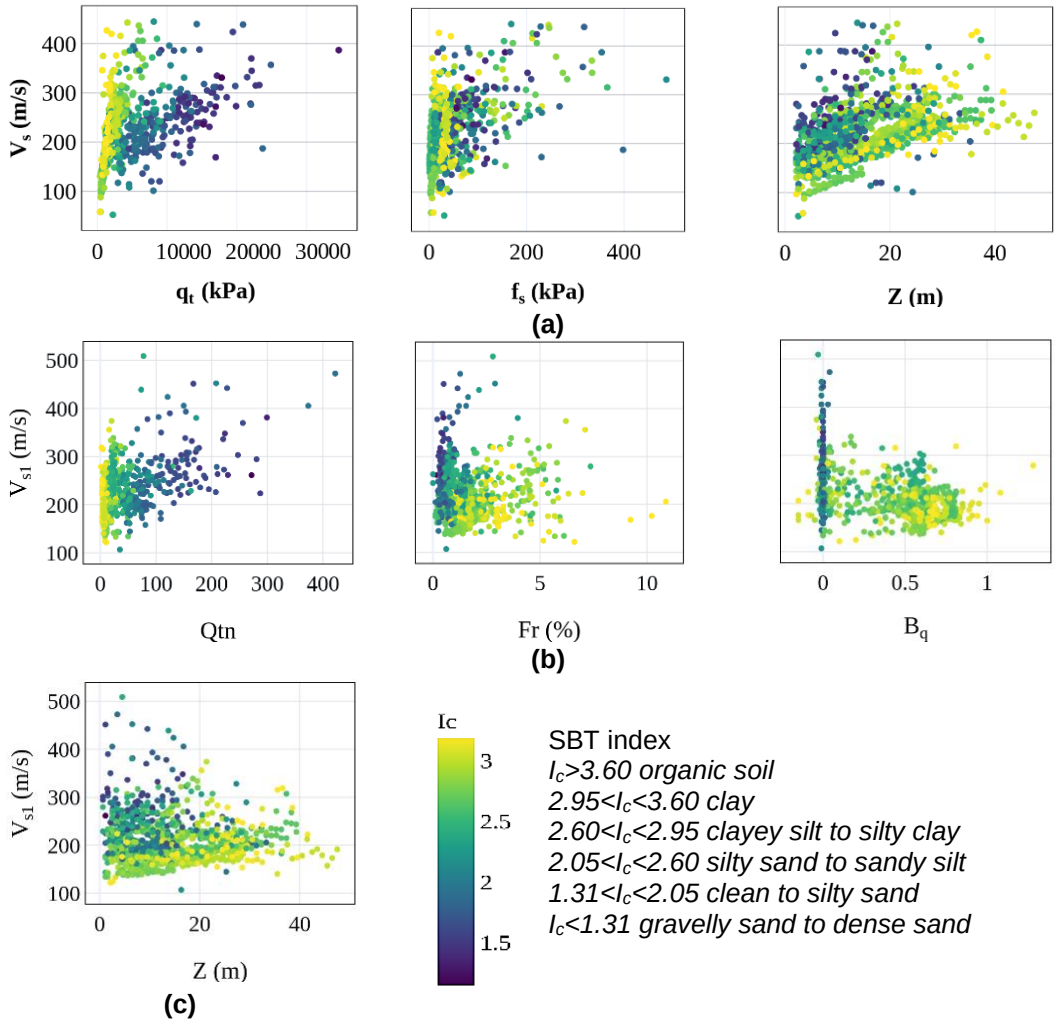

Figure 4-7. Relationship between (a) V_s and direct, (b) V_{s1} and normalized CPTu-based parameters and (c) V_{s1} and depth.

The next step in setting up the empirical CPTu-V_s and -V_{s1} correlations was the assessment of the functional forms of the regression. To this end, the efficiency of existing regression models for V_s prediction discussed in Chapter 4 served as the basis for testing more than 50 nonlinear regression functions (see Appendix). The importance and performance of each model were evaluated based on the statistical parameters R^2, RMSE and the standard error of the coefficients (SE). The models with a low SE ratio (SE/coefficient value), high R^2 and low RMSE were used as predictors. Table 4-1 provides the selected regression equations for general soils based on acceptable R^2, RMSE and SE ratio. Additional details are presented in the Appendix (Tables A1 and A3). The following points were observed.

- q_t is the governing CPTu parameter and I_c is the most important soil indicator in the CPTu-*Vs* correlation (Eq. (4-1)).
- The use of q_t and f_s alone cannot predict V_s properly for general soil types.
- Applying depth in non-stress-normalized equations is important, with an increase in R^2 by 3% (Eq. (4-2)).
- Applying B_q together with q_t, Z and I_c, produces a slightly improved result in terms of R^2 and RMSE and makes Eq. (4-3) the best correlation.
- The adoption of σ'_{v0} as an indicator of the stress state slightly outperforms depth in sands, but not in general and clayey soils (Appendix, Table C1, comparison between Eqs. C7 and C8).
- Depth plays a crucial role in V_{s1} correlations for general and clayey soils. Its role questions the use of stress-normalized V_s for the two groups (Appendix, Table C3, Eq. B5).

Table 4-1. Regression equations of V_s and CPTu parameters for general soils of Quebec

	Equation No.	Model equations	R^2	RMSE (m/s)
Non-stress-normalized V_s	Eq. (4-1)	$V_s = 3.666 q_t^{0.387} I_c^{1.133}$	0.618	37
	Eq. (4-2)	$V_s = 6.299 q_t^{0.329} I_c^{0.827} Z^{0.082}$	0.648	35
	Eq. (4-3)	$V_s = 3.868 q_t^{0.386} I_c^{0.881} Z^{0.048} (1 + B_q)^{0.225}$	0.658	35
Stress-normalized V_s	Eq. (4-4)	$V_{s1} = 84.652 Q_{tn}^{0.194} I_c^{0.371}$	0.367	39

To compare the R^2 of normalized and non-normalized correlations, the predicted V_{s1} values were transformed into V_s. Figure 8 shows that the V_{s1} correlation resulted in a relatively lower R^2 using Eq. (4-4). The remaining dependency of Vs on depth after stress normalization could explain this finding (Appendix, Table C3, Eq. B5).

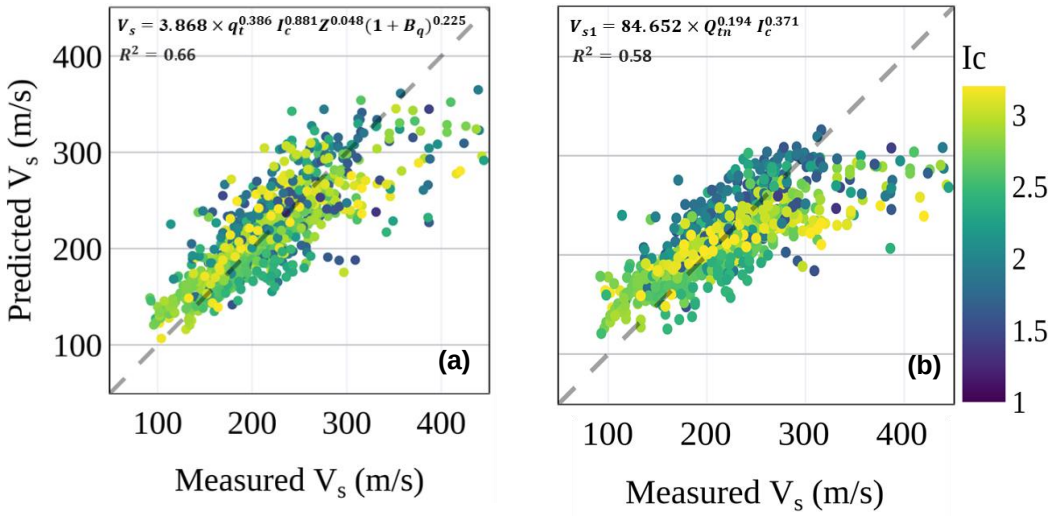

Figure 4-8. Comparison of measured and predicted V_s of regression functions for general soil type by using (a) Eq. (4-3) and (b) Eq. (4-4). R^2 is the coefficient of determination between the transformed predicted V_{s1} and the measured V_s.

Consequently, Eq. (4-3) is considered appropriate for general soil types within the range of 90 < V_s < 445 m/s. However, it is more suitable for values of V_s < 340 m/s because 97.5% of data are below this limit (less than two standard deviations). In terms of RMSE, the uncertainty in V_s estimation with Eq. (4-3) was 35 m/s. A comparison of the other V_s correlations obtained by invasive methods (i.e. SPT-N in (Tsai et al., 2019)) showed that the regression CPTu-V_s model had a lower level of uncertainty.

4.5.2.Correlations for specific soil types

The soil classification conducted in section 4-3 revealed that transitional soils represent a relatively important group of soils and their differentiation into one of the two main soil types (clay-like or sand-like) is a challenging task at risk of misclassification. Karray and Hussein (2017) demonstrated that V_{s1}–Q_{tn} correlations exhibit different trends with respect to grain sizes, and D_{50} = 0.2 mm can be recognized as the threshold for separating sands from clays. In the current study, the V_{s1}–Q_{tn} relationships were examined to distinguish the behavior of transitional soils with respect to I_c as an indicator of soil type.

Figure 4-9a shows visually that the correlations between $(V_{s1}/Q_{tn})^{\alpha}$ and I_c increased with an increase in α. For instance, for α = 0.75, a strong positive nonlinear correlation was identified between (V_{s1}/Q_{tn}) ratio and I_c. However, the increase in exponent α resulted in two different behaviours. For $I_c \leq 2.2$, the discrepancy decreased in such a way that a linear correlation was observed between (V_{s1}/Q_{tn}) ratio and I_c. For $I_c > 2.2$, the scattering remained unchanged (Figure 4-9b).

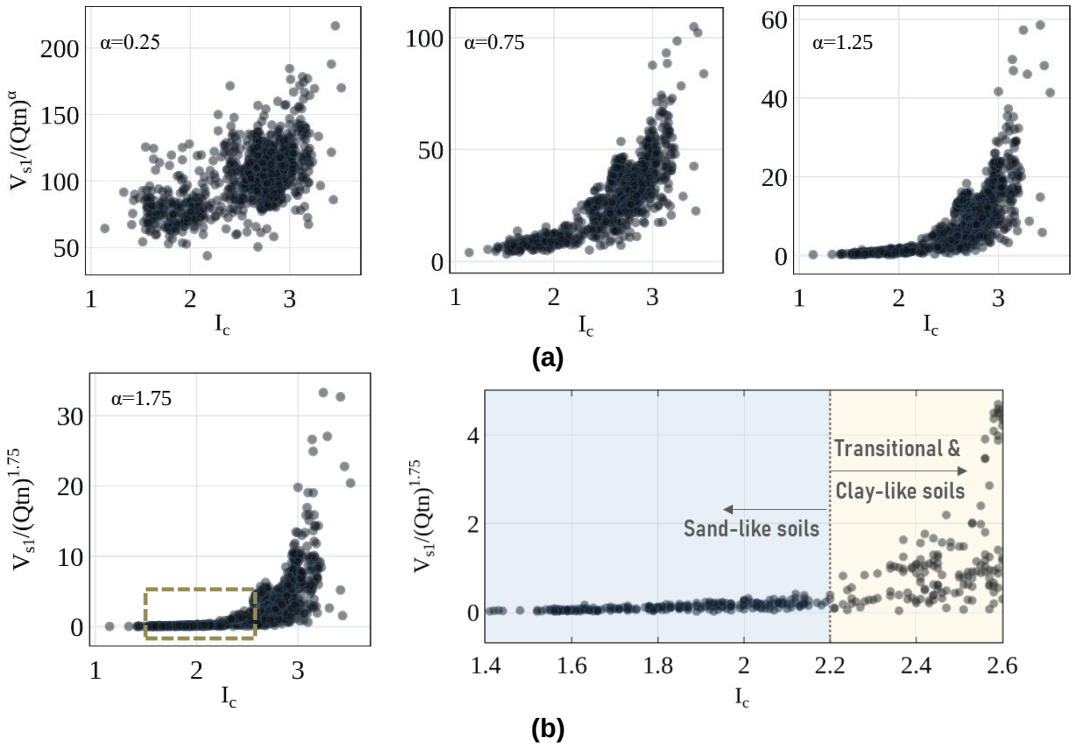

Figure 4-9. Relationships of $V_{s1}/(Q_{tn})^{\alpha}$ ratio with I_c: (a) variations with the increase in exponent α, and (b) different behaviors of sand-like ($I_c < 2.2$) and clay-like ($I_c > 2.2$) soils when α = 1.75.

The classification of sand-like soils ($I_c < 2.2$) from the clay-like ($I_c > 2.2$) soils was also examined by visual inspection using the scatterplot of I_c-B_q (Figure 4-10a). The limit of $B_q < 0.1$ was observed for sandy soils. The V_{s1} distributions of the two classes indicate that the V_{s1} of the sandy soils tend to have relatively higher and more dispersed values compared with the clay soils (Figure 4-10b).

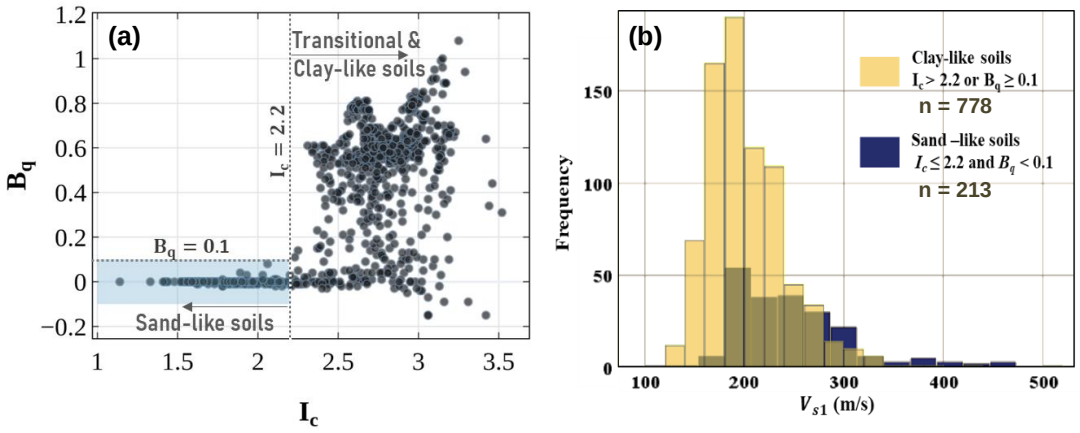

Figure 4-10. (a) Variation in B_q and I_c of data pairs, and (b) distributions of Vs_1 based on soil type behavior.

Owing to the different behaviors of cohesive (clay-like) and cohesionless (sand-like) soils presented in Figure 4-9b, regression equations were developed based on soil behavior types and stress-normalized parameters (see Appendix). Soil behavior type indexes I_c and B_q were used to define the two soil categories.

- Clay: $I_c > 2.2$ or $B_q \geq 0.1$
- Sand: $I_c \leq 2.2$ and $B_q < 0.1$

The resulting regression models are summarized in Table 4-2 which shows that the discrepancy in the fitting model for clayey soils was considerably lower (higher R^2 and lower RMSE) than that of the model developed for sand-like soil. The other observed points are as follows:

- Using depth as a direct parameter of the stress state improved the accuracy of the clay-specific models.
- In the sand-specific models, consideration of the effective stress resulted in a slight increase in R^2 (0.52) than what was the case with depth ($R^2 = 0.51$) (Appendix, Table C1, Eqs. A7 and A8).
- Stress-normalized V_s was inapplicable for the development of clay-specific models due to the dependency of V_{s1} on depth Z (Appendix, Table C3, Eq. B5). In the sand-specific models, however, a slightly higher accuracy was obtained when stress normalization was performed. The transformed predicted V_{s1} using Eq. (4-9) showed a marginally higher R^2 and better performance compared with that using Eq. (4-8) (Figure 4-11).

Table 4-2. Soil-specific regression equations of V_s and CPTu parameters

	Equation No.	Model equations	R^2	RMSE (m/s)
		Clay-like soils		
Non-stress-normalized V_s	Eq. (4-5)	$V_s = 19.285 q_t^{0.274} Z^{0.138}$	0.675	33
	Eq. (4-6)	$V_s = 7.86 q_t^{0.324} I_c^{0.61} Z^{0.099}$	0.700	32
	Eq. (4-7)	$V_s = 5.303 q_t^{0.371} I_c^{0.657} Z^{0.069} (1 + B_q)^{0.16}$	0.702	32
		Sand-like soils		
Non-stress-normalized V_s	Eq. (4-8)	$V_s = 4.416 q_t^{0.378} I_c^{0.53} \acute{\sigma}_{Vo}^{0.053}$	0.52	43
Stress-normalized V_s	Eq. (4-9)	$V_{s1} = 36.305 Q_{tn}^{0.361} {I_c}^{0.476}$	0.421	45

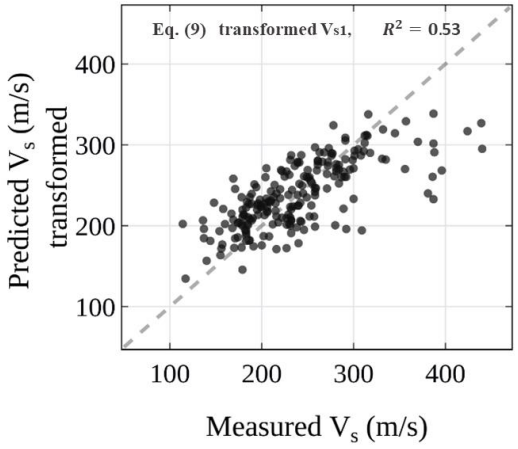

Figure 4-11. Comparison of measured and predicted V_s for the sand-like stress-normalized model (Eq. (4-9)). R^2 is the coefficient of determination between transformed predicted V_{s1} and measured V_s.

Figures 4-12 presents the linear correlations between the measured and predicted V_s using Eq. (4-3) for the two considered specific soil types, namely, clay- and sand-like soils. The correlations from Eq. (4-3) appeared to be similar to the developed soil-specific correlations from Eqs. (4-6) and (4-9). However, improved results were obtained when the regression analyses were conducted separately for sand-specific soil types (Eq. (4-9), R^2 = 0.53).

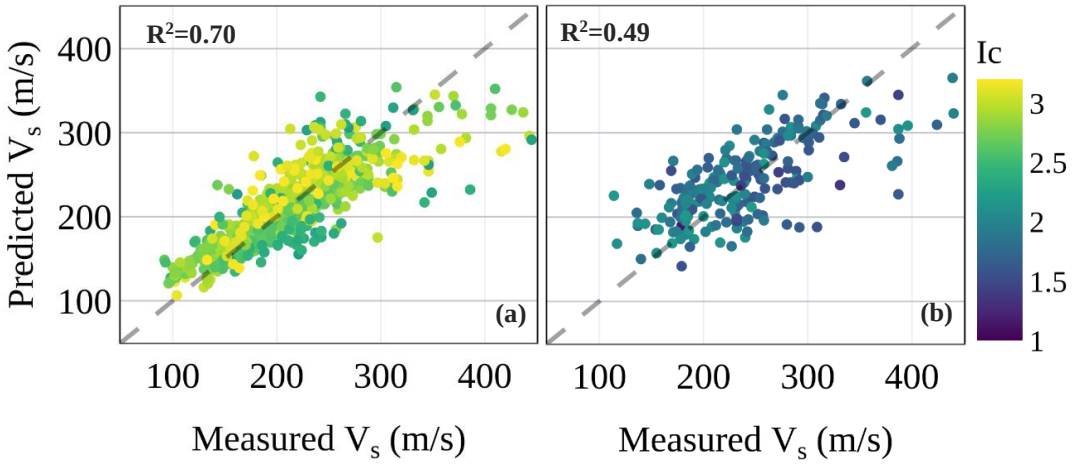

Figure 4-12. Comparison of measured and predicted V_s using Eq. (4-3) for (a) clay-like and (b) sand-like soils.

4.5.2.1. Case of clays

The soil database consisted of measurements from different locations and different postglacial sedimentary basins. One of the potential sources of uncertainty in the determination of soil geotechnical properties is the presence of different minerals, their texture and sedimentation conditions; for marine clays, a potential source of uncertainty is the variable effect of salt leaching (Locat and St-Gelais, 2014). Clays in these regions are sensitive and could be the cause of numerous geotechnical failures. The potential variability in soil composition in glaciomarine environments led to the study of the clays of the two postglacial sedimentation basins (i.e. Laflamme and Champlain) individually. Figure 4-13a presents the variations of the V_s–Z of four types of clays that dominantly existed in the database: mixture of clays and organic soils, mixture of clays and clayey silts, transitional clays and sensitive clays. Different V_s–Z relationships were observed based on each type of clay, but overall, the sensitive clays had the lowest values of V_s compared with the other clay types, except for the clays with I_c > 2.95, which exhibited highly dispersed V_s. Figure 4-13b suggests that depth could predict most of the variability of V_s for the Laflamme clays, but higher V_s dispersion was observed in the Champlain clays. This dispersion can be attributed to the large area covered by the Champlain basin and the differences in the rock sources, namely, the Canadian Shield and the Appalachian Mountain (Fulton et al., 1986).

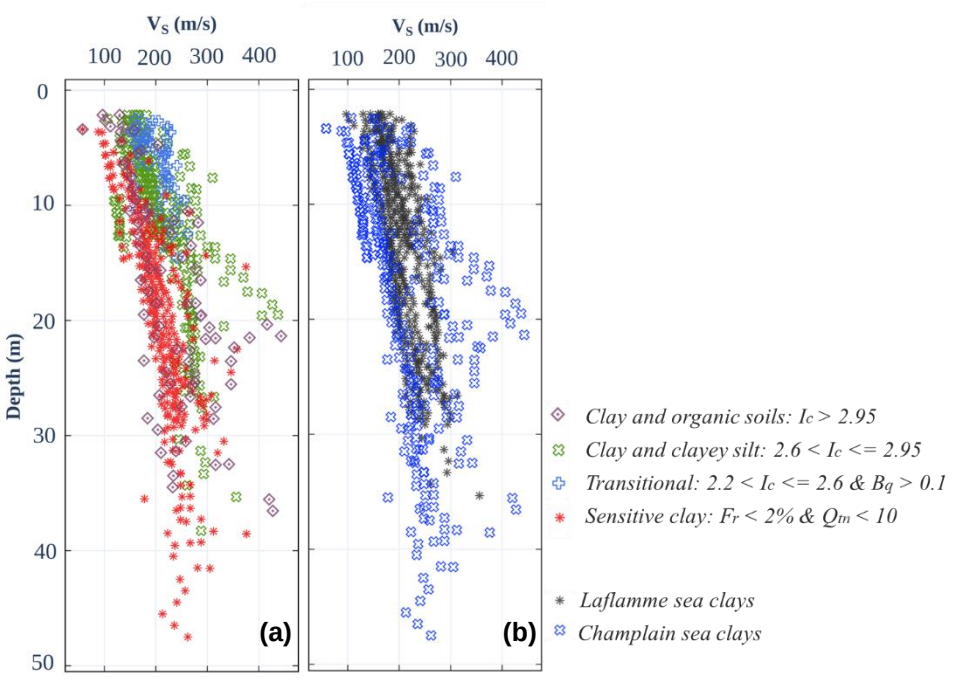

Figure 4-13. Variation of measured V_s against depth based on the (a) SBTs of clay-like soils and (b) Laflamme and Champlain sea locations.

It is worthy to consider V_s correlations depending only on q_t and Z, particularly when using the non-piezocone CPT profile in which f_s measurement is subject to uncertainties. This issue is particularly challenging in sensitive soils where f_s shows relatively low values. The higher R^2 in clay models (Eqs. (4-5), (4-6) and (4-7)) occurs likely due to the stronger correlation between V_s-depth and -q_t in clays (Appendix, Table C1, Eq. A4) and suggests the development of regression functions based on these two parameters. Table 4-3 presents the selected regression equations for specific clays of the Quebec region. Given that the data were classified using CPTu indicators, the regression equations for clays (Table 4-3) are simpler and show better fit than the equations developed for mixed soil types (e.g. Eq. (4-3)). As expected, a higher R^2 and a lower RMSE were achieved for the regression function of Laflamme clays in comparison with Champlain clays (Eqs. (4-11) and (4-12)).

Table 4-3. Regression equations developed for specific clays

Equation No.	Model equations	R^2	RMSE (m/s)	Remarks
Eq. (4-10)	$V_s = 11.86 q_t^{0.327} Z^{0.161}$	0.709	27	Sensitive clay
Eq. (4-11)	$V_s = 12.201 q_t^{0.359} Z^{0.070}$	0.819	17	Laflamme
Eq. (4-12)	$V_s = 8.591 q_t^{0.378} Z^{0.158}$	0.718	40	Champlain

4.6. Validations and comparisons of CPTu–V_s profiles

Figures 4-14 to 4-16 present V_s profiles estimated using the CPTu–V_s regression functions for general soils (V_s^{**}, Eq. (4-3)), specific soil types (V_s^{***}, Eqs. 4-7 and 4-12), Laflamme clays (V_s^{Lf}, Eq. (4-14)) and Champlain clays (V_s^{Ch}, Eq. (4-15)) in three representative sites. The sites were selected to visually demonstrate the capability and efficiency of the developed regression models in predicting V_s for the various soil types. In general, the predicted V_s corresponded well to the measured values (V_s^{*}), although several inconsistencies were noted.

Figure 4-14 illustrates heterogeneous fine-grained soils with alternation of clay, silty clay and in some parts sandy soils. The profile begins with thin shallow sandy soils then developed into fairly soft silty clay and clay deposits. The CPTu parameters fluctuate rapidly over a short distance, causing the variability in the predicted V_s. The predicted and measured V_s trends correspond well and increased steadily with depth, but the predicted V_s by specific soil type equations (V_s^{***}), experiences sharp fluctuations in some depths due to the evident variations in CPTu parameters. Figure 4-15 shows the results for fine-grained soils with alternating of soft clay and silty clay in Laflamme sediments. The values of V_s estimated by the general soil type correlation (V_s^{**}), V_s^{Lf} and measured V_s are consistent and increase steadily with depth. Figure 4-16 presents a profile of continuous marine Champlain silty clay sediments where the CPTu parameters (q_t, f_s and u_2) increased steadily with depth. The measured and estimated V_s values exhibit a similar trend, that is, they persistently increased with depth.

However, the V_s^{Ch} shows better prediction of measured V_s. In particular, for a depth of more than 21 m, V_s^{**} underestimates the V_s values.

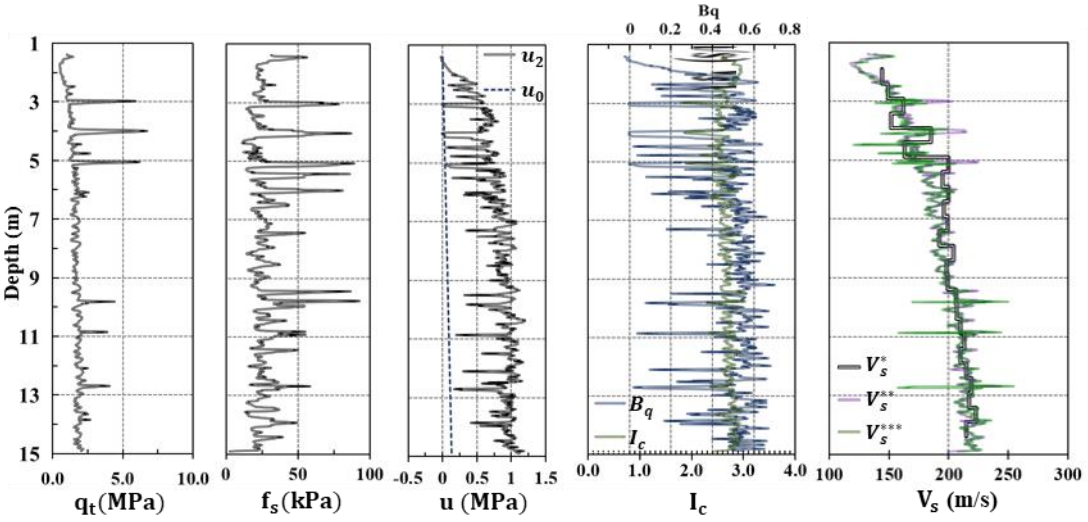

V_s^*: in-situ measured; V_s^{**}: prediction using Eq. (4-3); V_s^{***}: prediction using Eq. (4-7) and Eq. (4-12).

Figure 4-14. Observed CPTu parameters and predicted V_S profiles (SCPT-30AF) representative of heterogeneous transitional soils with alternation of clay and silt clay. © Mohammad Salsabili, 2022.

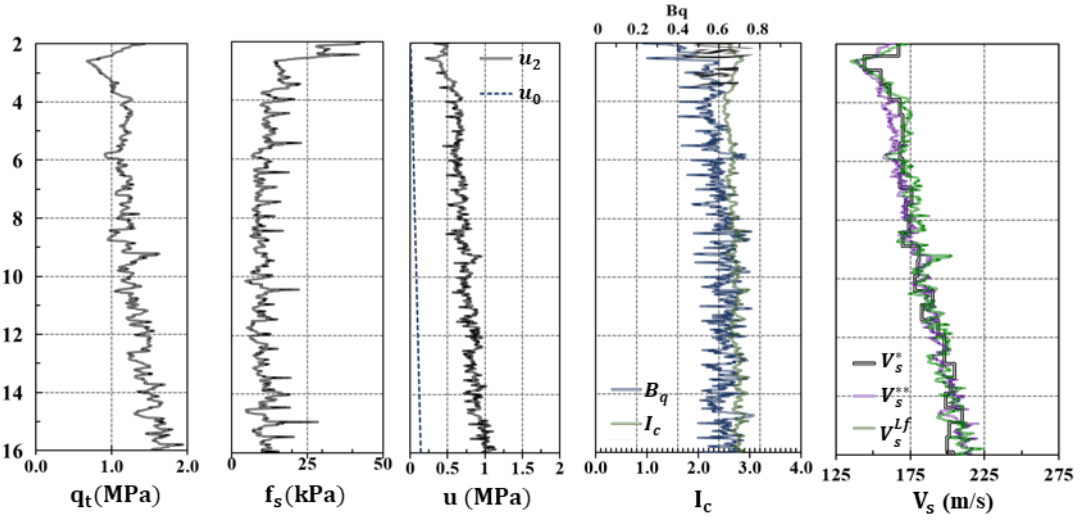

V_s^*: in-situ measured; V_s^{**}: prediction using Eq. (4-3); V_s^{Lf}: prediction using Eq. (4-14)

Figure 4-15. Observed SCPTu parameters and predicted V_S profiles for a site in Laflamme Sea basin (SCPT-45AVF) representative of a continuous marine clayey layer. © Mohammad Salsabili, 2022.

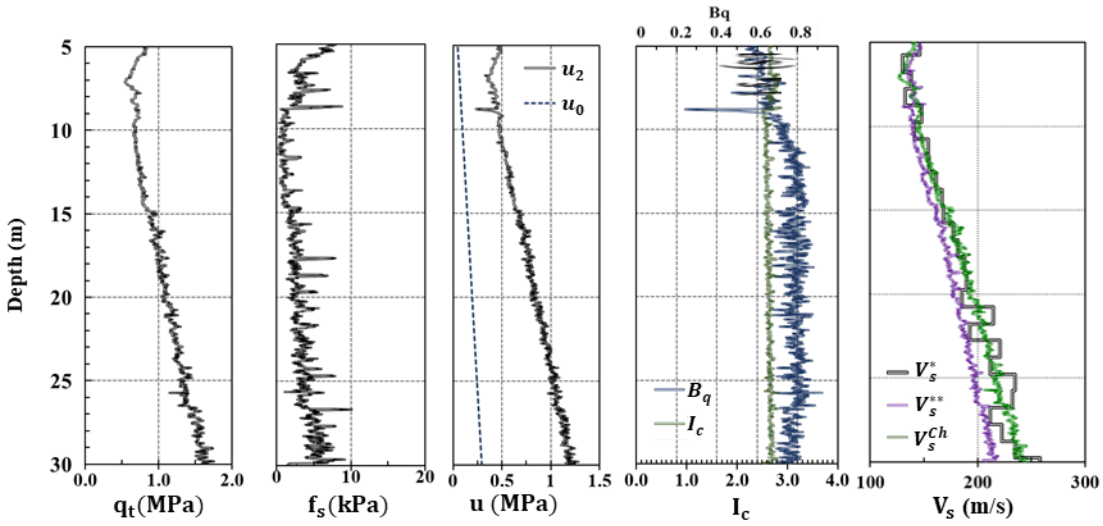

V_s^*: in-situ measured; V_s^{**}: prediction using Eq. (4-3); V_s^{Ch}: prediction using Eq. (4-15)

Figure 4-16. Observed SCPTu parameters and predicted V_s profiles for a site in Champlain Sea basin (CMPZ-15-01) representative of a continuous marine silty and clayey layer. © Mohammad Salsabili, 2022.

4.7. Conclusion

Regional correlation equations were developed between shear wave velocities (V_s) and CPTu parameters in postglacial sediments along St. Lawrence and Saguenay River valleys. A dataset was built by performing SCPTu field measurements at 40 test sites in Champlain and Laflamme seas. The examined sediments ranged from fine-grained silty clays to gravely sands. Nonlinear multiple regression analyses were performed to assess the relationships between soil geotechnical properties and shear wave velocity. The results showed that CPTu-V_S correlations are affected by the soil type and sedimentation environment. The major findings of the study are summarized below.

- The application of existing V_s correlation equations presents the risk of overestimation or underestimation of V_s due to the potential differences in geological age and the deposition environment. The consideration of the geological age (Pleistocene or Holocene) is important for estimating unbiased V_s values.
- The general model developed for a wide range of soil types can provide reliable predictions by using normalized indicators, such as B_q and I_c.

- B_q and I_c are key parameters in regression models and soil classifications. I_c helps improve the fitting results, and B_q is effective in the classification of transitional soil as a categorical variable.

- $(V_{s1}/Q_{tn})^{\alpha}$–I_c relationships are suggested to differentiate transitional soils. In this study, different correlations were observed with different values of I_c and the exponent α. On the basis of the observed trends, I_c=2.2 was established as the threshold between clay- and sand-like soils.

- Slightly improved results can be obtained from sand-specific regression models when stress-normalized V_s and CPTu parameters are applied. Stress normalization, however, is not recommended for clay-specific models due to the remaining dependency of V_{s1} on depth.

- Compared with the use of depth, the adoption of σ'_{v0} as an indicator of the stress state in sands provides better results. In clays, applying the direct measurement of depth is recommended.

- Depth is a leading parameter in the prediction of V_s in fine-grained soils and can predict most of the variability of V_s for Laflamme clays; however, high dispersion occurs for Champlain clays. This high dispersion may be explained by the large study area in the Champlain basin and the potential differences in the mineral compositions of soil deposits, sedimentation and successive erosional processes.

In the developed models, the performance of CPTu-V_s correlations was evaluated with R^2 and RMSE parameters. A possible explanation for the R^2 (=0.66) and RMSE (=35 m/s) values in the best model for general soil type was the mixing of different soil types. When the soil type was classified as clay-like and sand-like soil, R^2 improved to 0.70, and RMSE decreased to 32 m/s in the clay models. For sand, R^2 was determined to be 0.52 with RMSE = 43 m/s. In conclusion, although uncertainty exists in sand models, the bias observed using global V_s correlations is mitigated, and the predicted V_s values can provide first-hand estimates for regional seismic site classification.

Funding

This research was partially funded by the Natural Sciences and Engineering Research Council of Canada (NSERC) and Hydro-Quebec under project funding no. RDCPJ 521771–17.

Acknowledgements

The authors would like to acknowledge the Quebec Ministry of Transportation (MTQ) and the members of the CERM-PACES project of UQAC for their cooperation and for providing access to the database.

Conflicts of Interest

The authors declare no conflict of interest.

CHAPTER 5

PROBABILISTIC APPROACH FOR SEISMIC MICROZONATION INTEGRATING 3D GEOLOGICAL AND GEOTECHNICAL UNCERTAINTYT

Mohammad Salsabili [1], Ali Saeidi [1], Alain Rouleau [1] and Miroslav Nastev [2]

[1] Département des Sciences Appliquées, Université du Québec à Chicoutimi, G7H 2B1 Saguenay, Canada; mohammad.salsabili1@uqac.ca; alain_rouleau@uqac.ca

[2] Geological Survey of Canada, G1K 9A9 Quebec City, QC, Canada; miroslav.nastev@canada.ca

Abstract

A novel probabilistic methodology for regional seismic site characterization is proposed and applied to a region with highly heterogeneous surficial geology and varying soil sediment thickness and stiffness. The method combines various sources of geological and geotechnical uncertainties to develop a 3D shear-wave velocity (V_S) model and evaluate the associated uncertainties. A 3D geological model of the unconsolidated deposits was developed using geostatistical interpolation and simulation methods. Sequential indicator simulations produced a quantitative geologic model that explicitly quantified geological uncertainties based on the likelihood of specific soil types occurring. In situ measurements and multivariate statistical analysis allowed the development of empirical correlations between V_S, geotechnical parameters, depth, and soil types. The resulting 3D V_S values were estimated on the basis of V_S-depth correlations and the probability of occurrence of each soil type. In this approach, the propagated uncertainty was also quantified by considering the combined variance. Seismic microzonation mapping was then conducted by transforming the 3D V_S model into 2D maps that represent the spatial distributions of the time-averaged shear-wave velocity of the top 30 m ($V_{S,30}$) and the fundamental site period (T_0), along with their respective spatial uncertainties. The results indicate that microzonation maps and their uncertainties are influenced by the thickness, occurrence probability, and geotechnical properties of soils. The proposed method can be used to assess the probabilistic seismic risk at local and regional scales in areas with geologically and geotechnically complex soil properties.

Keywords: seismic microzonation, 3D geological model, geotechnical model, shear-wave velocity, uncertainty

5.1. Introduction

Local site conditions tend to modify the amplitude and frequency of incoming seismic waves (Seed et al., 1976). This phenomenon is known as the site effect, and it depends on the geotechnical (e.g. soil type, shear modulus, damping ratio) and geological (e.g. stratigraphy, basin topography, thickness) properties of soil sediments. Site-effect parameters such as the time-averaged shear-wave velocity of the top 30 m ($V_{s,30}$) and the fundamental site period (T_0) are reliable proxies for regionally evaluating seismic shaking amplification (Thompson et al., 2014; Heath et al., 2020) and seismic microzonation mapping (SM Working Group, 2015; Licata et al., 2019; Molnar et al., 2020).

Although shear-wave velocity (V_s) is recognized as a simple, effective and representative parameter for determining site effects, obtaining sufficient direct V_s measurements in regional site characterization studies is challenging. As a proxy, the available geotechnical data represent a useful data source for estimating V_s (Oliveira et al., 2020). In this case, empirical V_s correlations with geotechnical parameters (Mayne and Rix, 1995; Robertson, 2009) or depth (Motazedian et al., 2011; Podestá et al., 2019) are suggested for addressing the scarcity of V_s measurements. However, specific depositional environments, such as the presence of soft sensitive clays, which is frequently observed in Eastern Canada (Locat and St-Gelais, 2014), hinder the use of existing global regression equations, potentially resulting in estimation biases (McGann et al., 2015a; Salsabili et al., 2022).

Several seismic microzonation studies in Eastern Canada have used multilayered geological models as a basis for predicting the spatial variability of $V_{s,30}$ and T_0, as well as their associated uncertainties (Motazedian et al., 2011; Rosset et al., 2015; Nastev et al., 2016a and 2016b). For example, Rosset et al. (2015) developed three different $V_{s,30}$ models for the Montreal region using predictive equations for V_s as a function of depth: a single-layer model based on total soft soil thickness, a four-layer model based on geological and geotechnical information from borehole data, and a composite model that combined the characteristics of the two previous models. In the Ottawa and St. Lawrence Valleys, Nastev et al. (2016a) assigned a typical V_s-depth function to postglacial sediments and uniform V_s values to glacial

sediments and bedrock units. In these studies, the best expert (deterministic) 3D geological model was used in the sequential development of geotechnical models and the mapping of $V_{s,30}$ and T_0. They analyzed the uncertainty propagated to $V_{s,30}$ and/or T_0 using the first-order, second-moment (FOSM) approach, focusing solely on the statistical uncertainty related to V_s (geotechnical uncertainty). This approach, however, neglects the spatial uncertainty and the heterogeneity associated with the 3D geological model.

Geospatial modeling can be achieved using spatial variability. Spatial variation refers to the dissimilarity of pair values of a random variable as a function of distance (Isaaks and Srivastava, 1989). The spatial variation in soil properties has been modeled using random field theory, which decomposes the spatial variation into a deterministic trend function and its residuals (Fenton, 1999; Fenton and Griffiths, 2003). This method can also be used to address problems with sparse and nonstationary data (Wang et al., 2018; Zhao and Wang, 2020). In recent soil engineering practices, geostatistical methods have also been used to predict spatially-correlated geotechnical properties, such as cone resistance and V_s (Vessia et al., 2020; Hallal and Cox, 2021). However, few attempts have considered the influence of soil geological uncertainty on the prediction of geotechnical properties (Zhang et al., 2021). The geostatistical approach has the advantage of being able to provide quantitative spatial predictions of soil types (probabilistic geological model) prior to estimating geotechnical properties, while also providing an assessment of spatial uncertainty.

The objective of this paper is to conduct seismic microzonation mapping while considering the uncertainties associated with both geological and geotechnical models. The study was conducted over the city of Saguenay in Eastern Canada, which is a region with highly heterogeneous surficial geology and soil layers of varying thickness and stiffness. Geostatistical and multivariate statistical analyses were used to determine the spatial distribution and propagated uncertainties of seismic site parameters ($V_{s,30}$ and T_0). Lithological heterogeneity was characterized through spatial simulation of the main geological units present in the study area (e.g. clay, sand and gravel). The resulting model depicts the probability of occurrence of geological units and their related spatial uncertainties based on the simulation

variance. Multivariate statistical analysis was performed to develop the empirical V_S correlations. The geotechnical model was then built by combining the estimated occurrence probabilities of the soil units and the V_S empirical correlations for each soil type. Thus, a consistent spatial distribution of the respective V_S values and their uncertainties were determined in 3D. Finally, the 3D V_S model was transformed into 2D maps that show the spatial distributions of $V_{S,30}$ and T_0, as well as their related spatial uncertainties.

5.2. Methodology and procedure

The methodology for developing a seismic microzonation map and the uncertainties at each step are presented in Figure 5-1. This methodology includes three major steps: (I) the development of probabilistic geological models, (II) the development of geotechnical models and (III) the mapping of soil properties. Uncertainties must be considered for each step. Below, we explain the different uncertainties that affect each step, as well as the methodology used to quantify the uncertainties in the geological and geotechnical models and in the mapping of soil properties. Numerical examples are used to clarify the approach.

5.2.1. Considered uncertainties

As illustrated in Figure 5-1, soil variability is primarily rooted in two sources of uncertainty: (1) uncertainty resulting from the inherent variability of the natural process and (2) knowledge-related uncertainties arising from the statistical inference of a limited number of samples or measurement imprecisions, i.e., statistical uncertainty or measurement error (Wang et al., 2016). In addition, transformation uncertainty is introduced in the geotechnical variability when field or laboratory measurements are transformed into design soil properties using empirical or other correlation models, e.g. V_S-CPT or V_S-SPT correlations (Phoon and Kulhawy, 1999a; Wang et al., 2016). The propagation of the uncertainty to the design soil properties depends primarily on the combination of the applied analytical methods and probabilistic analysis. Analytical methods vary from simple linear or empirical models to sophisticated

constitutive models including nonlinearity or elastoplasticity (Kaggwa and Kuo, 2011). Based on the complexity of the selected probabilistic and analytical methods the response uncertainty varies from a single conventional statistical variance of averages to multiple probability density functions.

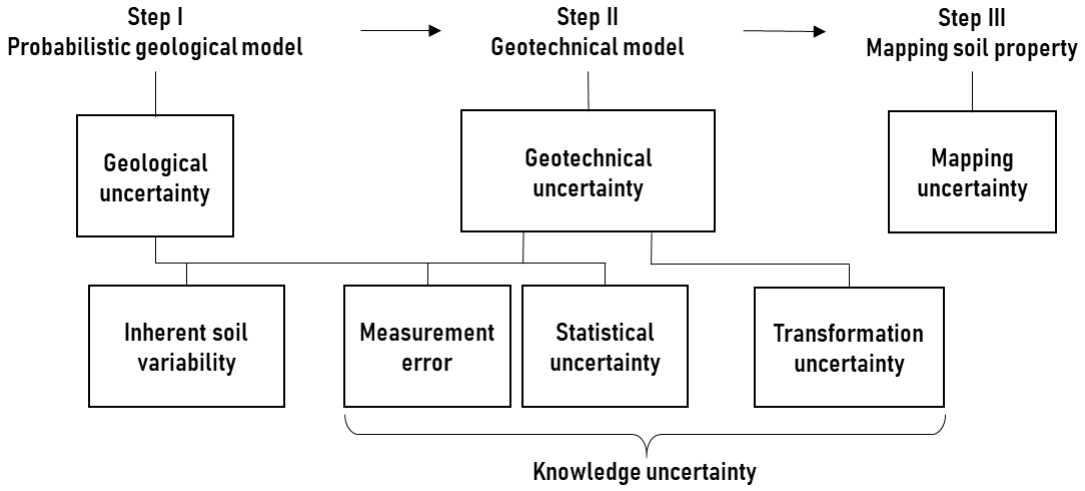

Figure 5-1. Variabilities and uncertainties affecting seismic microzonation mapping. © Mohammad Salsabili, 2022.

5.2.2.Geo-modelling: development of geological and geotechnical models

A quantitative geological model obtained by geostatistical simulation is presented, along with the probability of occurrence of the soil types. Probabilities are suggested to describe the different aspects of the uncertainty. The “simulation variance” is introduced as a quantitative measure of geological uncertainty (Yamamoto et al., 2014; Salsabili et al., 2021). Soil units are treated as Bernoulli variables with an outcome of either zero or one, and the variance ($\sigma^2(x_i)$) is computed based on the discrete probability distribution of a random categorical variable (x_i) with an event probability of p_i (Equation (5-1) and Figure 5-2).

$$\sigma^2(x_i) = p_i(1-p_i), \qquad x_i \in \{0,1\}, i \in \{1,\dots,k\} \tag{5-1}$$

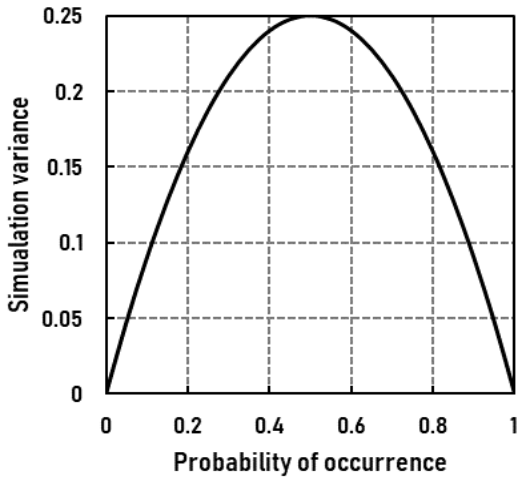

Figure 5-2. Simulation variance for a Bernoulli variable as a function of the probability of occurrence. When the probability of an outcome is close to 0 or 1, the variance (or uncertainty) is low; while, when the probability of this outcome is 0.5, the variance is maximal and equal to 0.25. © Mohammad Salsabili, 2022.

The flexibility of this approach is demonstrated in Figure 5-3, which shows an example of 2D grid cells of a binary soil unit (e.g. clay or sand). The certainty in distinguishing between the two soil units is represented by the probability of occurrence (Figure 5-3a). The values of 0 and 1 represent zones with sand or clay only. On the other hand, uncertain zones have probability values between 0 and 1; a probability of 0.5 conveys no information to distinguish the soil unit as either sand or clay and thus represents the maximum uncertainty. To develop the respective geotechnical model and its associated uncertainty, a deterministic or probabilistic interpretation of the geological model can be used. Figure 5-3b presents the *deterministic* interpretation of the geological model, in which the highest probability of occurrence is used to represent the soil type of the cells. The input geotechnical parameters are arbitrarily assumed to be:

$$V_{s,sand} = 400\,{}^{m}/_{s}, V_{s,clay} = 200\ {}^{m}/_{s}\ , \sigma_{Vs,sand} = \sigma_{Vs,clay} = \ 40\,{}^{m}/_{s}.$$

It is clear that the local value on the V_s map varies sharply based on the cell's soil type, whereas the σ_{Vs} map is uniform, with $\sigma_{Vs,sand} = \sigma_{Vs,clay}$. The V_s map will be determined solely by the binary variation of the soil units, not by the p_i values; difficulties arise in determining V_s

when the probability is approximately 0.5. In the *probabilistic* approach, the mean ($E(Z\ )$) and combined variance ($\sigma^2(Z)$) of a random geotechnical variable (z_i) with a variance of $\sigma^2(z_i)$ are determined using Equations (5-2) and (5-3).

$$E(Z\ ) = \sum_{i=1}^{k} p_i \times\ z_i\ , \tag{5-2}$$

$$\sigma^2(Z\ ) = \sum_{i=1}^{k} \left(p_i \times (\sigma^2(z_i) + {z_i}^2)\right) - E(Z)^2\ \ , \tag{5-3}$$

For the example given in Figure 5-3, Equations (5-2) and (5-3) can be rewritten as follows:

$$V_s^{cell}\ =\ p_{clay} \times\ V_{s,clay}\ + p_{sand} \times\ V_{s,sand}\ , \tag{5-4}$$

$$\sigma^2_{V_s^{cell}} = \left(p_{clay} \times \left(\sigma^2_{Vs,clay} + V^2_{s,clay}\right) + p_{sand} \times \left(\sigma^2_{Vs,sand} + V^2_{s,sand}\right)\right) - (V_s^{cell})^2, \tag{5-5}$$

where V_s^{cell} and $\sigma^2_{V_s^{cell}}$ are the mean and combined variance of an example grid cell with probabilities of occurrence of p_{clay} for clay and p_{sand} for sand. Figure 5-3c presents the probabilistic interpretation of the geological model. V_s and its associated variance values vary gradually based on the p_i values. The resulting variance ($\sigma^2_{V_s^{cell}}$) considers the "combined variance" of both the geological and geotechnical variables, and the uncertainty of the geological model will also be reflected in the V_s map. The uncertainty in V_s is lowest when the simulation variance is zero (i.e., when $p_i = 1.0$) and highest when all members are equally probable (i.e., when $p_i = 0.5$). This approach contributes to a more realistic model of V_s and its associated uncertainties. It also allows for an interpretation in the uncertain zone based on transitional or mixed soil units, e.g. clayey sand or sandy clay, which is often referred to as a fuzzy interpretation in the spatial context (Wellmann and Regenauer-Lieb, 2012). Fuzziness is caused by imprecision and uncertainty, which are the main consequences of grouping similar soil units into broad categories with a certain level of ambiguity (McBratney and Odeh, 1997).

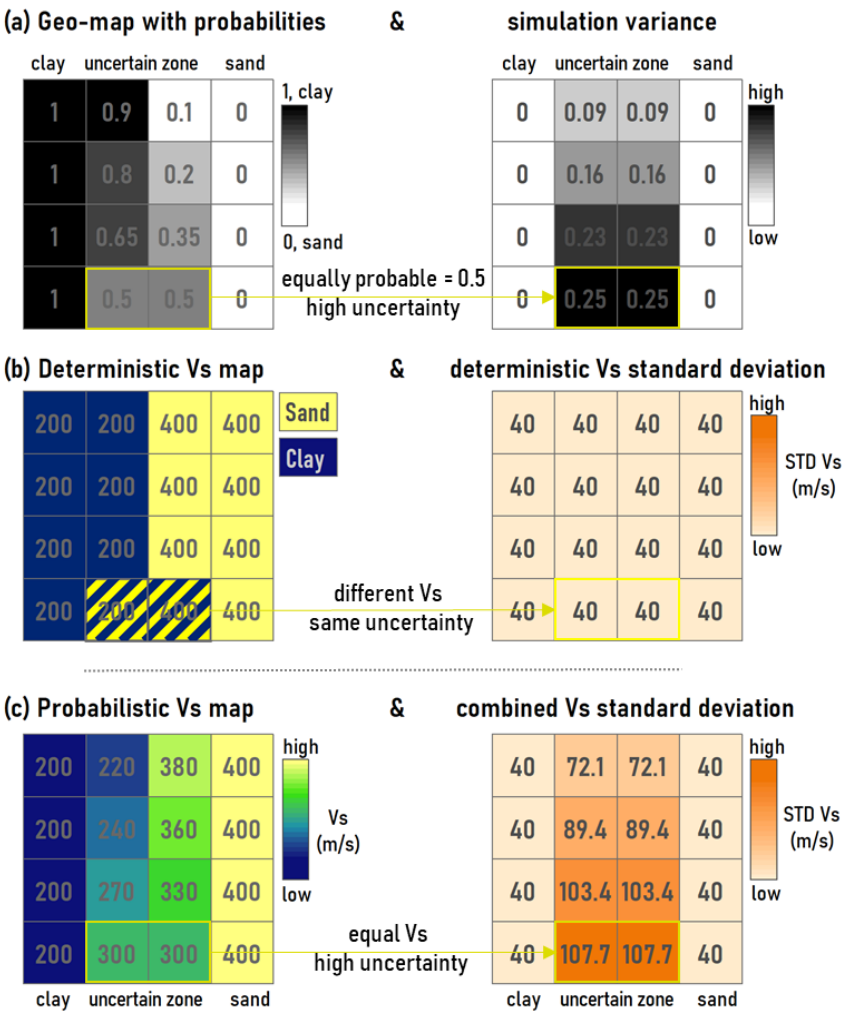

Figure 5-3. Numerical 2D grid cells presenting the methodology of probabilistic seismic mapping; (a) probability of possible outcomes for each soil unit in each cell and their visualized uncertainties (simulation variance); (b) deterministic V_s and uncertainty maps; (c) probabilistic V_s and uncertainty maps; ($V_{s,sand} = 400\,{}^{m}/_{s}, V_{s,clay} = 200\,{}^{m}/_{s}, \sigma_{Vs,sand} = \sigma_{Vs,clay} = 40\,{}^{m}/_{s}$). © Mohammad Salsabili, 2022.

5.2.3.Mapping of soil properties

After the soil properties have been evaluated in 3D, a straightforward procedure for mapping local site conditions while considering uncertainties was used to transform the 3D models into a 2D map. Figure 5-4 presents a schematic cross-section of the three dominant

geologic layers in the Saguenay region (from top to bottom): postglacial soils, glacial deposits (till) and bedrock. The glacial deposits and bedrock units were assumed to have uniform V_s values, whereas the average V_s value of the postglacial soil was obtained by transforming the 3D grid cells to 2D maps. Equations (5-6) and (5-7) indicate how to transform the 3D grid cells into a 2D map with the time-average V_s values and their related propagated uncertainties. The propagated uncertainty was calculated using the FOSM approach as an analytical approximation for the mean and standard deviation of the design variable (Nadim, 2007). FOSM analysis is a parametric method that can be used under the assumption of normality. Otherwise, nonparametric approaches can be used for the determination of V_s in each block, particularly in the presence of a trend and non-normal distribution. In this context, *V*s can be estimated via bootstrap resampling or geostatistical simulation.

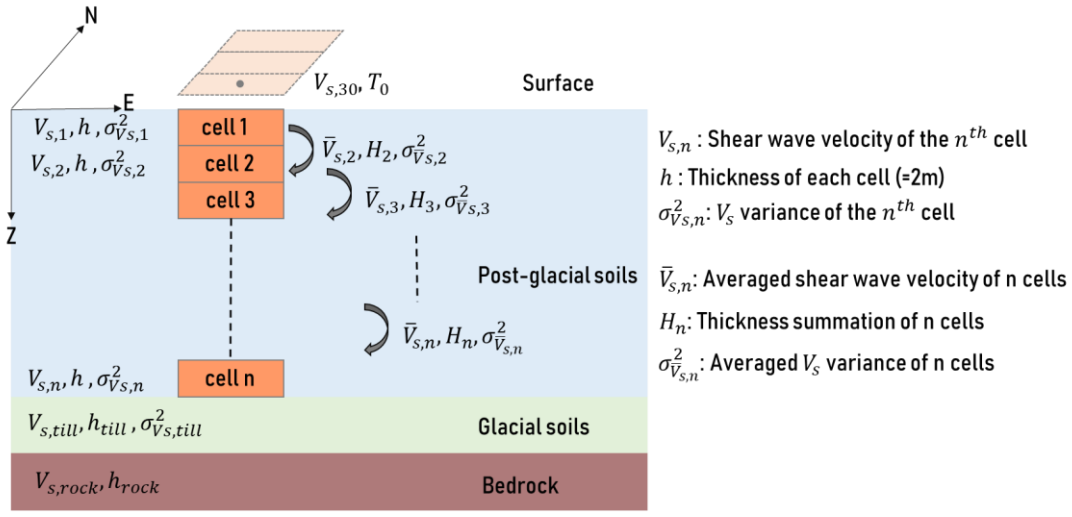

Figure 5-4. A schematic cross-section of a 3D model that contains postglacial, glacial and bedrock geological layers. © Mohammad Salsabili, 2022.

$$\text{For n cells, } \bar{V}_{s,n} = f(V_{s,n}) = \frac{H_n}{\sum_{m=1}^{n} \frac{h}{V_{s,m}}} \text{ and} \tag{5-6}$$

$$\sigma^2_{\bar{V}_{s,n}} = \sum_1^n \left(\frac{\partial f}{\partial V_{s,n}}\right)^2 \times \sigma^2_{Vs,n} \ , \tag{5-7}$$

where the thickness of each cell is assumed to be h = 2 m and $H_n = H_{n-1} + h$.

5.3. Saguenay City study area

Saguenay City was selected as the study area due to its relatively high seismic hazard (https://earthquakescanada.nrcan.gc.ca/) and the presence of heterogeneous Quaternary sediments with complex spatial and vertical architecture. It is the largest municipality within the Saguenay–Lac-Saint-Jean region, covering 1136 km² with a population of 147,100. The recent most important seismic event was the 1988 M 6.0 Saguenay earthquake. The epicenter of the earthquake, which had a mid-crustal depth of 29 km, was 35 km south of the downtown area (Du Berger et al., 1991). The earthquake's secondary effects included soil liquefaction, rock falls and landslides observed within a 200-km radius of the epicenter (Lamontagne, 2002).

The bedrock in the Saguenay region is part of the Grenville province of the Canadian Shield, which is composed mainly of crystalline Precambrian rocks (Davidson, 1998). Based on the surficial geology maps, cross-sections and subsurface data (LaSalle and Tremblay, 1978; Daigneault et al., 2011; CERM-PACES, 2013), the soil deposits can be grouped into four major categories: till, gravel, clay and sand (Figure 5-5).

- Till: This glacial sediment is located at the base of the stratigraphic soil column; it is compact and semi-consolidated. Till is the most widespread soil unit in the study area and ranges in thickness from a few meters to >10 m at certain locations. With the exception of rock outcrops, till covers the bedrock elsewhere, representing an important assumption in the 3D modelling approach.
- Gravel: This coarse sediment is mainly of glaciofluvial and alluvial origin; it consists of gravel, sand and sometimes till. This unit is occasional in the region, often in contact with till, sand or clay units.
- Clays: These fine postglacial sediments are the most present soil type by volume in the study area. They are composed mainly of silt, silty clays and clay. They have a general thickness of up to 10 m and may attain a maximum thickness of >100 m in the lowlands.
- Sand: This group consists mainly of coarse glaciomarine deltaic and prodeltaic sediments, and alluvial sands composed of sand and gravely sands.
- Other unconsolidated sediments can also be found in minor proportions including loose postglacial sediments (alluvium, floodplain sediments, organic sediments, etc.) and

occasional landslide colluvium. For the purpose of this study, they are classified into sand, clay and/or gravel mainly based on the encountered grain size.

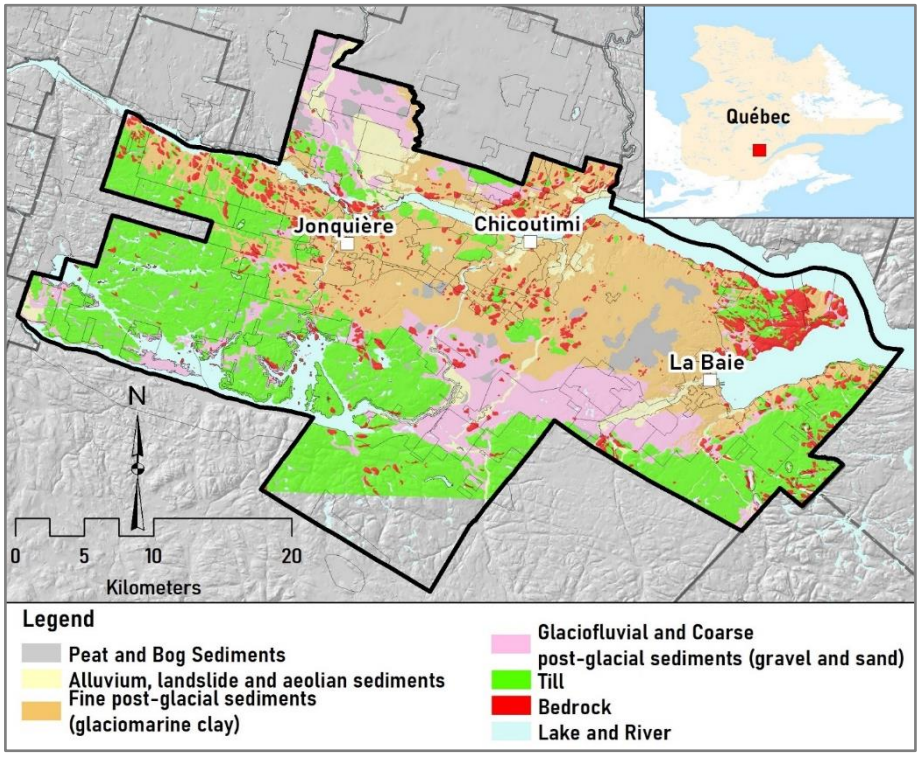

Figure 5-5. Saguenay city study area: surficial geology map (modified from Daigneault et al. 2011). © Mohammad Salsabili, 2022.

5.4. 3D probabilistic geological modelling

Geostatistical simulation is widely used to model the spatial architecture of major lithofacies in reservoir and mineral resource modeling (Deutsch, 2006; Pyrcz and Deutsch, 2014). Sequential indicator simulation (SIS) represents a practical approach for cases without an obvious genetic shape that can be incorporated into object-based modeling. It makes use of indicator kriging (IK), in which the Monte Carlo simulation draws a precise category at each location (Deutsch, 2006). IK is commonly used to estimate the probability of distribution or single-location uncertainty. However, given that it is based on the kriging estimator, it has been criticized for its smoothing effect (Chiles and Delfiner, 2009) and inability to reproduce spatial

heterogeneity. By contrast, SIS can reproduce the global histogram and variogram. SIS was used to determine the spatial boundaries of categorical variables (in this case, clay, sand and gravel) and to develop a model that captures the heterogeneity of soil properties prior to estimating geotechnical parameters (Salsabili et al., 2021). The geostatistical simulation requires a full 3D volume to determine the soil type of the glacial and postglacial deposits. Accordingly, the entire model space was subdivided into a raster with equal cell sizes (also referred to as voxels or blocks representing the smallest unit of a given soil type). Salsabili et al. (2021) developed the model on the basis of comprehensive datasets, including 3,524 borehole logs, 26 geological cross-sections, and 973 virtual boreholes. They were combined to create the total soil and till thickness maps and to generate the bedrock topography. The space between the top and bottom of each interface was filled with 75 m × 75 m × 2 m blocks to perform the geostatistical simulation. Then, the 3D model of soil type was created by using sequential indicator simulation. The spatial statistics of a target variable were reproduced with a set of alternative models of categorical variable spatial distributions called realizations. (Deutsch and Journel, 1997). The method consists of three steps, which are as follows:

i) Transformation of soil types into 3 indicator variables as clay, sand and gravel

$$i(u_\alpha; k) = \begin{cases} 1 & if\ category\ k\ prevails\ at\ location\ u\ , k = 1, \dots, 3. \\ 0 & otherwise \end{cases} \quad (5\text{-}8)$$

ii) Determination of indicator variograms to model the spatial continuity of the indicator soil types;

iii) Simulation of the soil types honoring field observations at sampled locations (conditional simulation) in a sequential and reproducible manner.

Overall, 100 realizations are generated using the conditional SIS method to determine the probability of occurrence (p_i) for each of the postglacial deposits: clay, sand and gravel. The resulting probability values are used to estimate the associated simulation variance (uncertainty). Figures 5-6 and 5-7 show the probabilistic interpretations of the plan and cross-section of the 100 SIS realizations in an area where all four surficial soil units are present.

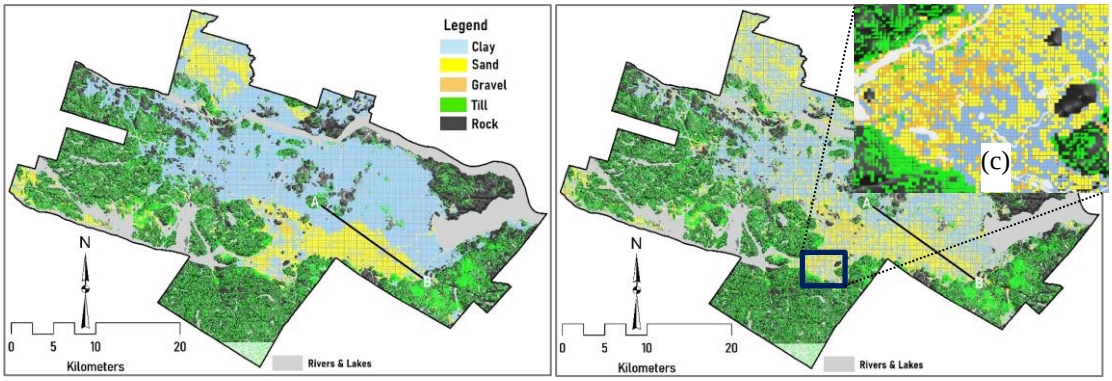

Figure 5-6. Map of (a) soil units with the highest probability of occurrence at the ground surface, and (b) one SIS realization showing sand, clay and gravel. (c) Local blown-up showing the surface soil variability in the SIS map. © Mohammad Salsabili, 2022.

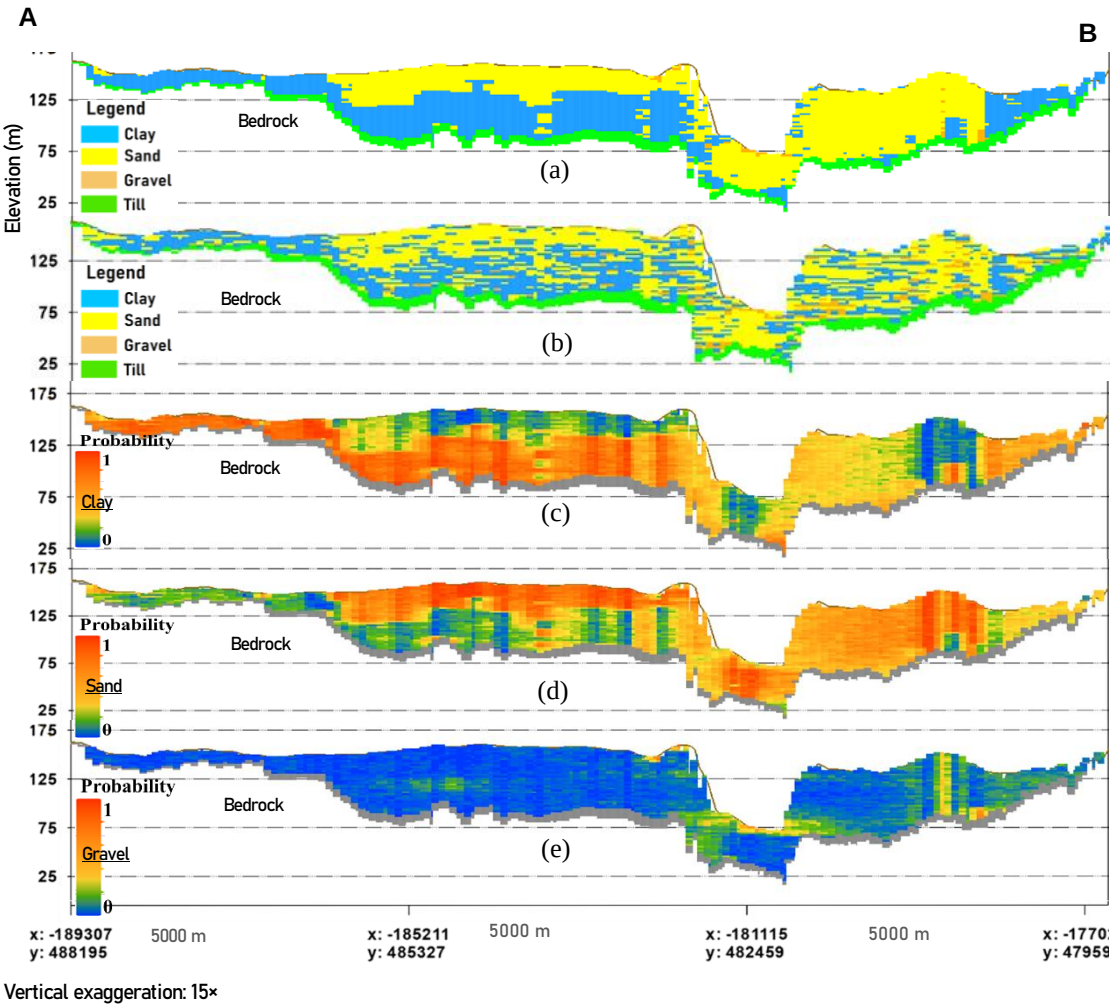

Figure 5-7. Stratigraphic cross-sections A-B: (a) soil units with the highest probability of occurrence; (b) one SIS realization of sand, clay and gravel. Individual probabilities of occurrence for: (c) clay, (d) sand and (e) gravel obtained from a set of 100 conditional SIS realizations. © Mohammad Salsabili, 2022.

5.5. Development of the 3D Geotechnical model

For practical convenience and because the term “geotechnical model” has different meanings in the literature related to stability analysis (Phoon and Tang, 2019), the geotechnical model considered in this paper is valid within the limits of elastoplastic behavior before ultimate failure. In this context, the geotechnical model was created similarly to the 3D geologic model in terms of engineering parameters, i.e., V_S. The procedure includes two main steps: (I) developing V_S empirical correlations and (II) creating a 3D V_S model that incorporates the probabilistic geologic model and V_S empirical correlations.

5.5.1. V_S empirical correlations

In situ V_S measurements can be obtained by invasive methods, such as cross-hole or downhole, as well as non-invasive methods, such as refraction or surface wave methods (Hunter and Crow, 2012; Garofalo et al., 2016a, 2016b). The seismic piezocone penetration test (SCPTu) is an invasive method that provides optimized V_S intervals and continuous penetration results, allowing the development of reliable empirical correlations between V_S and strength-based soil parameters. CPTu profiling provides continuous logs of the interpreted soil stratigraphy (Prins and Andresen, 2021). Interpretations are based on the values of the CPTu parameters, such as the cone tip resistance (q_t), sleeve friction and friction ratio in former studies (Robertson and Campanella, 1983) and the normalized cone resistance and sleeve friction in later studies (Robertson, 2009, 2016). For the development of V_S empirical correlations, we 1) perform SCPTu field tests, 2) collect and store existing data in a database, 3) develop CPTu–V_S correlations by using the results of 15 SCPTu surveys, and 4) estimate V_S on the basis of CPT and SPT data by using empirical correlations for the entire study area. The final step involves developing V_S–depth correlations to assist in determination of the 3D V_S values.

5.5.1.1. Field testing program

Fifteen SCPTu soundings were carried out using a standard type 2 piezocone with the following specifications: 60° apex angle, 10 cm^2 base area of the conical tip and 150 cm^2 sleeve area with the filter located at the shoulder. A dual-array seismic cone mounted on the top of the piezocone allows the measurement of the arrival of vertically propagating seismic body waves. For a given depth, the SCPTu method generates four types of data: V_S, raw cone tip resistance q_c, frictional cone resistance f_s and penetration pore pressure u_2. The field program followed principally the ASTM D5778-12 procedure and preprocessing, and corrections were done in accordance with Lunne et al. (2002) and Robertson (2009). SCPTu surveys were performed at the penetration rate of 2 cm/s. High-resolution CPTu data were collected every 1 cm, and V_s values were recorded at every 50 cm depth interval. Shear-wave velocities were determined from seismic signals by applying the cross-correlation algorithm (Campanella and Stewart, 1992). The cone tip was corrected, and q_c and f_s were cross-correlated by using the software CPeT-IT (GeoLogismiki, 2014). The predrill depth was assessed by applying the geological 3D model (Salsabili et al., 2021) prior to performing the field test. The maximum depth of testing was set to 30 m. The termination conditions were reached at the bedrock contact or in the presence of very stiff soil, such as till or gravel, where the pushing force reached the maximum. The ground water table in saturated drained soils (e.g., sands) was identified on the basis of pore water pressure ($u_0 \sim u_2$) and that in clayey soils was determined through dissipation tests. In some cases, before the sounding hole was destroyed, a piezometer was installed to measure the piezometric level. Precautions were taken in soils above the groundwater table that were saturated due to capillarity.

5.5.1.2. Geotechnical database

The database contains more than 700 samples with various laboratory tests on physical properties such as unit weight, permeability, natural water content, Atterberg limits, plasticity and liquidity index, in addition to mechanical properties such as pre-consolidation stress, compression index, and sensitivity. Herein, the sensitivity of the fine-grained sediments

shows high variability and ranges between 1 and ~2700, however, most of the data vary from 1 to 50 with a median of 44. Natural water content (w) data range between 9 and 70%. Most of the plasticity index data vary from 5 to 25% and more than 50% of the data show a liquidity index greater than one. The majority of the unit weight data ranges between 17 and 19 kN/m^3 with an average of 18 kN/m^3. The correlation between unit weight and depth was founded weak (R square ~ 0.2).

In-situ tests with invasive methods were conducted during three field campaigns:

i) 15 recent SCPTu surveys were conducted by the Université du Québec à Chicoutimi (UQAC) research group. The data include the complete set of q_t, f_s, u_2 and V_s measurements.

ii) Ninety-one CPT profiles were obtained during the 1980s and 1990s by the Quebec Ministry of Transport (MTQ). The CPT data set is limited to measurements of q_c and f_s. For the purposes of the present study, the CPT logs were digitalized, and V_s was calculated using the developed site-specific CPT-V_s correlation for sand or clay soils.

iii) Sixty-four standard penetration tests (SPTs) were acquired during the 1980s and 1990s by the MTQ. The results were incorporated in the determination of the geotechnical properties of coarse-grained soils.

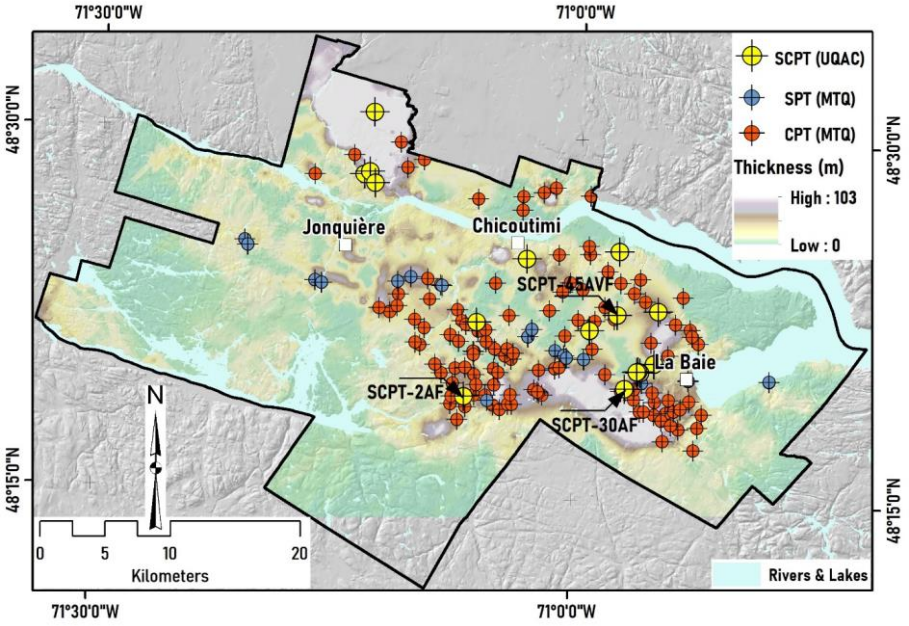

Figure 5-8. Distribution of geotechnical test sites. The background presents soil thickness (modified from Salsabili et al., 2021), and validation was conducted at the three indicated sites by arrows and labels. © Mohammad Salsabili, 2022.

5.5.1.3. Development of CPTu-V_s correlation

After the data processing, 568 CPTu-V_s data pairs were retained for analysis. Figure 5-9 shows a histogram and descriptive statistics of the V_s values with an approximate normal distribution. The V_s values were assumed to be consistent between two measurements, and the midpoint of each interval was assumed to be the depth (D) of the measured V_s.

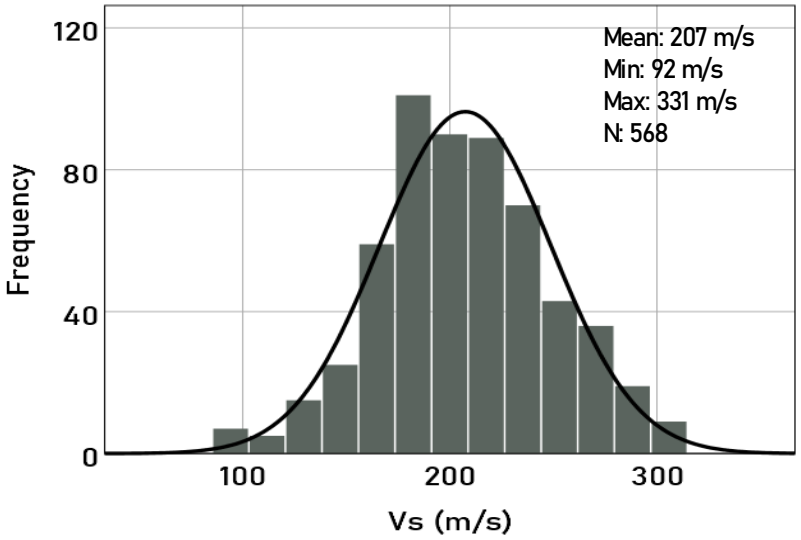

Figure 5-9. Distributions of the measured shear-wave velocity V_s; the black line represents the normal distribution. © Mohammad Salsabili, 2022.

In this work, the general CPTu-V_s correlation was developed for postglacial soils using 568 data pairs (Equation (5-9)). By distinguishing between cohesive (clay-like) and cohesionless (sand-like) soils, simple and robust regression equations for non-piezocone profiles can be developed. The soil behavior type index (I_c) was used to classify soil into two categories: clay ($I_c > 2.6$) and sand ($I_c < 2.6$). The soil-specific CPT-V_s correlations for the clayey soil (Equation (5-10)) and for the sandy soil (Equation (5-11)) are indicated as follows:

$$\text{All soils: } V_s = 7.648 q_t^{0.35} I_c^{0.322} D^{0.031} (1 + B_q)^{0.653} \quad \text{N = 568} \quad R^2 = 0.692 \quad \text{(5-9)}$$

$$\text{Clay: } V_s = 10.052 q_t^{0.379} D^{0.085} \quad \text{N = 453} \quad R^2 = 0.813 \quad \text{(5-10)}$$

$$\text{Sand: } V_s = 38.757 q_t^{0.174} D^{0.099} \quad \text{N = 115} \quad R^2 = 0.545 \quad \text{(5-11)}$$

where q_t is in kPa; D is depth (m) and B_q is normalized pore pressure (for detailed calculation see Robertson, (2009)).

5.5.1.4. Vs-depth profile

The V_s -depth profile is the core of developing geotechnical model and is of interest as a proxy to predict the spatial variability of V_s (Motazedian et al. 2011, 2020; Rosset et al. 2015; Nastev et al. 2016). The depth, D, shows a significant correlation with the measured V_s and the trend can be found frequently in the V_s profiles. Considering V_s as a function of only the depth variable allows us to predict the V_s everywhere by knowing the depth values.

Following the retrieval and processing of the older MTQ CPT logs, 4600 averaged data pairs of q_t and f_s were generated at 50 cm intervals. The V_s values were predicted by using the developed empirical CPT–V_s correlations (Eqs. (5-10) and (5-11)) for sands and clays. In addition, the SPT data were converted into V_s by applying the empirical relationship of Ohta and Goto (1978) for gravel sediments. Then, linear and nonlinear V_s–depth regression analyses were conducted on SCPTu and CPT–V_s data for sand and clay soils (Eqs. (5-12) – (5-14)) and on SPT–V_s data for gravels (Eq. (5-15)). The results are also shown in **Error! Reference source not found.**. The standard deviations of the V_s–depth correlations were used as a measure of statistical uncertainty. Note that the data from CPT–*Vs* and particularly SPT–V_s were subject to epistemic uncertainties. These sources of uncertainty have not been considered in our methodology, due to the limitations in analytical calculations. The use of site-specific V_s correlations for the dominant soil types of the study area (sand and clay) is, however, intended to reduce the epistemic uncertainties.

Sand and Clay mixture: $\mathrm{V_s} = 144.9 + 2.55 \times \mathrm{D}$	$\sigma_{Vs,SC} = 34\ m/s$	$R^2 = 0.43$	(5-12)
Clay: $\mathrm{V_s} = 114.5 + 9.4 \times \mathrm{D}^{0.76}$	$\sigma_{Vs,clay} = 33\ m/s$	$R^2 = 0.59$	(5-13)
Sand: $\mathrm{V_s} = 150.47 \times \mathrm{D}^{0.149}$	$\sigma_{Vs,sand} = 21\ m/s$	$R^2 = 0.66$	(5-14)
Gravel: $\mathrm{V_s} = 46.86 + 61.55 \times \mathrm{D}^{0.50}$	$\sigma_{Vs,gravel} = 34\ m/s$	$R^2 = 0.52$	(5-15)

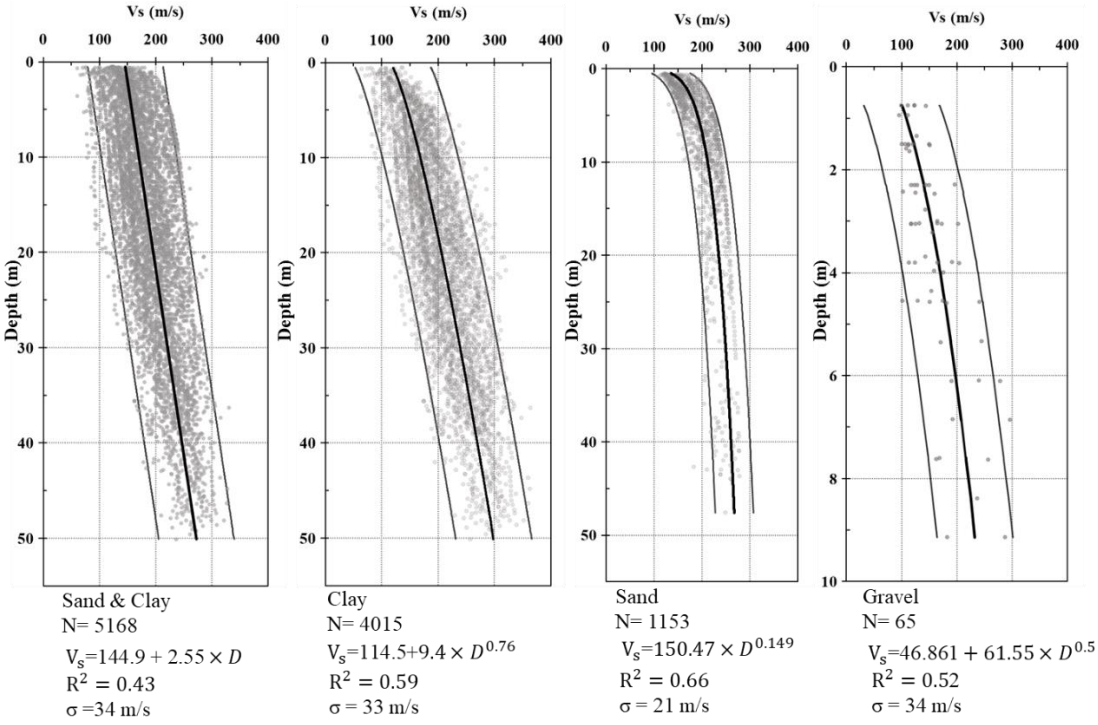

Figure 5-10. Interval V_s–depth relationships for postglacial sandy and clayey soils. Bold lines indicate average values; gray lines indicate ±2 standard deviations (σ).

5.5.2.3D Geotechnical modelling

A probabilistic method was used to estimate *Vs*. The V_s values for postglacial deposits were estimated on the basis of the probabilistic approach by using Eq. (5-2). The V_s values were calculated by using the V_s–depth profiles (Eqs. (5-13) - (5-15)) and the probability of soil occurrence (p_i). Then, the associated uncertainty was calculated on the basis of the combined variance approach (Eq. (5-3)) where the variance of the regression models for each soil type was incorporated for each block. Given that regression analysis removes the trend from the observed data, it allows residuals to behave as independent variables with a normal distribution, indicating that the V_s of each block is assumed to be normal. This assumption enables the application of parametric statistical methods, such as FOSM, in propagating the uncertainties in $V_{s,30}$ and T_0 mapping. Figure 5-11 presents the developed 3D geotechnical model, which indicates the spatial distribution of V_s, and its associated uncertainty is shown in Figure 5-11b. Due to the lack of V_s measurements in glacial deposits and bedrock and the

geological similarities between till and crystalline bedrock, the regional V_s values of the glacial deposits and bedrock were calculated from the data obtained by Motazedian et al. (2011) ($V_{s,till}$ = 580 m/s, $\sigma_{Vs,till}$=175 m/s) and Nastev et al. (2016b) ($V_{s,rock}$ = 2500 m/s).

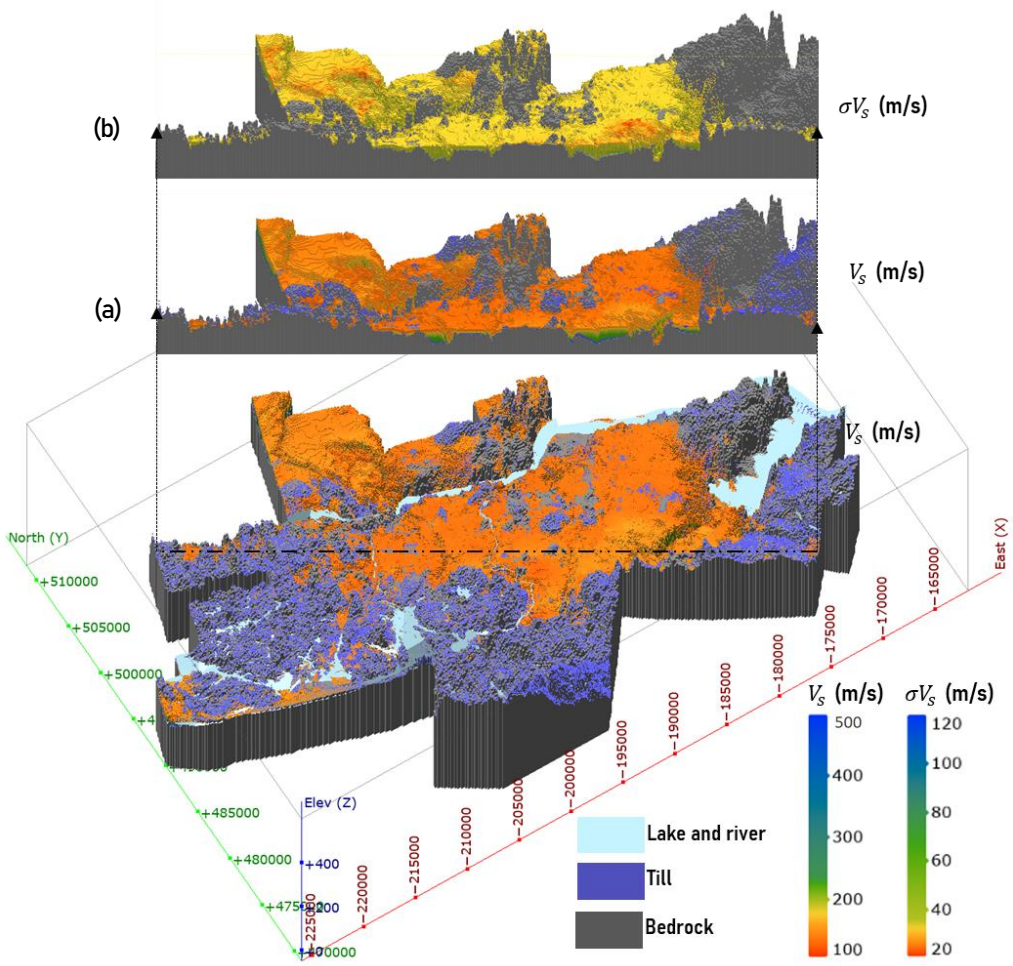

Figure 5-11. Probabilistic geotechnical model for the city of Saguenay: (a) 3D shear wave velocity and (b) associated V_s standard deviation. The color range indicates the V_s of postglacial deposits. The assumed uniform values for the glacial deposits were $V_{s,till}$ = 580 m/s and $\sigma_{Vs,till}$=175 m/s. © Mohammad Salsabili, 2022.

5.5.3. Validation

Three sites (Figure 5-8) composed of (1) sensitive clay soils, (2) transitional soil layers and (3) sandy soils with thin interbeds of clays, were selected to visually demonstrate the

capability and efficiency of the developed probabilistic and deterministic models in predicting the V_s values of the various soil types. In general, the predicted V_s values correspond fairly well to the measured values, although several inconsistencies were noted.

Soil classification was first performed using widely accepted CPTu-based charts and indices to determine the soil stratigraphy in selected SCPTu locations (Robertson, 2009, 2016). The normalized soil behavior type (SBTn) chart proposed by Robertson (2016) delineated the in situ behavior of soils, such as sensitivity, contractivity, or tendency to dilate, in addition to textural descriptions. Figure 5-12a shows a dominant fine-grained soil profile with alternating soft clay and silty clay sediment layers known as sensitive clays. Lower values of q_t and f_s and higher values of u_2 are typical indicators for distinguishing these soils. The CPTu parameters (q_t, f_s and u_2) fluctuate continuously over a short distance before stabilizing with depth, confirming the continuous stratigraphy of Laflamme-sensitive clays. Figure 5-12b depicts heterogeneous transitional soils with alternating clay and silty clay soils. The profile starts with interbedded thin (< 10 cm) sandy soils that transform into fairly soft transitional soils, most likely silty clay and clay soils. Figure 5-12c depicts a site with clean sandy soil interspersed with thin interbeds of fine-grained silt and clay soils. The variation in CPTu parameters indicates a sharp rather than a transitional change in soil behavior type.

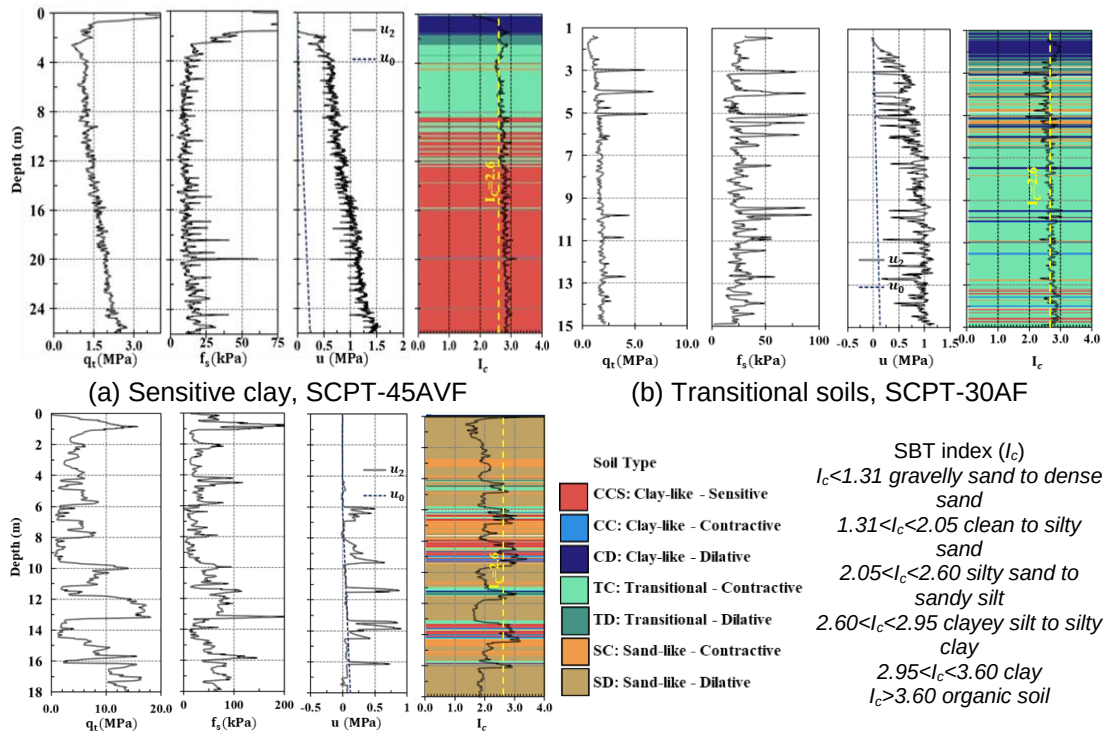

(a) Sensitive clay, SCPT-45AVF (b) Transitional soils, SCPT-30AF

(c) Sandy soils, SCPT-2AF

Figure 5-12. SCPTu profiles at three different sites composed of (a) sensitive clay soils, (b) transitional soil layers and (c) sandy soils with thin interbeds of clay; classification based on the *SBTn* chart (Robertson, 2016). © Mohammad Salsabili, 2022.

Figure 5-13 shows cross-sections of the 3D V_S block model and their associated standard deviations at the three representative SCPTu locations. Eq. (5-2) was calculated for each 3D block to generate the probabilistic V_S model V_s^p (Figure 5-13a). The respective standard deviations obtained from the combined variance (Eq. (5-3)) are illustrated in Figure 5-13b. As indicated earlier, the soil type behavior at these locations varies from top to bottom as follows: clayey, transitional and sandy soil. The resulting V_s^p values depend primarily on the depth and the probabilities of occurrence of the soil types. Based on Eq. (5-3), the resulting $\sigma_{V_s^p}$ values represent a combined standard deviation of $V_{s,clay}$, $V_{s,sand}$ and $V_{s,gravel}$, with their respective probabilities incorporated. The relatively higher $\sigma_{V_s^p}$ values for the sandy soil profile (Figure 5-13b bottom) than for the clayey soil (Figure 5-13b top) were attributed to higher heterogeneity in the sand profile, which resulted in higher simulation variance.

Figure 5-13c compares the measured V_s values using the SCPTu test, V_s predictions based on the deterministic V_s^d approach, and V_s predictions based on the probabilistic V_s^p approach. Essentially, the prediction methods serve as a good proxy for V_s measurements. In clays, which make up the majority of the study area, the estimated V_s values correspond closely to their measured counterparts. In transitional soils, we observed underestimations, but interestingly, the probabilistic approach provided better results. In sandy soils, due to intrinsic heterogeneity, the measured V_s values fluctuate considerably, and both the deterministic and probabilistic approaches underestimated V_s; however, in clay interbeds, the estimated V_s values were in good agreement with the measured values.

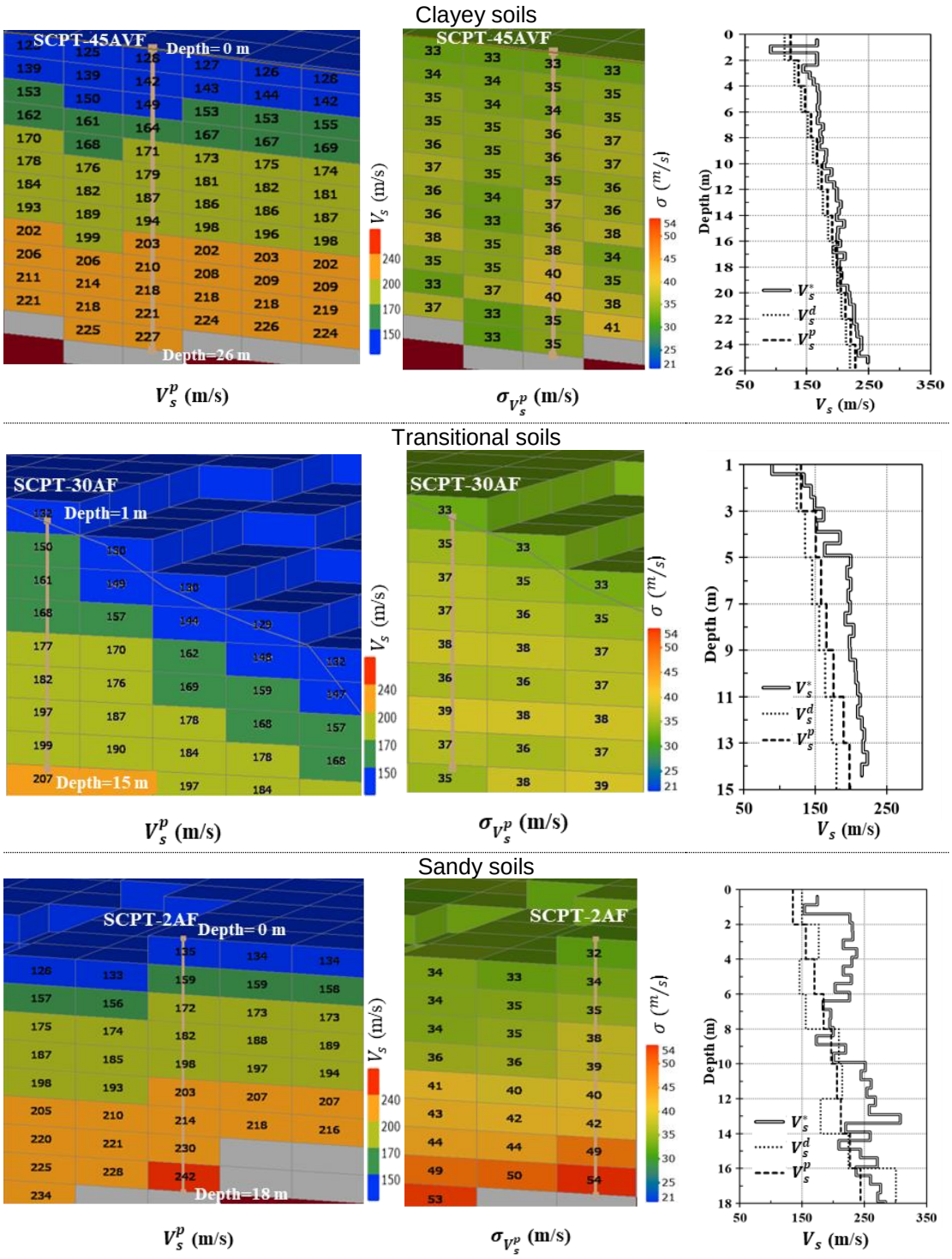

(a) probabilistic V_S model (b) V_S standard deviation (c) V_S profile

Figure 5-13. (a) Probabilistic 3D V_S block model and (b) associated standard deviations at the three different sites: from top to bottom, clayey, transitional and sandy soil; (c) comparison of the respective V_S profiles: SCPTu measurements (V_s^*), deterministic predictions (V_s^d), and probabilistic predictions (V_s^p). © Mohammad Salsabili, 2022.

5.6. $V_{s,30}$ and T_0 Mapping

Seismic site parameters, namely, the shear-wave velocity of the top 30 m, $V_{s,30}$, and the fundamental site period, T_0, were introduced to conduct site classifications. The computations were performed on a 2D raster with a cell size of 75×75 m based on the developed methodology. Based on the assumption that glacial sediments and bedrock have uniform V_s values, the time-averaged shear-wave velocity was first computed for postglacial soils from the ground surface down to the interface with the underlying glacial soils or bedrock (Figure 5-4). The estimation of $V_{S,30}$ was conducted for the first 30 m of soil as required. The averaged V_S values of a complete soil column, including the postglacial soils, till and rock, were also calculated. The $V_{S,30}$ and T_0 values for each 2D cell were calculated using Eq. (5-16) and Eq. (5-17).

$$V_{s,30} = \frac{30}{\frac{h_{pg}}{V_{s,pg}} + \frac{h_{till}}{V_{s,till}} + \frac{(30-h_{soil})}{V_{s,rock}}}, \tag{5-16}$$

$$T_0 = \frac{4 \times h_{soil}}{V_{s,avg}}, \tag{5-17}$$

where $V_{s,pg}$, $V_{s,till}$ and $V_{s,rock}$ (= 2500 m/s) are the shear-wave velocities of postglacial, glacial deposits and bedrock, respectively; $V_{s,pg}$ is computed using Eq. (5-6) with the incorporation of the 3D V_s model; $h_{soil} = h_{pg} + h_{till}$; and $V_{s,avg}$ is the soil average shear-wave velocities obtained by Eq. (5-18).

$$V_{s,avg} = \frac{h_{soil}}{\frac{h_{pg}}{V_{s,pg}} + \frac{h_{till}}{V_{s,till}}} \tag{5-18}$$

The final maps of the seismic site parameters are shown in Figure 5-14. At first glance, the spatial distribution of the seismic site parameters appears to follow the general variation patterns of surficial soil thickness (Figure 5-8). In shallow areas, where the thickness of the overlying soils is less than 30 meters, $V_{s,30}$ and T_0 exhibit the same pattern. The majority of the region was classified as rock or very stiff soil sites, with an average vibration period of less than 0.2 s, indicating that the seismic site response at these locations coincides at high frequencies,

similar to rock outcrops (Zhao et al., 2006). In contrast, regions with thicker sediments, where $V_{s,30}$ < 360 m/s and T_0 > 0.4 s, represent sites with seismic responses that resemble medium and soft soil behavior during seismic incidents. These zones will generally be sensitive to distant strong earthquakes with dominant low-frequency signals.

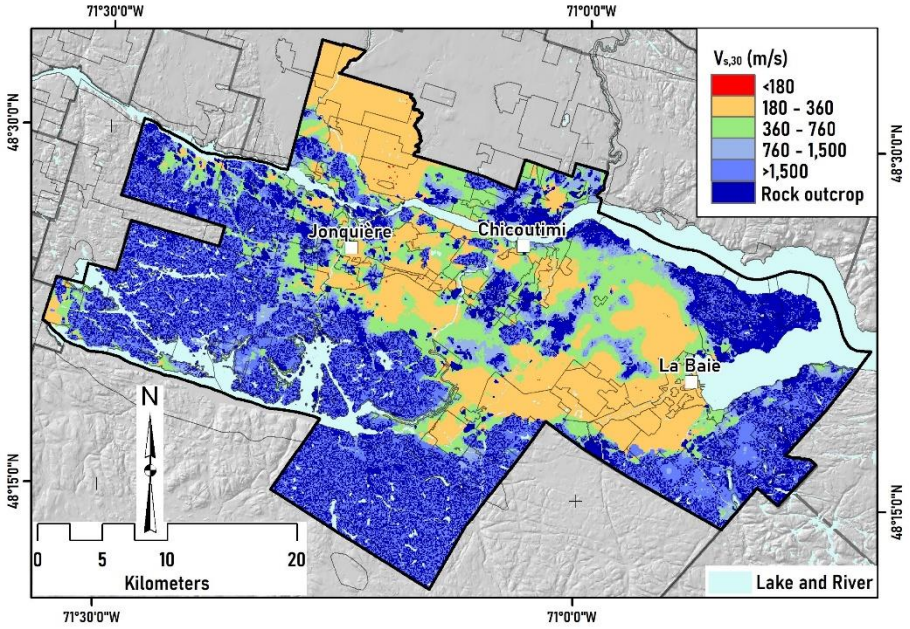

(a)

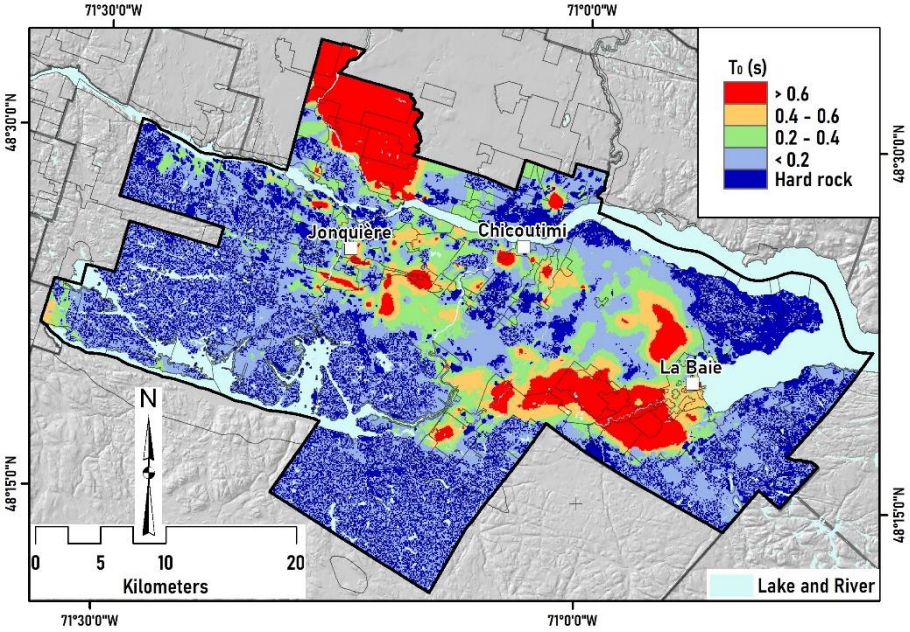

(b)

Figure 5-14. Spatial distribution of (a) $V_{s,30}$ and (b) fundamental site period, T_0. © Mohammad Salsabili, 2022.

5.6.1.Mapping uncertainty

The uncertainties associated with the seismic site parameters $V_{s,30}$ and T_0 were calculated by applying the FOSM method. The site parameters are given as the functions of the V_s of glacial and postglacial deposits, $f = f(V_{s,pg}, V_{s,till}, V_{s,rock})$. Eq. (5-7) can be rewritten as follows:

$$\sigma_f^2 = \left(\frac{\partial f}{\partial V_{s,pg}}\right)^2 \times \sigma_{Vs,pg}^2 + \left(\frac{\partial f}{\partial V_{s,till}}\right)^2 \times \sigma_{Vs,till}^2, \tag{5-19}$$

where σ_f^2, $\sigma_{Vs,pg}^2$, and $\sigma_{Vs,till}^2$ are the variances of the seismic site parameters, $V_{s,pg}$, and $V_{s,till}$, respectively.

Given that $f = V_{s,30}$, then Eq. (5-19) can be written as follows:

$$\sigma_{V_{s,30}}^2 = \left(\frac{30\times(\frac{h_{pg}}{V_{s,pg}^2})}{\left(\frac{h_{pg}}{V_{s,pg}}+\frac{h_{till}}{V_{s,till}}+\frac{(30-h_{soil})}{V_{s,rock}}\right)^2}\right)^2 \times \sigma_{Vs,pg}^2 + \left(\frac{30\times(\frac{h_{till}}{V_{s,till}^2})}{\left(\frac{h_{pg}}{V_{s,pg}}+\frac{h_{till}}{V_{s,till}}+\frac{(30-h_{soil})}{V_{s,rock}}\right)^2}\right)^2 \times \tag{5-20}$$

$\sigma_{Vs,till}^2$.

Similarly, considering that $f = T_0$, then Eq. () can be written as follows:

$$\sigma_{T_0}^2 = 16\left[\left(\frac{h_{pg}}{V_{s,pg}^2}\right)^2 \times \sigma_{Vs,pg}^2 + \left(\frac{h_{till}}{V_{s,till}^2}\right)^2 \times \sigma_{Vs,till}^2\right]. \tag{5-21}$$

Eqs. (5-20) and (5-21) were used to generate the uncertainty maps, including the complete soil column of postglacial and glacial deposits. The standard deviation $\sigma_{Vs,pg}$ was calculated using Eq. (5-7), but for glacial soils, a uniform $\sigma_{Vs,till}$ value of 175 m/s was assumed. It should be noted that in this study, $\sigma_{Vs,rock}^2$ was neglected to better reflect the uncertainty of only soil deposits. The spatial distributions of $\sigma_{V_{s,30}}$ and σ_{T_0} are shown in Figure 5-15a and 5-15b.

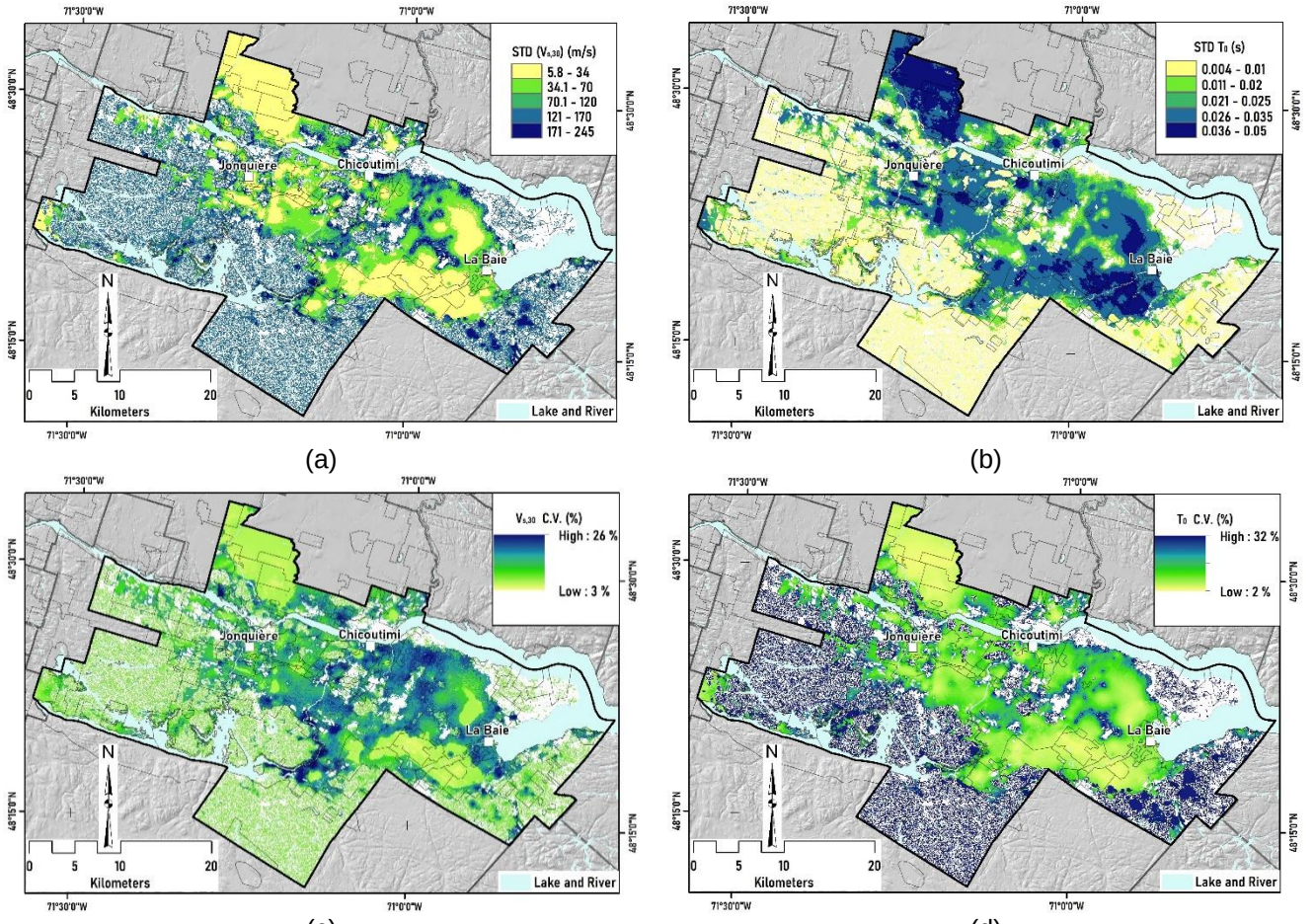

Figure 5-15. Spatial distributions of the associated uncertainties of seismic site parameters: (a) $\sigma_{V_{s,30}}$, (b) σ_{T_0}, (c) $V_{s,30}$ coefficient of variation, and (d) T_0 coefficient of variation. © Mohammad Salsabili, 2022.

Visual comparisons of Figure 5-15a and 5-15b with the corresponding spatial distributions in Figure 5-14 indicate that the uncertainties are approximately proportional to the modeled $V_{s,30}$ and T_0 values. Therefore, the distribution of $\sigma_{V_{s,30}}$ showed an approximately inverse spatial pattern relative to that of σ_{T_0}. Figures 5-15c and 5-15d present the coefficients of variation of $V_{s,30}$ and T_0, respectively. The areas with relatively high uncertainty in $V_{s,30}$ and T_0 are characterized by shallow deposits

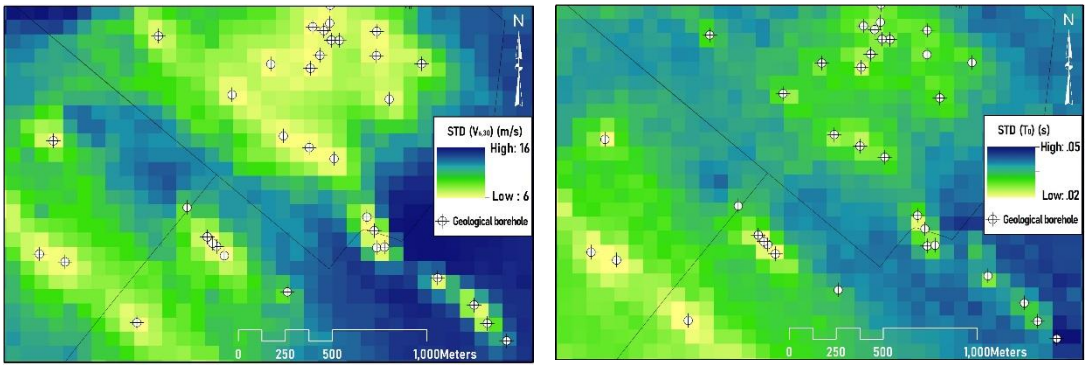

(a) (b)

Figure 5-16. The effect of spatial uncertainty in geological model on the uncertainties of seismic site parameters: (a) $\sigma_{V_{s,30}}$ and (b) σ_{T_0}. © Mohammad Salsabili, 2022.

The standard deviations shown in Figure 5 15 represent the model uncertainties that result from both the spatial variation of the geological soil units and the predicted V_S data. The efficiency of the developed methodology can be observed in Figure 5-16, which depicts the effect of geological uncertainty on the resulting geotechnical model. The certainty of the geological model is highest (p_i ~ 1) in the vicinity of the boreholes, and thus, the combined uncertainty of the geological and geotechnical models has its lowest value at these locations. In contrast, as the distance from the boreholes increases, the spatial uncertainty in the prediction of the soil units increases, leading to increased geotechnical model and seismic map uncertainty.

5.7. Conclusion

This study proposed a novel approach for determining the spatial uncertainties of the geological model and propagating these uncertainties to the geotechnical response variable V_S. A probabilistic approach for seismic site characterization was introduced to develop the 3D V_S model and to assess the uncertainty associated with combining various types of uncertainties in building the geological and geotechnical models. The model uncertainty was calculated using the combined variance of the probabilistic geological model and the variance of the V_S-depth regression model.

Given the complex stratigraphic setting and soil type heterogeneity of the study area, sequential indicator simulation was used to predict the probability of occurrence of the postglacial soil deposits. To quantify the uncertainty associated with the geological model, a method for determining the simulation variance was introduced.

Due to the lack of direct V_S measurements, it was necessary to supplement the V_S values inferred from existing CPT logs, which covered most of the study area. SCPT surveys were conducted to develop empirical site-specific CPT-V_S correlations for postglacial sediments in the study area, thereby reducing the epistemic uncertainties associated with the use of existing global correlations.

The V_S correlation functions were developed using nonlinear regression analyses, which incorporated q_t, depth and the SBT indicators for general soil types. In soil-specific correlations, the depth and q_t control the significant variability of V_S, and the developed CPT-V_S correlations were proposed for clay-like and sand-like soils.

The final output consisted of maps of the main site effect parameters $V_{S,30}$ and T_0, the uncertainties of which were assessed by using a 3D V_S model. The $V_{S,30}$ and T_0 spatial distributions appear to follow the general variation patterns of the surficial soil thickness. In shallow sediments, the $V_{s,30}$ and T_0 maps represent rock or very stiff soil conditions, with seismic responses in short vibration periods ≤ 0.2 s. In contrast, regions with thicker sediments denote sites with potential responses that resemble medium to soft soil conditions, with longer vibration periods dominating.

The respective $\sigma_{V_{s,30}}$ and σ_{T_0} maps represent the inherent random and epistemic uncertainty in the models, which are associated with both the spatial variability of the geological units and the statistical dispersion of the V_S data. As a result, the combined uncertainty of the geological and geotechnical models decreases in the vicinity of the geological boreholes due to the higher certainty of the geological model. In contrast, as the distance from the boreholes increases, the spatial uncertainty increases, resulting in greater uncertainties of $V_{S,30}$ and T_0.

Funding

This research was partially funded by the Natural Sciences and Engineering Research Council of Canada (NSERC) and Hydro-Quebec under project funding no. RDCPJ 521771 – 17.

Acknowledgments

The authors would like to thank the members of the CERM-PACES project for their cooperation and for providing access to the database.

Conflicts of Interest

The authors declare no conflicts of interest.

CONCLUSION

The study presents a multistep procedure to conduct seismic microzonation mapping in the complex and heterogeneous geological environment underlying the Saguenay City territory. The main seismic site parameters considered in the analyses were the average shear-wave velocity of the top 30 m ($V_{s,30}$), the average shear-wave velocity for the total thickness of the surficial sediments ($V_{s,avg}$) and the fundamental site period (T_0). Standard site classification based on ranges of $V_{s,30}$, $V_{s,avg}$ and T_0 values defines site classes including hard rock, moderately fractured and weathered rock, stiff and dense unconsolidated soil, loose sandy soil, and soft clayey soil. Such classification provided a straightforward basis for mapping local site responses in earthquake hazard analysis. Although shear-wave velocity (V_s) is known as a simple, effective and representative parameter for the determination of the site effect, the acquisition of sufficient direct V_s measurements is challenging in regional site characterization studies. Therefore, the acquisition of V_s measurements and the development of local empirical correlations between V_s, geotechnical parameters, depth, and soil types assisted in developing the 3D V_s estimation over the study area and reducing the epistemic uncertainty of using global correlations. Moreover, because of geological soil heterogeneity, the assessment of uncertainty in the determination of soil properties and site classes is essential.

To realistically address the soil variability and assess the associated uncertainties, a novel probabilistic approach for seismic site characterization was introduced. The method struggled to consider the uncertainty for a combined treatment of various sources of uncertainties in each step, namely, from developing the geological model to estimating the geotechnical parameters.

First, the performance of site classification schemes and seismic site parameters are analyzed. Four different classification schemes were applied and compared: NBCC, Eurocode 8, fundamental site period and the hybrid approach based on the combination of the main site parameters. All of the classification methods have their own advantages and limitations concerning the local geological and geotechnical conditions. As an overall conclusion, site

classification based on $V_{s,30}$ is generally consistent with the geological and geotechnical conditions of the study area. However, the results may be further improved by considering $V_{s,avg}$ in shallow (H<30 m) and T_0 in deeper soil sediments (H>30 m) as secondary parameters. In such a case, the impact of the stiffness and thickness of the surficial sediments will be better accounted for. The following specific remarks are also worth mentioning.

- A strong correlation between $V_{S,30}$ and T_0 was observed in shallow sediments (H<30 m), and a relatively weaker correlation was observed in deeper sediments (H>30 m), whereas the correlation between $V_{s,avg}$ and T_0 was practically inexistent. This suggests that the addition of $V_{s,rock}$ to the V_s soil in the top 30 m improves the correlation between $V_{s,30}$ and T_0. Due to this strong correlation, NBCC site classification yields similar patterns as the T_0 scheme.
- The site classification based on T_0 is affected considerably more by the thickness of the overlying sediments than by $V_{S,avg}$. Therefore, most of the shallow deposit conditions have a resonance period <0.2 s, which highlights the potential for seismic amplification in the short period range.
- Eurocode 8 does not include the hard-rock site condition, as is the case with site class A in the NBCC. Classification of rock sites into two categories helps distinguish the site effect in crystalline hard rocks and more fractured sedimentary rock formations.
- Hybrid site classification proposes a multitude of classification parameters, which, in certain cases, may lead to confusion in selecting the appropriate site class. However, the results arrange the site conditions mainly into two major groups: rock and soft soils. Stiff and medium stiffness soils share only a limited part of the study area as opposed to the NBCC site classification.

Second, a combined multistep methodology of interpolation and simulation was incorporated to develop a 3D geological model of soil deposits. The method focused on considering geologic rules of stratification, reducing the effect of skewness of the observation points, and modelling the uncertainties in predicting soil units. The interpolation procedure incorporated various sources of data, such as borehole logs, rock outcrops and shallow-till data; these sources of data were invaluable in soil thickness mapping. Providing bedrock and till deposit maps allowed us to consider the geologic rule of stratification of the basal till and the exclusion of low- and zero-thickness data from the simulation process of the discontinuous layers (i.e., clay, sand and gravel). The results of the validation and cross-validation verify that

empirical Bayesian kriging (EBK) is an appropriate interpolation method, producing an accurate outcome in regional studies involving extensive data with complexity. Next, the occurrence probabilities of soil units were generated by using sequential indicator simulation (SIS). The results indicated that the assumption of a continuous stratigraphic layer for the clay and for the sand and gravel units as drawn in the geological sections does not correspond to the real spatial variability of these layers. This observation is supported by the abrupt discontinuity and repetition of the deposits in the 3D model. The simulation of the soil type also assists in considering the spatial soil variability and its associated uncertainty. Therefore, the areas identified with increased uncertainty are characterized by considerable stratigraphic inconsistency and require further in situ measurements.

Third, invasive seismic piezocone penetration tests (SCPTu) were conducted, and empirical CPTu-V_s correlations for postglacial sediments were developed using nonlinear multiple regression analyses. Due to the scarcity of direct V_s measurements, it was necessary to supplement the V_s values with inferred values from the available CPT logs, which cover most of the study area. Developing region-specific correlations reduced the epistemic uncertainties associated with using existing global correlations. The CPTu-V_s correlations were developed for a wide range of postglacial sediments of the Champlain and Laflamme seas. A dataset was built by collecting SCPTu measurements at 40 test sites in sediments ranging from fine-grained silty clays to gravely sands. The results show that CPTu-V_s correlations were affected by the soil type and sedimentation environment. The major findings of the study are summarized below.

- The application of the existing V_s correlation equations presents the risk of overestimating or underestimating V_s values due to probable differences in geological age and the deposition environment. The results revealed that consideration of the geological age (Pleistocene or Holocene) is important in estimating unbiased V_s values.
- The general model developed for a wide range of soil types can provide reliable predictions by using normalized indicators, such as normalized pore water pressure (B_q) and soil behavior type index (I_c).

- B_q and I_c are key parameters in regression models and soil classifications. I_c helps improve the fitting results, and B_q is effective in the classification of transitional soil as a categorical variable.

- $(V_{s1}/Q_{tn})^{\alpha}$–I_c relationships are suggested to differentiate transitional soils. In this study, different correlations were observed with different values of I_c and the exponent α. On the basis of the observed trends, I_c=2.2 was established as the threshold between clay- and sand-like soils.

- Slightly improved results can be obtained from sand-specific regression models when stress-normalised V_s and CPTu parameters are applied. Stress normalisation, however, is not recommended for clay-specific models due to the remaining dependency of V_{s1} on depth.

- Compared with the use of depth, the adoption of σ'_{v0} as an indicator of the stress state in sands provides better results. In clays, applying the direct measurement of depth is recommended.

- Depth is a leading parameter in the prediction of V_s in fine-grained soils and can predict most of the variability of V_s for Laflamme-sea clays; however, high dispersion occurs for Champlain-sea clays. This high dispersion may be explained by the large study area in the Champlain basin and the potential differences in the mineral compositions of soil deposits, sedimentation and successive erosional processes.

Finally, a probabilistic approach for seismic site characterization was applied to develop the 3D V_s model and assess the associated uncertainty. The uncertainty model was assessed using the combined variance of the probabilistic geological model and the variance associate with the V_s-depth regression models. The V_s correlation functions were developed using nonlinear regression analyses with the incorporation of depth and q_t for clay-like and sand-like soils. Considering the complex stratigraphic setting and soil type heterogeneity, the method of determining the simulation variance was implemented. The final output consisted of mapping the main site effect parameters $V_{s,30}$ and T_0, and assessing their respective uncertainties by using a 3D V_s model. The $V_{s,30}$ and T_0 spatial distributions appear to follow the general variation patterns of the surficial soil thickness. In shallow sediments, the $V_{s,30}$ and T_0 maps represent rock or very stiff soil conditions, with seismic responses in short vibration periods ≤ 0.2 s. In contrast, regions with thicker sediments denote sites with potential responses that resemble medium to soft soil conditions, with dominating longer vibration

periods. The respective $\sigma_{V_{s,30}}$ and σ_{T_0} maps represent the inherent random and epistemic uncertainty in the models, which are associated with both the spatial variability of the geological units and the statistical dispersion of the V_S data. As a result, the combined uncertainty of the geological and geotechnical models decreases in the vicinity of the geological boreholes due to the higher certainty of the geological model. In contrast, as the distance from the boreholes increases, the spatial uncertainty increases, resulting in greater uncertainties of $V_{s,30}$ and T_0.

LIMITATIONS AND PERSPECTIVES FOR FUTURE RESEARCH

The followings are some of the issues and limitations recognized during this research process as interesting avenues for further investigation.

I. Stratigraphic sections over the Saguenay territory have been considered “hard data” in this thesis. Nevertheless, these sections are conceptual models and they are affected by uncertainties, both epistemic and inherent. These conceptual geological sections are constructed using stratigraphic logs from a number of real boreholes, and a larger number of virtual boreholes were used as supplementary data points. The virtual boreholes are regularly spaced and their main purpose is to reduce the sparsity of the data points for the subsequent construction of 3D stratigraphic models. The data from both the real boreholes and the virtual boreholes are affected by uncertainties. For the real boreholes, uncertainties are related, for instance, to the simplifications that are required in constructing the stratigraphic column, since finer layers cannot be considered individually. Also, the level of uncertainty varies with the drilling method, as only a limited number of drilling methods involve the coring of soft sediments. Concerning the use of virtual boreholes, this method requires the application of geological judgement by an expert geologist. The level of uncertainty of the resulting model varies with the degree of knowledge that the geologist has previously developed on the considered geological context. Other sources of uncertainty affecting these stratigraphic sections would very likely be identified by further thinking about the construction process of these sections. All of these sources of uncertainty should be investigated in future studies, and their relative importance should be evaluated with respect to applications such as seismic microzonation.

II. The V_S-depth profiles were developed using invasive geophysical and geotechnical tests particularly obtained by SCPT, CPT and SPT surveying. This type of method

is hampered by its depth limitations as well as its incapability to work in coarse and stiff soils. Further investigation is suggested to be performed with the use of non-invasive geophysical methods, such as surface wave analyses (e.g. microtremors) and seismic reflections. In order to determine the V_s of bedrock and glacial deposits, the seismic reflection test is recommended since there is no direct V_S measurement for these geological units in the Saguenay region.

III. In developing the 3D V_s model, we suggest considering the spatial autocorrelation of the V_s data and the corresponding spatial uncertainties. When the spatial correlation is considered, it is first possible to spatially estimate the V_s values, then it is possible to quantify the uncertainty of the estimates, and finally, it contributes to reducing the uncertainty in the V_s model.

IV. The uncertainty of seismic site parameters (such as $V_{s,30}$) was assessed based on geological and geotechnical uncertainties. Further research can be conducted to determine how uncertainties affect the assessment of amplification factors. The National Building Code of Canada (NBCC) can be used for this purpose, in order to apply the uncertainties in $V_{s,30}$ to the site factors. Based on the amplification factors and associated uncertainties, the final seismic microzonation map will provide optimistic or pessimistic seismic hazard models.

V. The empirical approach in the determination of site classes and assigning associated amplification factors overlooks the complex nature of the subsurface structures, such as the 3D basin model that potentially can cause unprecedented amplifications e.g. basin-edge or buried valley focusing amplification effect. The developed probabilistic 3D geotechnical model allows to perform detailed seismic site response analyses using numerical methods. We suggest applying quantitative analyses of site effects with earthquake scenarios, using standard equivalent linear and nonlinear analyses (e.g. SHAKE and DEEPSOIL). The analyses can be applied to several specific areas (based on our resulting maps), such as urban and emergency sites, important buildings and infrastructures.

LIST OF REFERENCES

Anbazhagan P, Parihar A and Rashmi HN (2012) Review of correlations between SPT N and shear modulus: A new correlation applicable to any region. *Soil Dynamics and Earthquake Engineering* 36. Elsevier: 52–69. DOI: 10.1016/j.soildyn.2012.01.005.

Andrus RD, Mohanan NP, Piratheepan P, et al. (2007) Predicting shear-wave velocity from cone penetration resistance. *Proceedings of the 4th International Conference on Earthquake Geotechnical Engineering* (1454): 12.

Aranze (2104) User Manual for Leapfrog Geo version 2.1.

Asten MW and Boore D (2006) Comparison of Shear-Velocity Profiles of Unconsolidated Sediments Near the Coyote Borehole (CCOC) Measured with Fourteen Invasive and Non-invasive Methods Editorial. *Journal of Environmental & Engineering Geophysics* 10(2): 85–85. DOI: 10.2113/jeeg10.2.85.

Bard P-Y and Riepl-Thomas J (1999) Wave propagation in complex geological structures and their effects on strong ground motion. In: E. Kausel and G. Manolis (ed.) *Wave Motion in Earthquake Engineering*. Southampton, Great Britain: WIT Press, pp. 1–45.

Boore DM and Atkinson GM (2008) Ground-motion prediction equations for the average horizontal component of PGA, PGV, and 5%-damped PSA at spectral periods between 0.01 s and 10.0 s. *Earthquake Spectra* 24(1): 99–138. DOI: 10.1193/1.2830434.

Borcherdt RD (1994) Estimates of Site-Dependent Response Spectra for Design (Methodology and Justification). *Earthquake Spectra* 10(4): 617–653. DOI: 10.1193/1.1585791.

Borcherdt RD and Glassmoyer G (1992) On the characteristics of local geology and their influence on ground motions generated by the Loma Prieta earthquake in the San Francisco Bay region, California. *Bulletin of the seismological society of America* 82(2). The Seismological Society of America: 603–641.

Bouchard R and Tavenas F (1983) Origine de la preconsolidation des argiles du Saguenay , Quebec. *Canadian geotechnic journal* 20: 315–328. DOI: 10.1139/t83-034.

Braganza S and Atkinson GM (2017) A model for estimating amplification effects on seismic hazards and scenario ground motions in southern Ontario. *Canadian Journal of Civil Engineering* 44(6): 441–451. DOI: 10.1139/cjce-2016-0471.

Brandenberg SJ, Bellana N and Shantz T (2010) Shear wave velocity as function of standard penetration test resistance and vertical effective stress at California bridge sites. *Soil Dynamics and Earthquake Engineering* 30(10). Elsevier: 1026–1035. DOI: 10.1016/j.soildyn.2010.04.014.

BSSC (2015) NEHRP Recommended Seismic Provisions for New Buildings and Other Structures, 2015 Edition, Volume I: Part 1 Provisions, Part 2 Commentary, FEMA Rep. No. P-1050-1. National Institute of Building Sciences Washington, DC.

Building Seismic Safety Council (2009) NEHRP Recommended Seismic Provisions for New Buildings and Other Structures, FEMA P-1050. *Fema P-750*. National Institute of Building Sciences Washington, DC. Available at: http://www.fema.gov/media-library-data/20130726-1730-25045-1580/femap_750.pdf.

Cai G, Puppala AJ and Liu S (2014) Characterization on the correlation between shear wave velocity and piezocone tip resistance of Jiangsu clays. *Engineering Geology* 171. Elsevier B.V.: 96–103. DOI: 10.1016/j.enggeo.2013.12.012.

Campanella RG and Stewart WP (1992) Seismic cone analysis using digital signal processing for dynamic site characterization. *Canadian Geotechnical Journal* 29(3). NRC Research Press: 477–486.

Campbell KW and Bozorgnia Y (2008) NGA ground motion model for the geometric mean

horizontal component of PGA, PGV, PGD and 5% damped linear elastic response spectra for periods ranging from 0.01 to 10 s. *Earthquake Spectra* 24(1): 139–171. DOI: 10.1193/1.2857546.

Campbell KW and Bozorgnia Y (2014) NGA-West2 ground motion model for the average horizontal components of PGA, PGV, and 5% damped linear acceleration response spectra. *Earthquake Spectra* 30(3): 1087–1114. DOI: 10.1193/062913EQS175M.

Castellaro S, Mulargia F and Rossi PL (2008) VS30: Proxy for seismic amplification? *Seismological Research Letters* 79(4). Seismological Society of America: 540–543.

CEN (2004) *Eurocode 8: Design of Structures for Earthquake Resistance - Part 1 : General Rules, Seismic Actions and Rules for Buildings*. European Standard EN 1998-1:2004, Comité Européen de Normalisation.

CERM-PACES (2013) Résultat du Programme d'Acquisition de Connaissances sur les Eaux Souterraines de la Région Saguenay-Lac-Saint-Jean. Chicoutimi: Centre d'Études sur les Ressources Minérales, Université du Québec à Chicoutimi. Available at: http://paces.uqac.ca/programme.html (accessed 29 April 2021).

Chesnaux R, Lambert M, Walter J, et al. (2017) A simplified geographical information systems (GIS) -based methodology for modeling the topography of bedrock : illustration using the Canadian Shield. Applied Geomatics. DOI: 10.1007/s12518-017-0183-1.

Chiles J-P and Delfiner P (2009) *Geostatistics: Modeling Spatial Uncertainty*. John Wiley & Sons.

Clayton CRI (2011) Stiffness at small strain: research and practice. *Géotechnique* 61(1). Thomas Telford Ltd: 5–37.

Cowan EJ, Beatson RK, Ross HJ, et al. (2003) Practical implicit geological modelling. In: *Fifth international mining geology conference*, 2003, pp. 17–19.

Cubrinovski M, Wotherspoon LM, Bradley BA, et al. (2015) Applicability of existing empirical shear wave velocity correlations to seismic cone penetration test data in Christchurch New Zealand. *Soil Dynamics and Earthquake Engineering* 75. Elsevier: 76–86. DOI: 10.1016/j.soildyn.2015.03.021.

Daigneault R-A, Cousineau P, Leduc E, et al. (2011) *Rapport final sur les travaux de cartographie des formations superficielles réalisés dans le territoire municipalisé du Saguenay-Lac-Saint-Jean*. *Quebec City: Ministère des Ressources naturelles et de la Faune du Québec*.

Davidson A (1998) *Geological Map of the Grenville Province: Canada and Adjacent Parts of the United States of America*.

De Kemp EA (2000) *Three-Dimensional Integration and Visualization of Structural Field Data :Tools for Regional Subsurface Mapping = Integration et Visualisation 3-D de Données Structurales de Terrain : Outils Pour La Cartographie Géologique Régionale*. Université du Québec à Chicoutimi. Available at: http://theses.uqac.ca/resume_these.php?idnotice=12127333%5Cnhttp://theses.uqac.ca/resume_these.php?idnotice=12127333&onglet=ti.

Deutsch C V. (2006) A sequential indicator simulation program for categorical variables with point and block data: BlockSIS. *Computers and Geosciences* 32(10): 1669–1681. DOI: 10.1016/j.cageo.2006.03.005.

Deutsch C V and Journel AG (1997) GSLIB : Geostatistical Software Library and User ' s Guide Second Edition Preface to the Second Edition.

Dobry R, Borcherdt RD, Crouse CB, et al. (2000) New site coefficients and site classification system used in recent building seismic code provisions. *Earthquake spectra* 16(1): 41–67.

Du Berger R, Roy DW, Lamontagne M, et al. (1991) The Saguenay (Quebec) earthquake of November 25, 1988: seismologic data and geologic setting. *Tectonophysics* 186(1–2). Elsevier: 59–74.

El-Ramly H, Morgenstern NR and Cruden DM (2002) Probabilistic slope stability analysis for practice. *Canadian Geotechnical Journal* 39(3): 665–683. DOI: 10.1139/t02-034.

Elkateb T, Chalaturnyk R and Robertson PK (2003) An overview of soil heterogeneity : quantification and implications on geotechnical field problems. 15: 1–15. DOI: 10.1139/T02-090.

Fenton GA (1999) Estimation for stochastic soil models. *Journal of Geotechnical and Geoenvironmental Engineering* 125(6). American Society of Civil Engineers: 470–485.

Fenton GA and Griffiths D V. (2003) Bearing-capacity prediction of spatially random c - ø soils. *Canadian Geotechnical Journal* 40(1): 54–65. DOI: 10.1139/t02-086.

Ferrari F, Apuani T and Giani GP (2014) Rock Mass Rating spatial estimation by geostatistical analysis. *International Journal of Rock Mechanics and Mining Sciences* 70. Elsevier: 162–176. DOI: 10.1016/j.ijrmms.2014.04.016.

Finn WDL and Ruz F (2015) Amplification effects of thin soft surface layers: A study for NBCC 2015. *Geotechnical, Geological and Earthquake Engineering* 37(April): 33–44. DOI: 10.1007/978-3-319-10786-8_2.

Foulon T, Saeidi A, Chesnaux R, et al. (2018) Spatial distribution of soil shear-wave velocity and the fundamental period of vibration–a case study of the Saguenay region, Canada. *Georisk* 12(1): 74–86. DOI: 10.1080/17499518.2017.1376253.

Fulton RJ, Fenton MM and Rutter NW (1986) Summary of quaternary stratigraphy and history, Western Canada. *Quaternary Science Reviews* 5(C). Pergamon Journals Ltd.: 229–241. DOI: 10.1016/0277-3791(86)90189-7.

Gallipoli MR and Mucciarelli M (2009a) Comparison of site classification from VS30, VS10, and HVSR in Italy. *Bulletin of the Seismological Society of America*. DOI: 10.1785/0120080083.

Gallipoli MR and Mucciarelli M (2009b) Comparison of site classification from VS30, VS10, and HVSR in Italy. *Bulletin of the Seismological Society of America* 99(1): 340–351. DOI: 10.1785/0120080083.

Garofalo F, Foti S, Hollender F, et al. (2016a) InterPACIFIC project: Comparison of invasive and non-invasive methods for seismic site characterization. Part II: Inter-comparison between surface-wave and borehole methods. *Soil Dynamics and Earthquake Engineering* 82. Elsevier: 241–254. DOI: 10.1016/j.soildyn.2015.12.009.

Garofalo F, Foti S, Hollender F, et al. (2016b) InterPACIFIC project: Comparison of invasive and non-invasive methods for seismic site characterization. Part II: Inter-comparison between surface-wave and borehole methods. *Soil Dynamics and Earthquake Engineering* 82. Elsevier: 241–254. DOI: 10.1016/j.soildyn.2015.12.009.

GeoLogismiki (2014) CPeT-IT User's Manual v.1.4. Available at: https://www.geologismiki.gr/Documents/CPeT-IT/CPeT-IT manual.pdf (accessed 27 March 2022).

Ghofrani H, Atkinson GM and Goda K (2013) Implications of the 2011 M9.0 Tohoku Japan earthquake for the treatment of site effects in large earthquakes. *Bulletin of Earthquake Engineering* 11(1): 171–203. DOI: 10.1007/s10518-012-9413-4.

Giustini F, Ciotoli G, Rinaldini A, et al. (2019) Mapping the geogenic radon potential and radon risk by using Empirical Bayesian Kriging regression: A case study from a volcanic area of central Italy. *Science of the Total Environment* 661. Elsevier B.V.: 449–464. DOI: 10.1016/j.scitotenv.2019.01.146.

Goovaerts P (1999) Geostatistics in soil science : state-of-the-art and perspectives.: 1–45.

Hallal MM and Cox BR (2021) An H/V geostatistical approach for building pseudo-3D Vs models to account for spatial variability in ground response analyses Part I: Model development. *Earthquake Spectra* 37(3): 2013–2040. DOI: 10.1177/8755293020981989.

Hassani B and Atkinson GM (2016) Applicability of the NGA-west2 site-effects model for central and eastern North America. *Bulletin of the Seismological Society of America* 106(3): 1331–1341. DOI: 10.1785/0120150321.

Heath DC, Wald DJ, Worden CB, et al. (2020) A global hybrid VS30 map with a topographic slope–based default and regional map insets. *Earthquake Spectra* 36(3): 1570–1584. DOI: 10.1177/8755293020911137.

Hegazy YA and Mayne PW (2006) A Global Statistical Correlation between Shear Wave Velocity and Cone Penetration Data. 40861(May 2006): 243–248. DOI: 10.1061/40861(193)31.

Holzer TL, Padovani AC, Bennett MJ, et al. (2005) Mapping NEHRP VS30 site classes. *Earthquake Spectra* 21(2): 353–370. DOI: 10.1193/1.1895726.

Huang S, Huang M and Lyu Y (2019) A novel approach for sand liquefaction prediction via local mean-based pseudo nearest neighbor algorithm and its engineering application. *Advanced Engineering Informatics* 41. Elsevier: 100918. DOI: 10.1016/j.aei.2019.04.008.

Hunter JA and Crow HL (2012) Shear wave velocity measurement guidelines for canadian seismic site characterization in soil and rock. *Geological Survey of Canada*: 227. DOI: 10.4095/291753.

Hunter JA and Crow HL (2015) EARTH SCIENCE SECTOR GENERAL INFORMATION PRODUCT 110 e Shear Wave Velocity Measurement Guidelines for Canadian Seismic Site Characterization in Soil and Rock. DOI: 10.4095/291753.

Hunter JA, Benjumea B, Harris JB, et al. (2002) Surface and downhole shear wave seismic methods for thick soil site investigations. *Soil Dynamics and Earthquake Engineering* 22(9–12): 931–941. DOI: 10.1016/S0267-7261(02)00117-3.

Hussien MN and Karray M (2015) Shear wave velocity as a geotechnical parameter: an overview. *Canadian Geotechnical Journal* 53(2): 252–272. DOI: 10.1139/cgj-2014-0524.

Imai T and Tonouchi K (1982) Correlation of N value with S-wave velocity and shear modulus. In: *Penetration testing. Proc. 2nd European symposium, Amsterdam, 1982*, 1982, pp. 67–72. DOI: 10.1201/9780203743959-11.

Isaaks EH and Srivastava MR (1989) *Applied Geostatistics*.

Jessell M, Aillères L, De Kemp E, et al. (2014) Next generation three-dimensional geologic modeling and inversion. *Society of Economic Geologists Special Publication* 18(18): 261–272.

Kaggwa WS and Kuo YL (2011) Probabilistic techniques in geotechnical modelling - Which one should you use? *Australian Geomechanics Journal* 46(3): 21–28.

Karray M and Hussien MN (2017) Shear wave velocity as function of cone penetration resistance and grain size for Holocene-age uncemented soils: a new perspective. *Acta Geotechnica* 12(5). Springer: 1129–1158.

Kishida T and Tsai C-C (2017) Prediction model of shear wave velocity by using SPT blow counts based on the conditional probability framework. *Journal of Geotechnical and Geoenvironmental Engineering* 143(4). American Society of Civil Engineers: 4016108.

Kring K and Chatterjee S (2020) Uncertainty quantification of structural and geotechnical parameter by geostatistical simulations applied to a stability analysis case study with limited exploration data. *International Journal of Rock Mechanics and Mining Sciences*

125(December 2018). Elsevier Ltd: 104157. DOI: 10.1016/j.ijrmms.2019.104157.

Krivoruchko K (2012) Empirical bayesian kriging. *ESRI: Redlands, CA.) Available at http://www. esri. com/news/arcuser/1012/empirical-byesian-kriging. html [Verified October 2018]*.

Krivoruchko K and Gribov A (2019) Evaluation of empirical Bayesian kriging. *Spatial Statistics* 32. Elsevier B.V.: 100368. DOI: 10.1016/j.spasta.2019.100368.

L'Heureux JS and Long M (2017) Relationship between shear-wave velocity and geotechnical parameters for Norwegian clays. *Journal of Geotechnical and Geoenvironmental Engineering* 143(6). DOI: 10.1061/(ASCE)GT.1943-5606.0001645.

Lamontagne M (2002) An overview of some significant eastern Canadian earthquakes and their impacts on the geological environment, buildings and the public. *Natural Hazards* 26(1): 55–67. DOI: 10.1023/A:1015268710302.

LaSalle P and Tremblay G (1978) Dépôts meubles Saguenay-Lac-Saint-Jean. Ministère des richesses naturelles.

Lee RL, Bradley BA, Ghisetti FC, et al. (2017) Development of a 3D velocity model of the Canterbury, New Zealand, region for broadband ground-motion simulation. *Bulletin of the Seismological Society of America* 107(5): 2131–2150. DOI: 10.1785/0120160326.

Li J and Heap AD (2008) A Review of Spatial Interpolation Methods for Environmental Scientists. *Australian Geological Survey Organisation* GeoCat# 68(2008/23): 154. DOI: http://www.ga.gov.au/image_cache/GA12526.pdf.

Liang M, Marcotte D and Benoit N (2014) A comparison of approaches to include outcrop information in overburden thickness estimation. *Stochastic Environmental Research and Risk Assessment* 28(7): 1733–1741. DOI: 10.1007/s00477-013-0835-6.

Licata V, Forte G and Antonio O (2019) *A Multi - Level Study for the Seismic Microzonation of the Western Area of Naples (Italy)*. Springer Netherlands. DOI: 10.1007/s10518-019-00665-6.

Locat J and St-Gelais D (2014) Nature of sensitive clays from Quebec. In: *Landslides in Sensitive Clays*. Springer, pp. 25–37.

Long M and Donohue S (2010) Characterization of Norwegian marine clays with combined shear wave velocity and piezocone cone penetration test (CPTU) data. *Canadian Geotechnical Journal* 47(7): 709–718. DOI: 10.1139/T09-133.

Lunne T, Powell JJM and Robertson PK (2002) *Cone Penetration Testing in Geotechnical Practice*. CRC Press. DOI: 10.1201/9781482295047.

Luzi L, Puglia R, Pacor F, et al. (2011) Proposal for a soil classification based on parameters alternative or complementary to Vs,30. *Bulletin of Earthquake Engineering* 9(6): 1877–1898. DOI: 10.1007/s10518-011-9274-2.

Madiai C and Simoni G (2004) Shear wave velocity-penetration resistance correlation for Holocene and Pleistocene soils of an area in central Italy. *International Symposium on Geotechnical and Geophysical Site Characterization* (January 2004): 1687–1694.

Mayne PW and Rix GJ (1995) Correlations Between Shear Wave Velocity and Cone Tip Resistance in Natural Clays. *Soils and Foundations* 35(2): 107–110. DOI: 10.3208/sandf1972.35.2_107.

McBratney AB and Odeh IOA (1997) Application of fuzzy sets in soil science: Fuzzy logic, fuzzy measurements and fuzzy decisions. *Geoderma* 77(2–4): 85–113. DOI: 10.1016/S0016-7061(97)00017-7.

McGann CR, Bradley BA, Taylor ML, et al. (2015a) Applicability of existing empirical shear wave velocity correlations to seismic cone penetration test data in Christchurch New

Zealand. *Soil Dynamics and Earthquake Engineering* 75. Elsevier: 76–86. DOI: 10.1016/j.soildyn.2015.03.021.

McGann CR, Bradley BA, Taylor ML, et al. (2015b) Development of an empirical correlation for predicting shear wave velocity of Christchurch soils from cone penetration test data. *Soil Dynamics and Earthquake Engineering* 75. Elsevier: 66–75. DOI: 10.1016/j.soildyn.2015.03.023.

Mirzaei R and Sakizadeh M (2016) Comparison of interpolation methods for the estimation of groundwater contamination in Andimeshk-Shush Plain, Southwest of Iran. *Environmental Science and Pollution Research* 23(3): 2758–2769. DOI: 10.1007/s11356-015-5507-2.

Molnar S, Cassidy JF, Castellaro S, et al. (2018) Application of Microtremor Horizontal-to-Vertical Spectral Ratio (MHVSR) Analysis for Site Characterization: State of the Art. *Surveys in Geophysics* 39(4). Springer Netherlands: 613–631. DOI: 10.1007/s10712-018-9464-4.

Molnar S, Assaf J, Sirohey A, et al. (2020a) Overview of local site effects and seismic microzonation mapping in Metropolitan Vancouver, British Columbia, Canada. *Engineering Geology* 270. Elsevier B.V. DOI: 10.1016/j.enggeo.2020.105568.

Molnar S, Assaf J, Sirohey A, et al. (2020b) Overview of local site effects and seismic microzonation mapping in Metropolitan Vancouver, British Columbia, Canada. *Engineering Geology* 270. Elsevier B.V: 105568. DOI: 10.1016/j.enggeo.2020.105568.

Moss RES (2008) Quantifying measurement uncertainty of thirty-meter shear-wave velocity. *Bulletin of the Seismological Society of America* 98(3): 1399–1411. DOI: 10.1785/0120070101.

Motalleb Nejad M, Manahiloh KN and Momeni MS (2017) Random-effects regression model for shear wave velocity as a function of standard penetration test resistance, vertical effective stress, fines content, and plasticity index. *Soil Dynamics and Earthquake Engineering* 103(October). Elsevier Ltd: 95–104. DOI: 10.1016/j.soildyn.2017.09.022.

Motazedian D, Hunter JA, Pugin A, et al. (2011) Development of a Vs 30 (NEHRP) map for the city of Ottawa, Ontario, Canada . *Canadian Geotechnical Journal* 48(3): 458–472. DOI: 10.1139/t10-081.

Motazedian D, Torabi H, Hunter JA, et al. (2020) Seismic site period studies for nonlinear soil in the city of Ottawa, Canada. *Soil Dynamics and Earthquake Engineering* 136. Elsevier: 106205.

Myers DE (1994) Spatial interpolation: an overview. *Geoderma* 62(1–3): 17–28. DOI: 10.1016/0016-7061(94)90025-6.

Nadim F (2007) Tools and strategies for dealing with uncertainty in geotechnics. *CISM International Centre for Mechanical Sciences, Courses and Lectures* 491: 71–95. DOI: 10.1007/978-3-211-73366-0_2.

Nakamura Y (1989) A method for dynamic characteristics estimation of subsurface using microtremor on the ground surface. *Railway Technical Research Institute, Quarterly Reports* 30(1).

Nastev M, Parent M, Ross M, et al. (2016) Geospatial modelling of shear-wave velocity and fundamental site period of Quaternary marine and glacial sediments in the Ottawa and St. Lawrence Valleys, Canada. *Soil Dynamics and Earthquake Engineering*. DOI: 10.1016/j.soildyn.2016.03.006.

Nastev M, Parent M, Benoit N, et al. (2016) Regional VS30 model for the St. Lawrence Lowlands, Eastern Canada. *Georisk*. DOI: 10.1080/17499518.2016.1149869.

NRC (2015) *National Building Code of Canada*. 14th ed. Canadian Commission on Building and Fire Codes, National Research Council of Canada, Ottawa, Ontario, Canada.

Ohta Y and Goto N (1978) Empirical shear wave velocity equations in terms of characteristic soil indexes. *Earthquake Engineering & Structural Dynamics* 6(2): 167–187. DOI: 10.1002/eqe.4290060205.

Oliveira L, Teves-Costa P, Pinto C, et al. (2020) Seismic microzonation based on large geotechnical database: Application to Lisbon. *Engineering Geology* 265. Elsevier B.V: 105417. DOI: 10.1016/j.enggeo.2019.105417.

Perret D, Charrois E and Bolduc M (2016) Shear Wave Velocity Estimation from Piezocone Test Data for Eastern Canada Sands (Quebec and Ontario) – Extended Version with Appendices. *Geological Survey of Canada*: 48. DOI: 10.4095/299413.

Phoon K-K and Kulhawy FH (1999a) Characterization of geotechnical variability. *Canadian Geotechnical Journal* 36(4): 612–624. DOI: 10.1109/MED.2015.7158899.

Phoon K-K and Kulhawy FH (1999b) Evaluation of geotechnical property variability. *Canadian Geotechnical Journal* 36(4). NRC Research Press: 625–639.

Phoon K, Nadim F, Uzielli M, et al. (2006) Soil variability analysis for geotechnical practice. *Characterisation and Engineering Properties of Natural Soils* (April 2016). DOI: 10.1201/noe0415426916.ch3.

Phoon KK and Tang C (2019) Characterisation of geotechnical model uncertainty. *Georisk* 13(2). Taylor & Francis: 101–130. DOI: 10.1080/17499518.2019.1585545.

Pilz J and Spöck G (2008) Why do we need and how should we implement Bayesian kriging methods. *Stochastic Environmental Research and Risk Assessment* 22(5): 621–632. DOI: 10.1007/s00477-007-0165-7.

Pinheiro M, Vallejos J, Miranda T, et al. (2016) Geostatistical simulation to map the spatial heterogeneity of geomechanical parameters: A case study with rock mass rating. *Engineering Geology* 205. Elsevier B.V.: 93–103. DOI: 10.1016/j.enggeo.2016.03.003.

Pitilakis K, Raptakis D, Lontzetidis K, et al. (1999) Geotechnical and geophysical description of euro-seistest, using field, laboratory tests and moderate strong motion recordings. *Journal of Earthquake Engineering* 3(3): 381–409. DOI: 10.1080/13632469909350352.

Pitilakis K, Riga E, Anastasiadis A, et al. (2018) Towards the revision of EC8: Proposal for an alternative site classification scheme and associated intensity dependent spectral amplification factors. *Soil Dynamics and Earthquake Engineering*. DOI: 10.1016/j.soildyn.2018.03.030.

Pitilakis KD, Anastasiadis A and Raptakis D (1992) Field and laboratory determination of dynamic properties of natural soil deposits. In: *Proceedings of the 10th world conference on earthquake engineering*, 1992, pp. 1275–1280.

Podestá L, Sáez E, Yáñez G, et al. (2019) Geophysical study and 3-D modeling of site effects in Viña del Mar, Chile. *Earthquake Spectra* 35(3): 1329–1349. DOI: 10.1193/080717EQS155M.

Prins LT and Andresen KJ (2021) A geotechnical stratigraphy for the shallow subsurface in the Southern Central Graben, North Sea. *Engineering Geology* 286(December 2019). DOI: 10.1016/j.enggeo.2021.106089.

Pyrcz MJ and Deutsch C V (2014) *Geostatistical Reservoir Modeling*. Oxford university press.

Remy N, Boucher A and Wu J (2009) *Applied Geostatistics with SGeMS: A User's Guide*. DOI: 10.1017/CBO9781139150019.

Robertson PK (1990) Soil classification using the cone penetration test. *Canadian Geotechnical Journal* 27(1). NRC Research Press: 151–158.

Robertson PK (2009) Interpretation of cone penetration tests - A unified approach. *Canadian Geotechnical Journal* 46(11): 1337–1355. DOI: 10.1139/T09-065.

Robertson PK (2016) Cone penetration test (CPT)-based soil behaviour type (SBT) classification system — An update. *Canadian Geotechnical Journal* 53(12): 1910–1927. DOI: 10.1139/cgj-2016-0044.

Robertson PK and Campanella RG (1983) Interpreation of cone penetration tests. Part I: sand. *Canadian Geotechnical Journal* 20(4): 718–733. DOI: 10.1139/t83-078.

Robertson PK and Wride CE (1998) Evaluating cyclic liquefaction potential using the cone penetration test. *Canadian Geotechnical Journal* 35(3): 442–459. DOI: 10.1139/t98-017.

Rohmer O, Bertrand E, Mercerat ED, et al. (2020) Combining borehole log-stratigraphies and ambient vibration data to build a 3D Model of the Lower Var Valley, Nice (France). *Engineering Geology* 270(May 2019). DOI: 10.1016/j.enggeo.2020.105588.

Rosset P, Bour-Belvaux M and Chouinard L (2015) Microzonation models for Montreal with respect to VS30. *Bulletin of Earthquake Engineering* 13(8): 2225–2239. DOI: 10.1007/s10518-014-9716-8.

Salsabili M, Saeidi A, Rouleau A, et al. (2021) 3D probabilistic modelling and uncertainty analysis of glacial and post-glacial deposits of the city of Saguenay, Canada. *Geosciences (Switzerland)* 11(5). Multidisciplinary Digital Publishing Institute: 204. DOI: 10.3390/geosciences11050204.

Salsabili M, Saeidi A, Rouleau A, et al. (2022) Development of empirical CPTu-Vs correlations for post-glacial sediments in Southern Quebec, Canada, in consideration of soil type and geological setting. *Soil Dynamics and Earthquake Engineering* 154(July 2021). Elsevier Ltd: 107131. DOI: 10.1016/j.soildyn.2021.107131.

Schneider JA, Randolph MF, Mayne PW, et al. (2008) Using Normalized Piezocone Tip Resistance. (November): 1569–1586.

Seed HB, Ugas C and Lysmer J (1976) Site dependent spectra for earthquake resistant design: Report No. EERC 74-12, Earthq. Engr. Res. Center. *Univ. of Calif, at Berkeley*.

Seed HB, Idriss IM and Arango I (1983) Evaluation of liquefaction potential using field performance data. *Journal of Geotechnical Engineering* 109(3): 458–482. DOI: 10.1061/(ASCE)0733-9410(1983)109:3(458).

Shano L, Raghuvanshi TK and Meten M (2020) Landslide susceptibility evaluation and hazard zonation techniques – a review. *Geoenvironmental Disasters* 7(1). DOI: 10.1186/s40677-020-00152-0.

Shearer PM and Orcutt JA (1987) Surface and near-surface effects on seismic waves—theory and borehole seismometer results. *Bulletin of the Seismological Society of America* 77(4). The Seismological Society of America: 1168–1196.

SM Working Group (2015) Guidelines for seismic microzonation. In: *Civil Protection Department and Conference of Regions and Autonomous Provinces of Italy*, 2015.

Talukder MK and Chouinard L (2016) Probabilistic methods for the estimation of seismic Faand Fvmaps—application to Montreal. *Bulletin of Earthquake Engineering*. DOI: 10.1007/s10518-015-9832-0.

TC4-ISSMGE (1999) *Manual for Zonation on Seismic Geotechnical Hazard, Revised Edition*.

Thompson EM, Wald DJ and Worden CB (2014) A VS30Map for California with geologic and topographic constraints. *Bulletin of the Seismological Society of America*. DOI: 10.1785/0120130312.

Tong LY, Che HB, Zhang MF, et al. (2018) Determination of shear wave velocity of Yangtze Delta sediments using seismic piezocone tests. *Transportation Geotechnics* 14: 29–40. DOI: 10.1016/j.trgeo.2017.09.005.

Tonni L and Simonini P (2013) Shear wave velocity as function of cone penetration test

measurements in sand and silt mixtures. *Engineering Geology* 163. Elsevier: 55–67. DOI: 10.1016/j.enggeo.2013.06.005.

Tsai CC, Kishida T and Kuo CH (2019) Unified correlation between SPT–N and shear wave velocity for a wide range of soil types considering strain-dependent behavior. *Soil Dynamics and Earthquake Engineering* 126(June). Elsevier Ltd: 105783. DOI: 10.1016/j.soildyn.2019.105783.

Uzielli M, Vannucchi G and Phoon KK (2005) Random field characterisation of stress-nomalised cone penetration testing parameters. *Geotechnique* 55(1). Thomas Telford Ltd: 3–20.

Vessia G, Di Curzio D and Castrignanò A (2020) Modeling 3D soil lithotypes variability through geostatistical data fusion of CPT parameters. *Science of the Total Environment* 698. Elsevier B.V.: 134340. DOI: 10.1016/j.scitotenv.2019.134340.

Wald DJ and Allen TI (2007) Topographic slope as a proxy for seismic site conditions and amplification. *Bulletin of the Seismological Society of America*. DOI: 10.1785/0120060267.

Walter J, Rouleau A, Chesnaux R, et al. (2018) Characterization of general and singular features of major aquifer systems in the Saguenay-Lac-Saint-Jean region. *Canadian Water Resources Journal* 43(2). Taylor & Francis: 75–91. DOI: 10.1080/07011784.2018.1433069.

Wang B (2020) Geotechnical investigations of an earthquake that triggered disastrous landslides in eastern Canada about 1020 cal BP. *Geoenvironmental Disasters*. DOI: 10.1186/s40677-020-00157-9.

Wang X, Wang H, Liang RY, et al. (2019) A semi-supervised clustering-based approach for stratification identification using borehole and cone penetration test data. *Engineering Geology* 248(November 2018). Elsevier: 102–116. DOI: 10.1016/j.enggeo.2018.11.014.

Wang Y, Cao Z and Li D (2016) Bayesian perspective on geotechnical variability and site characterization. *Engineering Geology* 203. Elsevier B.V.: 117–125. DOI: 10.1016/j.enggeo.2015.08.017.

Wang Y, Zhao T and Phoon K-K (2018) Direct simulation of random field samples from sparsely measured geotechnical data with consideration of uncertainty in interpretation. *Canadian Geotechnical Journal* 55(6). NRC Research Press: 862–880.

Wellmann JF and Regenauer-Lieb K (2012) Uncertainties have a meaning: Information entropy as a quality measure for 3-D geological models. *Tectonophysics* 526–529. Elsevier B.V.: 207–216. DOI: 10.1016/j.tecto.2011.05.001.

Wu C, Wu J and Luo Y (2011) Spatial interpolation of severely skewed data with several peak values by the approach integrating kriging and triangular irregular network interpolation.: 1093–1103. DOI: 10.1007/s12665-010-0784-z.

Yamamoto JK, Koike K, Kikuda AT, et al. (2014) Post-processing for uncertainty reduction in computed 3D geological models. *Tectonophysics* 633(1). Elsevier B.V.: 232–245. DOI: 10.1016/j.tecto.2014.07.013.

Yamazaki F and Molas G (1995) Attenuation of earthquake ground motion in Japan including deep focus events. *Bulletin of the Seismological Society of America* 85(5): 1343–1358. Available at: http://www.bssaonline.org/cgi/content/abstract/85/5/1343.

Zhang G, Robertson PK and Brachman RWI (2002) Estimating liquefaction-induced ground settlements from CPT for level ground. *Canadian Geotechnical Journal* 39(5). NRC Research Press: 1168–1180.

Zhang JZ, Huang HW, Zhang DM, et al. (2021) Quantitative evaluation of geological uncertainty and its influence on tunnel structural performance using improved coupled

Markov chain. *Acta Geotechnica* 6. Springer Berlin Heidelberg. DOI: 10.1007/s11440-021-01287-6.

Zhang M and Tong L (2017) New statistical and graphical assessment of CPT-based empirical correlations for the shear wave velocity of soils. *Engineering Geology* 226(May). Elsevier: 184–191. DOI: 10.1016/j.enggeo.2017.06.007.

Zhao JX, Zhang J, Asano A, et al. (2006) Attenuation relations of strong ground motion in Japan using site classification based on predominant period. *Bulletin of the Seismological Society of America* 96(3): 898–913. DOI: 10.1785/0120050122.

Zhao T and Wang Y (2020) Non-parametric simulation of non-stationary non-gaussian 3D random field samples directly from sparse measurements using signal decomposition and Markov Chain Monte Carlo (MCMC) simulation. *Reliability Engineering and System Safety* 203. Elsevier Ltd: 107087. DOI: 10.1016/j.ress.2020.107087.

APPENDICES

APPENDIX A

Electric CPT cone (Piezocone)

Technical Specification:

Gouda Geo-Equipment B.V.

Overall length	: 254 mm
Section area of conical tip	: 1,000 mm²
Apex angle of conical tip	: 60º
Surface of friction sleeve	: 15,000 mm²
Weight	: 1,480 gr
Power supply	: ± 10 Vdc (100 mA)
Signal output	: 0 – 5 Vdc
Screw thread	: Standard female GHD thread
Connector	: Standard gold-plated Lemo 10 pins
Working temperature	: 0 till 60 ºC
Storage temperature	: -40 till 85 ºC

Cone Resistance (q_c)

Available measuring ranges *)	: 0 – 25 kN (*0 – 25 MPa*) 0 – 50 kN (*0 – 50 MPa*) (standard) 0 – 100 kN (*0 – 100 MPa*)
Accuracy	: 0.25% of the full scale (FS)
Maximum allowable load	: 150% of the measuring range
Cone area factor	: 0.71

Local Sleeve Friction (f_s) + Cone Resistance (q_c)

Available measuring ranges *)	: 0 – 25 kN 0 – 50 kN (standard) 0 – 100 kN
Accuracy local sleeve friction	: 0.50% of the full scale (FS)
Maximum allowable load	: 150% of the measuring range
Sleeve area ratio	: 1.0

Inclination	**(biaxial)**
Available measuring range	: 0 – 25º (biaxial)
Accuracy	: < 0,5º

Pore Pressure (p)

Available measuring ranges *)	: 0 – 5 MPa (standard) 0 – 10 MPa 0 – 20 MPa
Accuracy	: 0.5% of the full scale (FS)

APPENDIX B

Triaxial seismic adapter (Seismic Module)

Technical Specification:

Gouda Geo-Equipment B.V.

Length: 380mm
Diameter: 44mm
Measuring orientation: X, Y and Z axis
Geophone: 3x Geospace GS-14-L3
Sensitivity: 290 mV/ips (± 15%)
Natural frequency: 28 Hz (± 20%)
Coil resistance: 570 Ohm (± 5%)
Coil inductance: 45 mh
Damping factor: 0.18 (± 30%)
Damping constant: 172
Displacement limit: 2.29 mm (0.09 in)
Inertial mass: 2.155 gr (0.076 oz)
Orientation angle: ± 180°
Operating temperature: -45° to +100°C
Storage temperature: -45° to +100°C
Shock resistance: 5000 G

APPENDIX C

List of developed regression equations

Table C1. Regression equation forms between V_s and CPTu parameters

Equation No.	Model equations	General soils		Clay		Sand	
		R^2	RMSE (m/s)	R^2	RMSE (m/s)	R^2	RMSE (m/s)
A1	$V_s = aq_t^b$	0.349	48	0.558	38	0.446	46
A2	$V_s = aq_t^b f_s^c$	0.375	47	0.564	38	0.456	45
A3	$V_s = aq_t^b I_c^c$	**0.618**	**37**	0.655	34	0.507	43
A4	$V_s = aq_t^b Z^c$	0.565	39	**0.675**	**33**	0.486	44
A5	$V_s = aq_t^b (1+B_q)^c$	0.457	44	0.631	35	0.454	45
A6	$V_s = a(q_t - \sigma_{v0})^b Z^c$	0.567	39	0.675	33	0.486	44
A7	$V_s = aq_t^b I_c^c \acute{\sigma}_{vo}^d$	0.645	35	0.692	32	**0.520**	**43**
A8	$V_s = aq_t^b I_c^c Z^d$	**0.648**	**35**	**0.70**	**32**	0.513	43
A9	$V_s = aq_t^b f_s^c Z^d$	0.624	37	0.69	32	0.501	43
A10	$V_s = aq_t^b Z^c (1+B_q)^d$	0.568	39	0.677	33	0.487	44
A11	$V_s = aq_t^b I_c^c Z^d (1+B_q)^e$	**0.658**	**35**	**0.702**	**32**	0.520	43

Table C2. Regression coefficients of Table C1

Equation No.	General soils					Clay					Sand				
	a	b	c	d	e	a	b	c	d	e	a	b	c	d	e
A1	57.245	0.171	-	-	-	18.705	0.325	-	-	-	12.876	0.321	-	-	-
A2	68.016	0.124	0.06	-	-	15.175	0.365	-0.03	-	-	17.109	0.266	0.054	-	-
A3	3.666	0.387	1.133	-	-	3.892	0.387	1.077	-	-	3.612	0.416	0.685	-	-
A4	37.959	0.169	0.172	-	-	19.285	0.274	0.138	-	-	15.477	0.284	0.074	-	-
A5	17.935	0.294	0.626	-	-	7.365	0.424	0.473	-	-	12.128	0.327	-3.242	-	-
A6	41.407	0.157	0.187	-	-	23.172	0.244	0.169	-	-	16.050	0.280	0.078	-	-
A7	5.93	0.312	0.762	0.095	-	8.651	0.290	0.423	0.124	-	4.416	0.378	0.530	0.053	-
A8	6.299	0.329	0.827	0.082	-	7.86	0.324	0.610	0.099	-	4.912	0.383	0.558	0.033	-
A9	50.034	0.092	0.092	0.186	-	28.873	0.187	0.056	0.168	-	22.279	0.213	0.067	0.080	-
A10	31.335	0.194	0.157	0.117	-	15.292	0.305	0.120	0.114	-	15.077	0.287	0.070	-1.256	-
A11	3.868	0.386	0.881	0.048	0.225	5.303	0.371	0.657	0.069	0.160	3.896	0.406	0.632	0.017	-2.831

Table C3. Regression equation forms between V_{s1} and CPTu parameters

Equation No.	Model equations	General soils		Clay		Sand	
		R^2	RMSE (m/s)	R^2	RMSE (m/s)	R^2	RMSE (m/s)
B1	$V_{s1} = aQ_{tn}^b$	0.348	40	0.249	36	0.393	47
B2	$V_{s1} = aQ_{tn}^b {F_r}^c$	0.309	41	0.246	36	0.408	46
B3	$V_{s1} = aQ_{tn}^b {I_c}^c$	**0.367**	**39**	0.249	36	**0.421**	**45**
B4	$V_{s1} = aQ_{tn}^b (1+B_q)^c$	0.352	40	**0.250**	**36**	0.393	47
B5	$V_{s1} = aQ_{tn}^b Z^c$	0.385	39	0.408	32	0.393	46

Table C4. Regression coefficients of Table C3

Equation No.	General soils					Clay					Sand				
	a	b	c	d	e	a	b	c	d	e	a	b	c	d	e
B1	144.88	0.128	-	-	-	136.80	0.157	-	-	-	68.111	0.285	-	-	-
B2	141.22	0.135	0.036	-	-	135.12	0.161	0.001	-	-	72.819	0.277	0.062	-	-
B3	84.652	0.194	0.371	-	-	126.28	0.162	0.065	-	-	36.305	0.361	0.476	-	-
B4	130.12	0.152	0.128	-	-	142.94	0.147	-0.048	-	-	68.662	0.283	0.555	-	-
B5	117.85	0.147	0.064	-	-	82.833	0.233	0.125	-	-	67.524	0.286	0.002	-	-

Table C5. Regression equation forms between V_S and CPTu parameters for specific clays

Equation No.	Model equations	Laflamme		Champlain		Sensitive clay	
		R^2	RMSE (m/s)	R^2	RMSE (m/s)	R^2	RMSE (m/s)
C1	$V_s = aq_t^b Z^c$	**0.819**	**17**	**0.718**	**40**	**0.709**	**27**
C2	$V_s = aq_t^b I_c^c Z^d$	0.822	17	0.721	40	0.709	27

Table C6. Regression coefficients of Table C5

Equation No.	Laflamme				Champlain				Sensitive clay			
	a	b	c	d	a	b	c	d	a	b	c	d
C1	12.201	0.359	0.070	-	8.591	0.378	0.158	-	11.860	0.327	0.161	-
C2	40.165	0.274	-0.718	0.139	4.407	0.381	0.675	0.134	11.484	0.324	0.048	0.162

Table C7. The ratio of the SE to the value of coefficient

SE / RC	Colour legend
< 10 %	
10 – 25 %	
25 –50 %	
> 50 %	

SE: Standard error of regression coefficients
RC: Regression coefficient values